

DESIGN AND CHARACTERIZATION OF A LONG  
PERIOD FIBER GRATING BASED SENSOR FOR  
MERCURY (II) IONS DETECTION

TAN SHIN YINN

DOCTOR OF PHILOSOPHY IN ENGINEERING

FACULTY OF ENGINEERING AND GREEN  
TECHNOLOGY  
UNIVERSITI TUNKU ABDUL RAHMAN  
OCTOBER 2018

**DESIGN AND CHARACTERIZATION OF A LONG  
PERIOD FIBER GRATING BASED SENSOR FOR  
MERCURY (II) IONS DETECTION**

By

**TAN SHIN YINN**

A thesis submitted to the Department of Electronic Engineering,  
Faculty of Engineering and Green Technology,  
Universiti Tunku Abdul Rahman,  
in partial fulfillment of the requirements for the degree of  
Doctor of Philosophy in Engineering  
October 2018

## **ABSTRACT**

### **DESIGN AND CHARACTERIZATION OF A LONG PERIOD FIBER GRATING BASED SENSOR FOR MERCURY (II) IONS DETECTION**

**Tan Shin Yinn**

Water is known as a very essential substance that all living beings cannot survive without, hence the purity of water has become a crucial issue. Recently, there have been enough cases reported in which the pollution of water bodies has become an appalling issue, especially those caused by heavy metals. Water pollution not only affects the nature ecosystems, but also causes harmful effects to human health. One of the heavy metals that requires attention is mercury. Many fresh and sea water areas have been reported to be contaminated by mercury, which is then ingested by aquatic life and pass through the food chain, ultimately reaching to humans. The exposure to mercury, even in small amounts, can lead to serious health problems. For example, the neurological development, renal organ systems and gastrointestinal functions of human bodies can be destroyed if overly exposed to mercury. Due to this, the monitoring of mercury content in water is important and a variety of measurements have been proposed and demonstrated over the years.

One of the commonly used sensors in monitoring mercury is optical-based sensors as it offers a variety of advantages, including its small size, light

weight, immunity to electromagnetic interference and its ease of signal transmission. However, most optical-based sensors required the measurands to be collected from the site before they can be tested in the laboratory. Due to this, the proposed sensors were only limited to a short and quick laboratory detection. This project explores the possibility of extending the detection outside the laboratory. The project proposed the use of an electric arc-induced Long Period Fiber Grating (LPFG) as the optical-based sensor for mercury detection because past research have proven that LPFG can be deployed kilometers away where an electric source is not needed at the sensing point. In other words, the application of LPFG can be extended to the real environment. This particular property of LPFG will help overcome the limitation of previously proposed sensors, where they were only limited to laboratory testing. Also, the unique property of LPFG, *i.e.* its sensitivity to external index, is another reason why LPFG is proposed as the optical-based sensor for monitoring mercury content in this project, as a slight change in the surrounding refractive index caused by mercury content can be investigated through its response. Throughout the years, not much research has been done on using LPFG as a mercury sensor. Hence, the techniques to enhance its sensitivity and the sensing agent that can tailor the surface of LPFG are explored in this research so that the LPFG will respond to the presence of mercury in water.

Another important aspect that should be considered in environmental studies such as water monitoring is long-term detection because it allows the collection of background data over a longer period of time. Also, it helps to

reveal important trends which can provide researchers with more solid proof in understanding environmental parameters. However, most of the proposed fiber sensors including LPFG were limited to short-term detection. When it comes to long-term monitoring, LPFG without protection may not be suitable to be used due to its brittle silica-based structure. Hence, another limitation is found in this aspect. In this project, a structure that can be used to protect the modified LPFG and prevent it from being broken by the harsh environment was constructed as well. The structure constructed in this project was similar to the structure of (Diffusive Gradient in Thin Films) DGT, which was proposed in 1994 for long-term detection purposes. With the protection offered by this structure, the LPFG can be used to monitor mercury (II) ions over a longer duration as the structure helps to overcome the weakness of LPFG, *i.e.* limited lifespan.

In conclusion, the purpose of this project is to solve both the limitations discussed earlier, *i.e.* to extend the sensing application of LPFG to outside of laboratory and to prolong the lifespan of LPFG for long term monitoring. A hybrid sensor which combined the features of both LPFG and DGT was proposed and demonstrated in this research to allow the application of real-time and long-term monitoring of mercury (II) ions in water. In the beginning stage of the research, the sensitivity of LPFG towards refractive index was enhanced. The shifting of the resonant wavelength of the LPFG in response to external refractive index was increased by applying thin film coating method. Also, the transmission loss of the LPFG was enhanced by introducing double-pass configuration into the experiment setup. The

improved LPFGs were then coated with gold nanoparticles and tested with different concentrations of mercury (II) ions solution. From the study, the resonant wavelengths of the coated LPFGs shifted to longer wavelength and its transmission power increased when it was exposed to mercury (II) ions. This proves that the LPFGs were able to detect the presence of mercury (II) ions with the coating agent. In the final stage of the research, a hybrid LPFG-DGT monitoring sensor system was constructed and demonstrated. The sensor was again experimented with different concentrations of mercury (II) solutions. Similarly, the resonant wavelength of the sensor shifted to longer wavelength and the transmission power increased. This result proves that the designed LPFG-DGT hybrid sensor was capable of performing real-time and long-term monitoring of mercury (II) ions in water bodies.

## ACKNOWLEDGEMENTS

I would like to take this golden opportunity to gratefully acknowledge the contribution of everyone who has encouraged and lent me a helping hand over the past few years towards the successful completion of this research.

First and foremost, I would like to express my sincere appreciation to Universiti Tunku Abdul Rahman for giving me this opportunity to develop and conduct this research. Thank you for providing the necessary information and instruments regarding the project that assisted me in gaining valuable knowledge and experiences in these few years.

Secondly, I would like to express my gratitude to my research supervisor, Prof. Ts. Dr. Faiz bin Abd Rahman, and my co-supervisor, Dr. Lee Sheng Chyan, who had always been patient with me in guiding and taking care of me throughout the development of this whole research. Prof. Faiz and Dr. Lee were great mentors who were willing to encourage me and share valuable opinions with me when I encountered challenges in my research.

Furthermore, I would also like to heartily thank my external co-supervisors, Prof. Dr. Hideki Kuramitz for offering me the opportunity to visit and perform part of the research in University of Toyama. I am deeply grateful for the experience gained in Japan as well as the training and advice provided by Prof. Hideki from time to time.

Last but not least, I would like to acknowledge, with gratitude, the support and love of my family, especially my grandmother, parents and brother. They have always been supportive and encouraged me.

Truly I have been blessed to have known them all. I truly appreciated every advice and opportunity offered.

## APPROVAL SHEET

This dissertation/thesis entitled “**DESIGN AND CHARACTERIZATION OF A LONG PERIOD FIBER GRATING BASED SENSOR FOR MERCURY (II) IONS DETECTION**” was prepared by TAN SHIN YINN and submitted as partial fulfillment of the requirements for the degree of Doctor of Philosophy in Engineering at Universiti Tunku Abdul Rahman.

Approved by:

---

(Prof. Ts. Dr. Faidz bin Abd Rahman)

Date:.....

Professor/Supervisor

Department of Electrical and Electronic Engineering

Lee Kong Chian Faculty of Engineering and Science

Universiti Tunku Abdul Rahman

---

(Dr. Lee Sheng Chyan)

Date:.....

Assistant Professor/Co-supervisor

Department of Electronic Engineering

Faculty of Engineering and Green Technology

Universiti Tunku Abdul Rahman

**FACULTY OF ENGINEERING AND GREEN TECHNOLOGY  
UNIVERSITI TUNKU ABDUL RAHMAN**

Date: \_\_\_\_\_

**SUBMISSION OF THESIS**

It is hereby certified that ***Tan Shin Yinn*** (ID No: ***14AGD06670***) has completed this thesis entitled “*Design and Characterization of a Long Period Fiber Grating Based Sensor for Mercury (II) Ions Detection*” under the supervision of Prof. Ts. Dr. Faidz bin Abd Rahman (Supervisor) from the Department of Electrical and Electronic Engineering, Lee Kong Chian Faculty of Engineering and Science, and Dr. Lee Sheng Chyan (Co-Supervisor) from the Department of Electronic Engineering, Faculty of Engineering and Green Technology.

I understand that University will upload softcopy of my thesis in pdf format into UTAR Institutional Repository, which may be made accessible to UTAR community and public.

Yours truly,

\_\_\_\_\_  
(*Tan Shin Yinn*)

## DECLARATION

I hereby declare that the thesis is based on my original work except for quotations and citations which have been duly acknowledged. I also declare that it has not been previously or concurrently submitted for any other degree at UTAR or other institutions.

Name TAN SHIN YINN

Date \_\_\_\_\_

## TABLE OF CONTENTS

|                                                                         | <b>Page</b>  |
|-------------------------------------------------------------------------|--------------|
| <b>ABSTRACT</b>                                                         | <b>ii</b>    |
| <b>ACKNOWLEDGEMENTS</b>                                                 | <b>vi</b>    |
| <b>APPROVAL SHEET</b>                                                   | <b>vii</b>   |
| <b>PERMISSION SHEET</b>                                                 | <b>viii</b>  |
| <b>DECLARATION</b>                                                      | <b>ix</b>    |
| <b>TABLE OF CONTENTS</b>                                                | <b>x</b>     |
| <b>LIST OF FIGURES</b>                                                  | <b>xiv</b>   |
| <b>LIST OF TABLES</b>                                                   | <b>xvii</b>  |
| <b>LIST OF ABBREVIATIONS</b>                                            | <b>xviii</b> |
| <br>                                                                    |              |
| <b>CHAPTER</b>                                                          |              |
| <br>                                                                    |              |
| <b>1.0 INTRODUCTION</b>                                                 | <b>1</b>     |
| 1.1 Research Motivations                                                | 1            |
| 1.2 Objectives                                                          | 5            |
| 1.3 Contributions                                                       | 6            |
| 1.4 Organization of Thesis                                              | 9            |
| <br>                                                                    |              |
| <b>2.0 THEORY AND PROPERTIES OF LONG PERIOD FIBER GRATINGS (LPFGs)</b>  | <b>12</b>    |
| 2.1 Introduction                                                        | 12           |
| 2.2 Wave model of Light                                                 | 12           |
| 2.3 Basic Theory of Long Period Fiber Grating                           | 17           |
| 2.4 Coupled Mode Theory                                                 | 18           |
| 2.5 Phase Matching Condition                                            | 22           |
| 2.6 Development of Fabrication Techniques of LPFG                       | 26           |
| 2.7 Sensitivity of LPFG towards External Influences                     | 27           |
| 2.7.1 Temperature Sensitivity                                           | 29           |
| 2.7.2 Refractive Index Sensitivity                                      | 30           |
| 2.7.3 Strain Sensitivity                                                | 32           |
| 2.8 Modifications of LPFG Sensitivity                                   | 33           |
| 2.8.1 Bending                                                           | 33           |
| 2.8.2 Etching                                                           | 34           |
| 2.8.3 Grating Period Optimization                                       | 35           |
| 2.9 Influence of Coupled Cladding Mode Order on the Sensitivity of LPFG | 36           |
| 2.10 LPFGs in the Turning Point                                         | 36           |
| 2.11 Applications of LPFG                                               | 37           |
| 2.11.1 Pressure Sensor                                                  | 37           |
| 2.11.2 Refractive Index Sensor                                          | 38           |
| 2.11.3 Biosensor                                                        | 39           |
| 2.12 Advantages of LPFG as a Sensor                                     | 40           |

|            |                                                                                         |            |
|------------|-----------------------------------------------------------------------------------------|------------|
| 2.13       | Summary                                                                                 | 41         |
| <b>3.0</b> | <b>FABRICATION OF ARC-INDUCED LPFG</b>                                                  | <b>42</b>  |
| 3.1        | Introduction                                                                            | 42         |
| 3.1.1      | Advantages of Arc-Induced LPFG                                                          | 42         |
| 3.1.2      | Disadvantages of Arc-Induced LPFG                                                       | 44         |
| 3.1.3      | History of Arc-Induced LPFG                                                             | 45         |
| 3.2        | Current Fabrication Setup for Arc-Induced LPFG                                          | 49         |
| 3.3        | Fabrication of Arc-Induced LPFGs                                                        | 52         |
| 3.3.1      | Preparation before Fabrication Process                                                  | 52         |
| 3.3.2      | Fabrication Process                                                                     | 53         |
| 3.3.3      | Flowchart of the Fabrication Process                                                    | 55         |
| 3.3.4      | Arc Generation and Gratings Formation on LPFG                                           | 56         |
| 3.3.5      | The Reproducibility of LPFGs Fabricated                                                 | 58         |
| 3.4        | Characterization of LPFGs Fabricated with Current Fabrication System                    | 60         |
| 3.4.1      | Sensing of Cargille Oils                                                                | 60         |
| 3.4.1.1    | Experimental Setup                                                                      | 60         |
| 3.4.1.2    | Results and Discussion                                                                  | 63         |
| 3.4.2      | Sensing of Sucrose Solutions                                                            | 69         |
| 3.4.2.1    | Experimental Setup                                                                      | 69         |
| 3.4.2.2    | Results and Discussion                                                                  | 71         |
| 3.5        | Summary                                                                                 | 74         |
| <b>4.0</b> | <b>SENSITIZATION OF ARC-INDUCED LPFG TOWARDS SURROUNDING REFRACTIVE INDEX</b>           | <b>75</b>  |
| 4.1        | Introduction of LPFG Sensitivity Enhancement                                            | 76         |
| 4.2        | Thin Film Coating                                                                       | 79         |
| 4.2.1      | Experiment Setup for LPFG Coating Process                                               | 81         |
| 4.2.1.1    | Results and Discussion                                                                  | 83         |
| 4.2.2      | Characterization of PE-coated LPFG towards Refractive Index                             | 87         |
| 4.2.2.1    | Results and Discussion                                                                  | 88         |
| 4.3        | Double-Pass Configuration                                                               | 91         |
| 4.3.1      | Single-Pass Configuration versus Double-Pass Configuration                              | 92         |
| 4.3.2      | Characterization of LPFG with Double-Pass Configuration                                 | 94         |
| 4.3.2.1    | Results and Discussion                                                                  | 96         |
| 4.3.3      | Characterization of PE-coated LPFG with Double-Pass Configuration                       | 99         |
| 4.3.3.1    | Results and Discussion                                                                  | 100        |
| 4.4        | Summary                                                                                 | 101        |
| <b>5.0</b> | <b>DETECTION OF MERCURY (II) IONS BY POLYELECTROLYTE-GOLD NANOPARTICLES COATED LPFG</b> | <b>103</b> |

|            |                                                                                                             |            |
|------------|-------------------------------------------------------------------------------------------------------------|------------|
| 5.1        | Introduction                                                                                                | 104        |
| 5.2        | Mercury in the Environment                                                                                  | 106        |
| 5.2.1      | Sources of Mercury                                                                                          | 106        |
| 5.2.2      | Impacts of Mercury                                                                                          | 107        |
| 5.2.2.1    | Environmental Impacts                                                                                       | 108        |
| 5.2.2.2    | Health Impacts                                                                                              | 109        |
| 5.3        | History of Mercury Detection                                                                                | 111        |
| 5.3.1      | Colourimetric Sensor                                                                                        | 112        |
| 5.3.2      | Fluorescent Sensor                                                                                          | 113        |
| 5.3.3      | Surface Enhanced Raman Scattering (SERS)                                                                    | 114        |
| 5.4        | Gold Nanoparticles Coated LPFG                                                                              | 115        |
| 5.4.1      | Interaction of Gold Nanoparticles with Mercury                                                              | 115        |
| 5.4.2      | Synthesis of Gold Nanoparticles                                                                             | 116        |
| 5.4.3      | Coating Process of LPFG                                                                                     | 117        |
| 5.4.4      | Experimental Setup                                                                                          | 119        |
| 5.5        | Results and Discussion                                                                                      | 121        |
| 5.5.1      | Coating of Gold Nanoparticles                                                                               | 121        |
| 5.5.2      | Mercury (II) Ions Detection with PE-AuNP coated LPFGs                                                       | 123        |
| 5.5.3      | Comparison of Responses Among Non-Coated, PE-only Coated and PE-AuNP Coated LPFGs towards Mercury (II) Ions | 132        |
| 5.6        | Summary                                                                                                     | 137        |
| <b>6.0</b> | <b>A NOVEL HYBRID LPFG-DGT SENSOR SYSTEM FOR LONG TERM MONITORING OF MERCURY (II) IONS</b>                  | <b>138</b> |
| 6.1        | Introduction                                                                                                | 139        |
| 6.2        | Diffusive Gradient in Thin Films                                                                            | 141        |
| 6.3        | Hybrid LPFG-DGT Sensor System for the Detection of Mercury (II) Ions                                        | 145        |
| 6.3.1      | Structure of Hybrid LPFG-DGT Sensor                                                                         | 145        |
| 6.4        | Experimental Setup                                                                                          | 148        |
| 6.5        | Results and Discussion                                                                                      | 150        |
| 6.5.1      | Mercury (II) ions Detection with Hybrid LPFG-DGT                                                            | 150        |
| 6.5.2      | Comparisons of Performances between Hybrid and Open Structure Sensor                                        | 157        |
| 6.6        | Summary                                                                                                     | 167        |
| <b>7.0</b> | <b>CONCLUSIONS AND FUTURE RECOMMENDATIONS</b>                                                               | <b>169</b> |
| 7.1        | Conclusions                                                                                                 | 169        |
| 7.2        | Future Recommendations                                                                                      | 171        |
|            | <b>PUBLICATIONS</b>                                                                                         | <b>173</b> |
|            | <b>REFERENCES</b>                                                                                           | <b>174</b> |

**APPENDIX A**  
**APPENDIX B**

**189**  
**190**

## LIST OF FIGURES

| Figures |                                                                                                                                                       | Page |
|---------|-------------------------------------------------------------------------------------------------------------------------------------------------------|------|
| 2.1     | Schematic diagram of the cylindrical waveguide                                                                                                        | 13   |
| 2.2     | Coupling principle of a LPFG                                                                                                                          | 17   |
| 3.1     | Current fabrication setup for producing arc-induced LPFGs                                                                                             | 51   |
| 3.2     | Flow chart of the fabrication process                                                                                                                 | 55   |
| 3.3     | Formation of arc-induced LPFG after 33 gratings                                                                                                       | 57   |
| 3.4     | Transmission spectra of four different LPFGs fabricated with the same arcing profile                                                                  | 59   |
| 3.5     | Experimental setup for testing with Refractive index matching oils                                                                                    | 62   |
| 3.6     | Spectra response of (a) LPFG 1; and (b) LPFG 2 in accordance to difference refractive indices                                                         | 65   |
| 3.7     | (a) Wavelength shift and (b) Transmission power of both LPFG 1 and LPFG 2 in accordance to the increment in surrounding refractive index              | 68   |
| 3.8     | (a) Wavelength shift and (b) Transmission power of both LPFG 1 and LPFG 2 in accordance to the increment in surrounding refractive index              | 73   |
| 4.1     | Schematic of the LPFG coated with bilayer of polyelectrolytes (PDDA/PSS) <sub>1</sub>                                                                 | 83   |
| 4.2     | Transmission spectra of (a) LPFG 1; and (b) LPFG 2 in water in accordance to the increment number of bilayers                                         | 86   |
| 4.3     | Wavelength shift of (a) LPFG 1; (b) LPFG 2 coated with increasing number of PE bilayers in accordance to different concentrations of sucrose solution | 90   |
| 4.4     | Illustration of (a) Single-Pass Configuration; (b) Double-Pass Configuration                                                                          | 93   |
| 4.5     | Experimental setup for (a) Single-pass configuration; (b) Double-pass configuration                                                                   | 95   |

|     |                                                                                                                                                                                                                        |     |
|-----|------------------------------------------------------------------------------------------------------------------------------------------------------------------------------------------------------------------------|-----|
| 4.6 | Comparison of spectra in accordance to external refractive index for (a) first LPFG; (b) second LPFG in both single- and double-pass configurations                                                                    | 98  |
| 4.7 | Comparison of normalized transmission attenuation for both single- and double-pass configurations in sucrose solutions ranging from 0 % to 60 %                                                                        | 101 |
| 5.1 | Schematic diagram of the PE-AuNP coated LPFG                                                                                                                                                                           | 119 |
| 5.2 | Wavelength shift of LPFG resonance wavelength after the deposition of AuNPs                                                                                                                                            | 122 |
| 5.3 | FESEM image of the gratings surface after the deposition of AuNPs at magnification of 20,000x                                                                                                                          | 122 |
| 5.4 | Transmission response of the first PE-AuNP coated LPFG towards mercury (II) solutions                                                                                                                                  | 125 |
| 5.5 | (a) Wavelength shift; (b) Transmission power responses of the PE-AuNP coated LPFG (first LPFG) towards different concentrations of mercury over time                                                                   | 126 |
| 5.6 | Transmission response of the second PE-AuNP coated LPFG towards mercury (II) solutions                                                                                                                                 | 130 |
| 5.7 | (a) Wavelength shift; (b) Transmission power responses of the PE-AuNP coated LPFG (second LPFG) towards different concentrations of mercury over time                                                                  | 131 |
| 5.8 | First comparison of (a) resonance wavelength shift of non-coated LPFG, PE-only coated LPFG and PE-AuNP coated LPFG; (b) normalized transmission power of non-coated LPFG, PE-only coated LPFG and PE-AuNP coated LPFG  | 134 |
| 5.9 | Second comparison of (a) resonance wavelength shift of non-coated LPFG, PE-only coated LPFG and PE-AuNP coated LPFG; (b) normalized transmission power of non-coated LPFG, PE-only coated LPFG and PE-AuNP coated LPFG | 136 |
| 6.1 | Structure of DGT (a) window, (b) cap, (c) membrane filter, (d) diffusive gel layer,                                                                                                                                    | 143 |

|      |                                                                                                                                                                                                                                                                                                                                   |     |
|------|-----------------------------------------------------------------------------------------------------------------------------------------------------------------------------------------------------------------------------------------------------------------------------------------------------------------------------------|-----|
|      | (e) resin gel layer, (f) plastic base.                                                                                                                                                                                                                                                                                            |     |
| 6.2  | Structure of the hybrid LPFG-DGT DGT (a) window, (b) upper plastic plate, (c) membrane filter, (d) diffusive gel layer, (e) window that exposed fiber gratings section, (f) PE-AuNP coated LPFG, (g) base (plastic plate); the upper and base plates were glued and sealed together into a sealed structure similar to DGT device | 146 |
| 6.3  | Experimental Setup of mercury detection by the hybrid LPFG-DGT sensor                                                                                                                                                                                                                                                             | 149 |
| 6.4  | (a) Transmission power response; (b) Transmission wavelength shift of the first hybrid sensor towards mercury (II) solutions                                                                                                                                                                                                      | 152 |
| 6.5  | Transmission response of the first hybrid sensor towards mercury solutions                                                                                                                                                                                                                                                        | 153 |
| 6.6  | (a) Transmission response; (b) Transmission wavelength shift of the second hybrid sensor towards mercury (II) solutions                                                                                                                                                                                                           | 156 |
| 6.7  | Diagram of the open structure sensor (a) window that exposed fiber gratings section, (b) PE-AuNP coated LPFG; both the upper plastic plate and base plate were glued together to seal the structure                                                                                                                               | 157 |
| 6.8  | First comparison of (a) Normalized transmission power; (b) Wavelength shift between the hybrid and open structure                                                                                                                                                                                                                 | 159 |
| 6.9  | Second comparison of (a) Normalized transmission power; (b) Wavelength shift between the hybrid and open structure                                                                                                                                                                                                                | 161 |
| 6.10 | Comparison of (a) Normalized transmission power; (b) wavelength shift between open structure (LPFG 1) and hybrid structure (LPFG 2) in 2.0 ppm mercury solution                                                                                                                                                                   | 165 |
| 6.11 | Diffusion of mercury (II) ions across diffusive gel until equilibrium is achieved; (a) Mercury (II) solution (measurand), (b) membrane filter, (c) diffusive gel layer, PE-AuNP coated LPFG                                                                                                                                       | 166 |

## LIST OF TABLES

| <b>Table</b> |                                                                                                                                  | <b>Page</b> |
|--------------|----------------------------------------------------------------------------------------------------------------------------------|-------------|
| 3.1          | Arcing profile of LPFG fabrication process                                                                                       | 53          |
| 3.2          | Comparison of the properties of four different LPFGs                                                                             | 60          |
| 3.3          | Comparison of refractive index sensitivity of LPFG 1 and LPFG 2                                                                  | 69          |
| 3.4          | Weight of sucrose and volume of deionised water required for the preparation of sucrose solutions with various concentrations    | 70          |
| 5.1          | Volume of mercury standard solution and deionised water required to prepare mercury (II) solutions with different concentrations | 120         |
| 6.1          | First comparison of response rate for the hybrid LPFG-DGT structure and open structure                                           | 158         |
| 6.2          | Second comparison of response rate for hybrid and open structure                                                                 | 160         |

## LIST OF ABBREVIATIONS

|       |                                           |
|-------|-------------------------------------------|
| AuNP  | Gold Nanoparticles                        |
| DGT   | Diffusive Gradient in Thin Films          |
| DI    | Deionized                                 |
| ESA   | Electrostatic Self-Assembly               |
| FESEM | Field Effect Scanning Electron Microscope |
| IMGs  | Index Modulated Gratings                  |
| IPA   | Isopropyl Alcohol                         |
| LB    | Langmuir-Blodgett                         |
| LPFG  | Long Period Fiber Grating                 |
| MFGs  | Mode Field Modified Gratings              |
| OSA   | Optical Spectrum Analyzer                 |
| PDDA  | Poly-dimethyl dially ammonium chloride    |
| PDGs  | Physical Deformation Gratings             |
| PE    | Polyelectrolyte                           |
| PSS   | Poly (sodium-p-styrenesulfonate)          |
| QDs   | Quantum Dots                              |
| RI    | Refractive Index                          |
| SERS  | Surface Enhanced Raman Scattering         |
| TIR   | Total Internal Reflection                 |
| UV    | Ultraviolet                               |

## CHAPTER 1

### INTRODUCTION

#### 1.1 Research Motivations

As we all know, water is one of the most important substances on earth as all living beings cannot survive without water. Therefore, the quality of water is extremely crucial. Nonetheless, the pollution of water has worsened in many places such as Africa and Asia in recent years (Abaspour *et al.*, 2011), and it was discovered that there were a few major causes which led to the pollution of water, including sewage and waste from factories (Dwivedi *et al.*, 2017). Usually, the discharge of wastewater from factories and chemical plants contained heavy metals such as mercury (Gworek *et al.*, 2016). Mercury is known to be one of the most toxic metals that is very poisonous to living beings because it can result in severe effects to both the environment and humans (Rocha, 2012). There are many cases reported in which fresh and sea water have been contaminated by mercury. The exposure to mercury, even in small amounts, can lead to severe health problems. For instance, mercury is a powerful neurotoxin which can impair neurological development (Fernandes *et al.*, 2012). Moreover, renal organ systems and gastrointestinal functions of human bodies can be damaged by mercury as well. Due to this, the pollution of water by mercury requires proper attention in order to maintain water quality demands.

Over the years, different sensors and detection devices had been proposed to monitor mercury content in water. One of the sensors that had been widely utilised was the optical-based sensor. It had been proven that optical-based sensors such as colourimetric sensors, fluorescent sensors, and others were able to detect and respond towards mercury (Du *et al.*, 2015; Li *et al.*, 2011; Fen *et al.*, 2011). However, most of the sensing devices proposed were mainly used for a quick examination and detection in the laboratory, instead of detection in real environmental conditions. The active sampling technique was often adopted in these demonstrated optical-based sensors, in which the water sample was collected from the real site first before being sent to the laboratory for a quick detection. If the detection was required to be extended outside the laboratory to the real environment, a limitation was found with these proposed sensors as they were only meant for laboratory testing. Hence, there is a demand to introduce a mercury sensor which can be used for both laboratory and real-world detection.

One of the researches done in 2017 suggested that Long Period Fiber Grating (LPFG) can be deployed in the real environment located kilometres away without the need of electric source at the sensing point (Yong *et al.*). Due to this discovery, it is proposed that LPFG is a suitable candidate for real-time mercury detection in this research as it can overcome the limitation found in other optical-based sensors proposed (they are limited to laboratory testing). Also, not much research has been done on applying LPFG as a mercury sensor. Hence, to tailor the LPFG to become a mercury sensor, the discovery of a sensing agent is required, which can be used to modify the surface of LPFG so

that its attenuation band changes during the exposure to mercury ions. LPFG has been known to be a commonly used fiber sensor that has been applied in different sensing applications as chemical sensors and biosensors. One of the most important characteristics of LPFG is that its resonance wavelength can be shifted by the changes in the refractive index of the surrounding medium (Shu *et al.*, 2002). Due to this, LPFG has brought inspiration to many researches, in which the sensitivity of LPFG towards the external medium was modified to detect targeted elements for different sensing applications. On the other hand, investigations have also been initiated with the purpose to look for different techniques that can improve the wavelength shift of LPFGs in accordance to the external index to maximise its performance as a sensor (Tan *et al.*, 2015). However, most of the proposed sensitization methods such as etching of the fiber cladding as well as fiber tapering techniques required complicated processes to modify the physical structure of the LPFG (Caucheteur *et al.*, 2005; Ding *et al.*, 2005). Hence, there is a need to improve and optimize the sensitivity of LPFG with a simpler enhancement process such as thin-film coating in this research before the LPFG is further modified for mercury ions detection. In 2009, it was suggested that the sensitivity and response of LPFG can be measured by a second interrogation technique, which is based on the variation in transmission loss of the LPFG resonant notch (Han *et al.*). Therefore, there is a possibility that applying another enhancement method in this research can increase the transmission loss of the LPFG, thereby increasing its sensitivity for transmission-based interrogation. By applying both enhancement methods, the responses of LPFG towards

mercury content can be investigated through both wavelength shift and variation in transmission loss.

Another aspect that is very crucial in the investigation of environmental water bodies is long-term monitoring. This is because the environment will be affected by many uncertainties caused by different factors such as the weather. Hence, in order to monitor a large-scale of water, long-term monitoring is a crucial process so that a more accurate prediction and prognosis about the environment can be achieved (Lohner *et al.*, 2013). However, most of the demonstrated sensors for detection of mercury including the proposed LPFGs, are not suitable to be deployed in the real environment for a long period of time due to their short lifespans, unless they are well sealed and protected by a structure that can prevent them from being broken by harsh environmental factors. Despite the easily broken silica-based structure of LPFG, it actually provides a wide range of advantages which enhances the possibility of deploying it in the real environment for a duration of time, including its immunity to electromagnetic interference and corrosion resistance (Bock *et al.*, 2007). Due to these, it is required to propose and construct a protective structure to seal the LPFGs so that they are well-protected and hence can be used for long-term monitoring of mercury ions in the real environment. The idea of the protective structure was adopted from a long-term monitoring device, which was introduced back in 1994 (Zhang and Davison *et al.*). The device was named as the Diffusive Gradient in Thin Film (DGT), and it was designed for deployment in water for a period of time to monitor the targeted contents. In other words, DGT had a durable and strong

structure which protected it from being destroyed by the environment. Similarly, if the LPFG was protected with a similar durable structure, it can be deployed for a longer period of time as the structure prolongs its lifespan.

The advantages and limitations found in LPFG had prompted the inspiration of this research to propose a hybrid LPFG-DGT sensor which is meant for real-time and long-term monitoring of mercury (II) ions in water. The research consists of the enhancement of LPFG sensitivity, the identification of a sensing agent and modification of the LPFG surface so that it can be used as a sensor to detect mercury (II) ions in water, as well as the construction of a hybrid LPFG-DGT sensor structure which protects the modified LPFG for long-term monitoring purpose.

## **1.2 Objectives**

This PhD research consists of three main objectives: (1) to fabricate, characterize and improve the sensitivity of LPFG towards the external refractive index; (2) to modify LPFG surface with gold nanoparticles for the detection of mercury (II) ions in water; as well as (3) to develop a hybrid LPFG-DGT sensor system for real time and long-term monitoring of mercury (II) ions in water.

### 1.3 Contributions

According to the research conducted, it is possible to divide and categorize the contributions of this research into three different sections. The first contribution focuses on the combination of two sensitivity enhancement methods, *i.e.* thin-film coating and double-pass configuration, in improving the sensitivity of LPFG towards the external refractive index (RI). In the second stage of this research, the novelty presented was focus on the coating of the combination of polyelectrolyte and gold nanoparticles on the LPFG, which enabled the sensor to detect mercury (II) ions in water. In the final stage of the research, the contribution was highlighted in the hybrid LPFG-DGT structure, which can protect and allow the sensor to be used for long-term and real-time monitoring of mercury (II) ions in water samples.

#### **Enhancement of the sensitivity of LPFG towards refractive index changes through the combination of thin-film coating and double-pass configuration**

The arc-induced LPFGs in this thesis had been improved by two different methods before they were employed in the sensing application. Experiments had proven that the first technique, thin-film coating, had successfully enlarged the wavelength shift of the LPFG resonance notch towards the surrounding refractive index changes when a certain thickness of coating was deposited. This enhancement method was simple, as it only required simple steps of immersing the LPFG in polyelectrolytes, and the deposition process

was fast due to the stronger ionic bonding involved. Furthermore, this deposition technique offered flexibility as the coating agents were not only limited to polyelectrolytes, but, any nano-materials that consisted of charges can also be adsorbed onto the charged surface. Thus, by applying this enhancement technique, the surface of LPFG was able to be tailored accordingly as the assembly of multi-material onto its surface was possible. On the other hand, results had proven that the second enhancement technique employed in this research could improve the refractive index sensitivity of LPFG up to almost double for transmission-based interrogation due to the longer path provided by the circulators. The advantage of applying this double-pass configuration is that it does not require a complicated modification process on the LPFG. Apart from this, it can be applied to almost all LPFGs that are used in different sensing applications, as it only requires the addition of circulators into the setup. By applying both enhancement methods, the LPFGs in this research have been sensitized for both wavelength-based and transmission-based interrogation.

### **Detection of mercury (II) ions by polyelectrolyte and gold nanoparticles coated LPFG**

The ability of the sensor to detect mercury (II) ions is the main highlight in this research and it is relatively important nowadays due to the pollution of water by mercury ions. A novel combination of coating materials which consists of polyelectrolyte bilayers and gold nanoparticles was proposed as the sensing agent towards mercury ions. A study on the detection of mercury (II)

ions by polyelectrolyte-gold nanoparticles coated LPFG demonstrated that the reaction between mercury (II) ions and gold nanoparticles had successfully modified the differential in effective refractive indices of LPFG core and cladding mode, thereby causing the output spectrum of LPFG to respond when in contact with mercury (II) ions. This proposed sensor does not require a complicated modification process, but only adopts a simple coating technique to modify its surface so that the LPFG transmission responds towards mercury (II) ions.

#### **Long-term and real-time monitoring of mercury (II) ions through the proposed hybrid LPFG-DGT structure device**

The study of the hybrid sensor structure shown in this thesis had combined the features of LPFG with another DGT device which is normally used for long-term monitoring. With this structure, the limitation of LPFG (its silica-based brittle structure) had been overcome. The LPFG was sealed and protected properly within the DGT structure, hence it could be deployed freely in water bodies for the monitoring of mercury (II) ions over a longer period of time, *i.e.* allows long-term detection of mercury (II) ions. Additionally, this sensor allowed the collection of data from time to time, which means that it can be used for real-time detection. This hybrid sensor structure also overcame the limitation found in other optical-based sensors because the protective hybrid structure allowed the direct deployment of the sensor in the real environment, which means that the detection process could be performed directly outside the laboratory.

## 1.4 Organization of Thesis

This thesis is split into seven chapters. The thesis is organized as follows:

The **first chapter** of this thesis explains the research motivations, objectives and the contributions of the work conducted, as well as the organization and arrangement of the thesis.

The **second chapter** in this thesis gives a general introduction to the fiber sensor used in this research, the Long Period Fiber Grating (LPFG) and the details containing the fundamentals and theory of LPFG, including the coupled mode theory and phase matching condition. Besides that, the history of different fabrication techniques of LPFG were explored. Sensitivity of LPFG towards different parameters and methods of sensitivity enhancement were also covered in this chapter. Lastly, this chapter also describes the applications and advantages of LPFG as a sensor.

**Chapter 3** demonstrates the electric arc discharge technique that was engaged in this research for fabricating LPFGs. In the beginning, the history of arc-induced fabrication technique is briefly described. The fabrication setup and process that were used to produce arc-induced LPFGs were also presented. Lastly, the performance and sensitivity of the LPFG produced were characterized in the final section of this chapter by conducting experiments with Cargille oil and sucrose solutions.

**Chapter 4** of this thesis concerns the work conducted for sensitizing the arc-induced LPFG towards external RI. Two enhancement techniques were investigated and described in this chapter, including the thin-film coating and double-pass configuration techniques. This chapter also presents the experiments of the sensitized LPFGs with sucrose solutions and Cargille oil in order to evaluate the influence of both enhancement techniques on the sensitivity of LPFG.

**Chapter 5** of this thesis introduces a novel nanoparticles coated LPFG for the detection of mercury (II) ions in water. A novel combination of coating agents was introduced. Also, the coating technique as well as coating process of the LPFG were described in detail. The performance of the coated LPFG towards mercury (II) ions was observed in the last part of this chapter, and attention was given to the comparison between coated and uncoated LPFG in order to investigate the role of gold nanoparticles in capturing mercury (II) ions.

**Chapter 6** of this thesis proposes a novel hybrid LPFG-DGT sensor system which can be applied for real-time and long-term monitoring of mercury (II) ions. The structure of the hybrid sensor was described and illustrated, and the performance of the hybrid sensor in detecting mercury (II) ions was investigated. Also, a comparison of the performances of the proposed hybrid structure and open structure was given in order to assure the role of the hybrid structure in prolonging the sensor response time.

The final chapter of this thesis, **Chapter 7**, concludes and summarizes the findings of the whole research. Last but not least, recommendations for potential future research were discussed in this chapter as well.

## **CHAPTER 2**

### **THEORY AND PROPERTIES OF LONG PERIOD FIBER GRATINGS**

#### **2.1 Introduction**

As stated in Chapter 1, the optical-based sensor that was chosen in this research was the LPFG. In this chapter, the fundamental and basic theory of LPFG are described in detail. It begins with a brief discussion on the wave model of light, coupled mode theory as well as the phase matching condition of LPFG. The chapter then proceeds with a brief overview on the development of different fabrication techniques. Furthermore, the sensitivity of LPFG towards external influences and the techniques to enhance its sensitivity are presented. Last but not least, different applications of LPFGs that have been demonstrated and the advantages of LPFG as sensor are discussed in this chapter.

#### **2.2 Wave Model of Light**

The propagation of light within an optical fiber is identical to the propagation of an electromagnetic wave inside a medium. Due to this, the light propagation in the fiber can be treated as a transverse electromagnetic wave. In order to make the analysis simpler, the radius of the fiber cladding is assumed to be infinitely larger than the fiber core, therefore, the analysis can

be reduced to calculations across one interface between core and cladding only (Mountfort, 2009).

As shown in Figure 2.1, an optical fiber is cylindrical in shape, which plays a role as the cylindrical dielectric waveguide in the propagation of light. In the figure, the radii of the fiber core and cladding are represented as  $a$  and  $r$ , while  $n_1$  and  $n_2$  indicate the refractive indices of fiber core and cladding, respectively. The occurrence of any point within the fiber is expressed as the coordinate of  $(r, \phi, z)$ , where  $\phi$  represents the angle between the meridional plane containing the point and the reference meridional plane, whereas  $z$  is the depth of that particular point further into the core of the fiber.

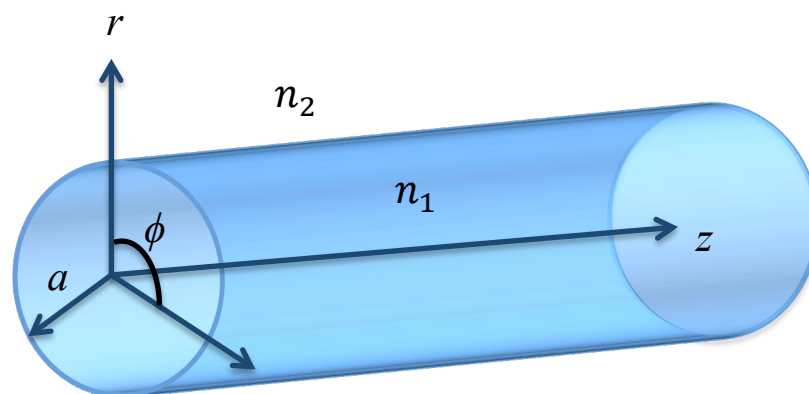


Figure 2.1 Schematic diagram of the cylindrical waveguide

By assuming the core of the fiber to be a perfectly source-free dielectric medium, the analysis of the nature of the fields that exist for the propagation of light within a fiber can be started from Maxwell's equation. Hence, both the electric and magnetic fields that occur in a source-free material can be expressed as:

$$\vec{\nabla} \cdot \vec{D} = 0 ; \quad (2.1)$$

$$\vec{\nabla} \cdot \vec{B} = 0 ; \quad (2.2)$$

$$\vec{\nabla} \times \vec{E} = -\frac{\partial \vec{B}}{\partial t} ; \quad (2.3)$$

$$\vec{\nabla} \times \vec{H} = \frac{\partial \vec{D}}{\partial t} ; \quad (2.4)$$

where  $\vec{B} = \mu \vec{H}$  is the magnetic flux density, while  $\vec{D} = \epsilon \vec{E}$  is the electric displacement vector. The analysis was then followed by performing curl on the equations to decouple both  $\vec{B}$  and  $\vec{D}$ . The equation then resulted as:

$$\vec{\nabla} \times \vec{\nabla} \times \vec{E} = -\mu \epsilon \frac{\partial^2 \vec{E}}{\partial t^2} \quad (2.5)$$

where  $\epsilon$  and  $\mu$  represent the permittivity and permeability, respectively. By applying the vector identities (Degree Two), equation (2.5) can then be expressed as:

$$\vec{\nabla}(\vec{\nabla} \cdot \vec{E}) - \nabla^2 \vec{E} = -\mu \epsilon \frac{\partial^2 \vec{E}}{\partial t^2} \quad (2.6)$$

The wave equations are then obtained:

$$\nabla^2 \vec{E} = \mu\varepsilon \frac{\partial^2 \vec{E}}{\partial t^2} ; \quad (2.7)$$

$$\nabla^2 \vec{H} = \mu\varepsilon \frac{\partial^2 \vec{H}}{\partial t^2} ; \quad (2.8)$$

A scalar quantity is then adopted to represent one of the two components in order to simplify the analysis and solve the wave equations above. Consequently, the wave equations are rewritten as below:

$$\nabla^2 \psi = \mu\varepsilon \frac{\partial^2 \psi}{\partial t^2} ; \quad (2.9)$$

$$\Rightarrow \frac{1}{r} \frac{\partial}{\partial r} \left( r \frac{\partial \psi}{\partial r} \right) + \frac{1}{r^2} \frac{\partial^2 \psi}{\partial \theta^2} + \frac{\partial^2 \psi}{\partial z^2} = \mu\varepsilon \frac{\partial^2 \psi}{\partial t^2} ; \quad (2.10)$$

Assuming the components are time-harmonic with an angular frequency of  $\omega$ , the following equation was obtained:

$$\psi = e^{j\omega t} \quad (2.11)$$

By applying the differentiation to the above equation, the equation below was obtained:

$$\frac{\partial \psi}{\partial t} = j\omega \psi ; \quad (2.12)$$

$$\frac{\partial^2 \psi}{\partial t^2} = -\omega^2 \psi ; \quad (2.13)$$

By substituting the differentiation equations (2.12) and (2.13) into equation (2.10):

$$\frac{\partial^2 \psi}{\partial r^2} + \frac{1}{r} \frac{\partial \psi}{\partial r} + \frac{1}{r^2} \frac{\partial^2 \psi}{\partial \phi^2} + \frac{\partial^2 \psi}{\partial z^2} = -\omega^2 \psi \mu \epsilon \quad (2.14)$$

Assuming the light is travelling along +z direction, the following Bessel's equation was then obtained by using the method of separation of variables.

$$\frac{\partial^2 R(r)}{\partial r^2} + \frac{1}{r} \frac{\partial R(r)}{\partial r} + \left\{ (\omega^2 \mu \epsilon - \beta^2) - \frac{v^2}{r^2} \right\} R(r) = 0 \quad (2.15)$$

Let  $q^2 = \omega^2 \mu \epsilon - \beta^2$ , radius  $r$  is smaller than  $a$ , and  $q^2 > 0$  in the fiber core. On the contrary, radius  $r$  is larger than  $a$ , and  $q^2 < 0$  for fiber cladding. The propagation constant can then be represented as:

$$\omega \sqrt{\mu \epsilon_2} < \beta < \omega \sqrt{\mu \epsilon_1} \quad (2.16)$$

Lastly, the solutions to the wave equations for both fiber core and fiber cladding can hence be represented as:

$$E_1 = AJ_v(ur) e^{jv\phi - j\beta z + j\omega t}; \quad r < a; \quad (2.17)$$

$$E_2 = BK_v(\omega r) e^{jv\phi - j\beta z + j\omega t}; \quad r > a \quad (2.18)$$

### 2.3 Basic Theory of the Long Period Fiber Grating

Basically, LPFG is produced by generating fiber gratings onto the surface of a single-mode fiber. Fiber gratings are created by producing axial periodic refractive index change on the optical fiber. Generally, the creation of a perturbation to the effective refractive index of the fiber guided mode can be described by:

$$\delta n_{eff}(z) = \overline{\delta n_{eff}}(z) \left\{ 1 + v \cos \left[ \frac{2\pi}{\Lambda} z + \phi(z) \right] \right\} \quad (2.19)$$

where  $\overline{\delta n_{eff}}(z)$  represents the direct current index change spatially averaged over a grating period, whereas  $v$  indicates the fringe visibility of the index change. On the other hand, the grating period and grating chirp of the LPFG are represented as  $\Lambda$  and  $\phi(z)$ , respectively.

Based on the coupling characteristic of the existed mode in the fiber grating, the fiber gratings can be divided into two types, *i.e.* fiber Bragg grating (FBG) and Long Period Fiber Grating. The main difference between FBG and LPFG is the length of grating period. The grating period of FBG is shorter than 100 micrometers, while LPFG has grating period of a few hundred micrometer. In terms of working principle, LPFG couples forward-propagating core mode to several cladding modes that are co-propagating in the similar direction. The coupling principle of a LPFG can be illustrated in Figure 2.2.

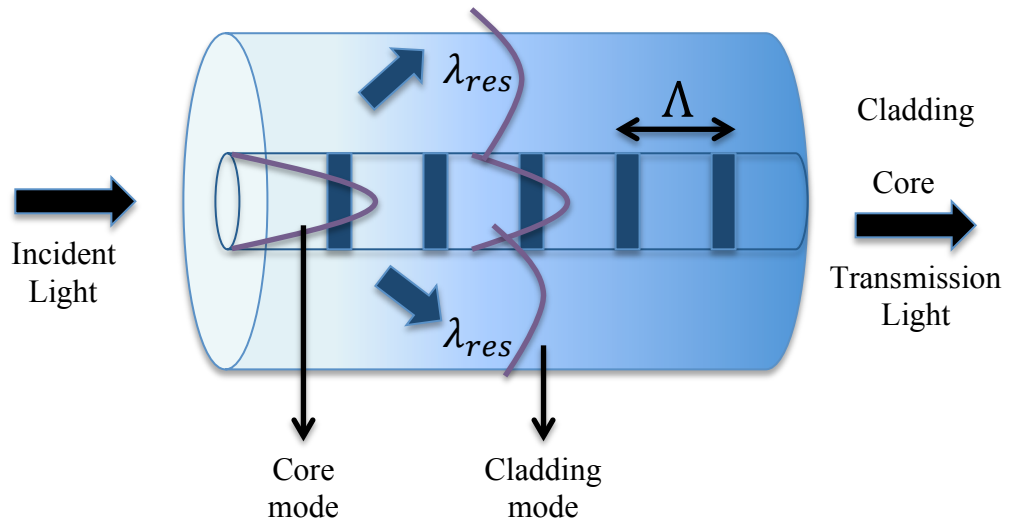


Figure 2.2 Coupling principle of a LPFG

As can be seen from the figure, LPFG can function as a broadband band rejection filter in transmission spectrum, which was the first application of LPFG being introduced. Hence, it is also called as the transmission grating. The resonant wavelength of the LPFG,  $\lambda_{res}$  will be discussed in later section.

## 2.4 Coupled Mode Theory

Coupled mode theory is a fundamental concept in optical waveguide technology that can be used to describe the energy of two waveguides that are in close proximity (Huang *et al.*, 1994). The basic principle of coupled mode theory is that energy can be transferred from one propagating mode to another as long as certain boundary conditions are satisfied (Huang *et al.*, 2009). However, the transfer of energy to another mode within a fiber core is prohibited in a single mode fiber. Due to this, the energy of core mode can

only be transferred by the coupling with cladding modes. In 1997, an analysis method was proposed to simplify the analysis of the mode coupling within a single mode fiber (Erdogan *et al.*). In the studies, the transverse component of the electric field is written as a superposition of the modes. Assuming the modes are in ideal waveguides and without the presence of grating perturbation, the superposition of the coupled mode can hence be represented as (Kaminow *et al.*, 2002):

$$\begin{aligned} \vec{E}_t(x, y, z, t) & \sum_j [A_j(z) \exp(i\beta_j z) + B_j(z) \exp(-i\beta_j z)] \cdot \\ \vec{e}_{jt}(x, y) & \exp(-i\omega t) \end{aligned} \quad (2.19)$$

where the coefficients of the amplitudes of  $j$ th modes travelling in  $+z$  and  $-z$  directions are expressed as  $A_j(z)$  and  $B_j(z)$ , respectively. In an ideal waveguide, there is no energy exchange between modes as the cladding modes are orthogonal. The coupling between modes will occur only when a dielectric perturbation is present. The changes in the forward and backward propagating amplitudes along the  $z$ -axis can be described by the general coupled-mode equation:

$$\frac{dA_j}{dz} = i \sum_k A_k (K_{kj}^t + K_{kj}^z) \exp[i(\beta_k - \beta_j)z] + i \sum_k B_k (K_{kj}^t - K_{kj}^z) \exp[-i(\beta_k + \beta_j)z] \quad (2.20)$$

$$\frac{dB_j}{dz} = -i \sum_k A_k (K_{kj}^t - K_{kj}^z) \exp[i(\beta_k + \beta_j)z] - i \sum_k B_k (K_{kj}^t + K_{kj}^z) \exp[-i(\beta_k - \beta_j)z] \quad (2.21)$$

where the transverse and longitudinal coupling coefficients between modes  $j$  and  $k$  are represented as  $K_{kj}^t$  and  $K_{kj}^z$ , respectively. In addition, the transverse coupling coefficient between both modes can be expressed as:

$$K_{kj}^t(z) = \frac{\omega}{4} \iint_{\infty} dx dy \Delta\epsilon(x, y, z) \vec{e}_{kt}(x, y) \cdot \vec{e}_{jt}^*(x, y) \quad (2.22)$$

where the perturbation towards the permittivity is represented as  $\Delta\epsilon$  and can be further expressed as:

$$\Delta\epsilon(x, y, z) = 2n_{eff}\delta n_{eff}(x, y, z) \quad (2.23)$$

On the other hand, the longitudinal coupling coefficient between modes  $j$  and  $k$  can be expressed similarly as the transverse coupling coefficient. However, the longitudinal coupling coefficient is usually neglected in the analysis as it is generally much smaller than the transverse coupling coefficient.

Generally, the formation of LPFG is mainly due to the creation of periodic gratings along the fiber core axis, which then induces a perturbation to the effective refractive index of the fiber guided core mode. The change in refractive index can be expressed as (Erdogan *et al.*, 1997):

$$\delta n_{eff}(z) = \overline{\delta n_{eff}}(z) \left\{ 1 + v \cos \left[ \frac{2\pi}{\Lambda} z + \phi(z) \right] \right\} \quad (2.24)$$

where  $\Lambda$  and  $v$  indicate the fiber grating period as well as the fringe visibility of the index change respectively. Furthermore,  $\overline{\delta n_{eff}}(z)$  represents the “dc”

index change spatially averaged over a grating period, whereas  $\phi(z)$  indicates the grating chirp.

By defining two new coefficients which represent the “dc” and “ac” coupling coefficients:

$$\sigma_{kj} = \frac{\omega n_{co}}{2} \overline{\delta n_{co}}(z) \iint_{core} dx dy \vec{e}_{kt}(x, y) \cdot \vec{e}_{jt}^*(x, y) \quad (2.25)$$

$$\kappa_{kj}(z) = \frac{v}{2} \sigma_{kj}(z) \quad (2.26)$$

The general coupling coefficient of the fiber can hence be represented as:

$$K_{kj}^t(z) = \sigma_{kj}(z) + 2\kappa_{kj}(z) \cos \left[ \frac{2\pi}{\Lambda} z + \phi(z) \right] \quad (2.27)$$

As mentioned in previous section, the mode couplings in a LPFG mainly occurs between the fundamental core mode and several propagating cladding modes. Specifically, the forward-propagating mode of amplitude  $A_1(z)$  is strongly coupled to co-propagating mode with amplitude  $A_2(z)$ . By only involving the amplitudes of both modes and making the synchronous approximation, the general coupled-mode equations (2.20) and (2.21) can be simplified and expressed as:

$$\frac{dR}{dz} = i\hat{\sigma}R(z) + i\kappa S(z) \quad (2.28)$$

$$\frac{dS}{dz} = -i\hat{\sigma}S(z) + i\kappa^* R(z) \quad (2.29)$$

where the new amplitudes are indicated as R and S:

$$R(z) = A_1 \exp \left[ -i(\sigma_{11} + \sigma_{22}) \frac{z}{2} \right] \exp \left( i\delta z - \frac{\phi}{2} \right) \quad (2.30)$$

$$S(z) = A_2 \exp \left[ -i(\sigma_{11} + \sigma_{22}) \frac{z}{2} \right] \exp \left( -i\delta z + \frac{\phi}{2} \right) \quad (2.31)$$

Furthermore, the “ac” coupling coefficient is indicated as  $\kappa = \kappa_{21} = \kappa_{12}^*$ , whereas the “dc” coupling coefficient is represented as  $\sigma_{11}$  and  $\sigma_{22}$  as discussed earlier in equation (2.25) and (2.26). The general “dc” coupling coefficient,  $\hat{\delta}$  can then be defined as:

$$\hat{\delta} = \delta + \frac{\sigma_{11} - \sigma_{22}}{2} - \frac{1}{2} \frac{d\phi}{dz} \quad (2.32)$$

The detuning is assumed to be constant along the fiber z-axis:

$$\delta = \frac{1}{2} (\beta_1 - \beta_2) - \frac{\pi}{\Lambda} = \pi \Delta n_{eff} \left[ \frac{1}{\lambda} - \frac{1}{\lambda_D} \right] \quad (2.33)$$

where  $\lambda_D = \Delta n_{eff} \Lambda$ . Both coupling coefficients are constants for a uniform forward-propagating coupled grating.

## 2.5 Phase Matching Condition

LPFG can be defined as a core-cladding coupling device formed by a periodic modulation of the refractive index of the fiber core. Generally, the period of the gratings formation in LPFG is within the range from 100  $\mu\text{m}$  to

1000  $\mu\text{m}$  (1 mm). To further the analysis on phase matching condition of LPFG, the grating formed on the fiber can be treated as an optical diffraction grating. An optical diffraction grating can be defined as the splitting or diffraction of lights into different modes travelling in different directions which is mainly caused by the periodic modulation formed on the optical fiber. By applying diffraction grating equation, the effect of the LPFG grating upon a light wave incident on the grating at an angle  $\theta_1$  can hence be represented as the equation below:

$$n \sin \theta_2 = n \sin \theta_1 + m \frac{\lambda}{\Lambda} \quad (2.34)$$

where  $m$  and  $\theta_2$  indicate the diffraction order and angle of the diffracted wave, respectively. The order of diffraction that usually dominates in fiber grating is first-order, which is represented as  $m = -1$ . On the other hand, the propagation constant of the travelling mode can be represented as:

$$\beta = \left(\frac{2\pi}{\lambda}\right) n_{eff} \quad (2.35)$$

By substituting the effective refractive index seen by the mode,  $n_{eff} = n \sin \theta$  into equation (2.34), the equation can then be rewritten as:

$$\beta_2 = \beta_1 + m \frac{2\pi}{\Lambda} \quad (2.36)$$

where the propagation constants in core and cladding modes are represented as  $\beta_1$  and  $\beta_2$ , respectively. In LPFG, the mode propagation constant of cladding will be larger than zero,  $\beta_2 > 0$  when the light coupled from fundamental core mode is travelling in a similar direction as the core mode. According to this condition, the resonant wavelength of the LPFG can be expressed as equation (2.37).

$$\lambda_{res} = (n_{eff}^{co} - n_{eff}^{cl,m})\Lambda \quad (2.37)$$

In the equation, the resonant wavelength of LPFG corresponding to  $m^{\text{th}}$  cladding mode is indicated by  $\lambda_{res}$ , whereas  $n_{eff}^{co}$  and  $n_{eff}^{cl,m}$  are the effective refractive indices of both core and cladding modes. As observed from the phase matching condition equation, the factors that can lead to the shifting of the resonant wavelength are the differential in effective index between core and cladding modes as well as the changes in fiber grating period. In summary, the basic principle of LPFG is mainly induced by the coupling between the fundamental core mode and several propagating cladding modes (James *et al.*, 2003; Lazaro *et al.*, 2009). Once the light is coupled into cladding modes, it will lead to the decay of light due to scattering loss. As a result, attenuation bands centered at wavelengths that satisfy the phase-matching condition are formed and observed at the output (Vengsarkar *et al.*, 1996).

The light experiences a high loss when it is travelling within cladding modes which then produces loss bands at resonance wavelengths in the

transmission spectrum. An analysis was conducted in 1999 to investigate the loss bands and it was discovered that the minimum transmission of the loss bands can be represented as (Kashyap, 1999):

$$T_m = 1 - \sin^2(\kappa_m L) \quad (2.38)$$

where  $L$  represents the length of the LPFG whereas  $\kappa_i$  indicates the coupling coefficient of the  $m^{\text{th}}$  cladding modes. As can be predicted from the equation, the minimum transmission of the loss bands is mainly dependent on the coupling coefficient of cladding modes. There are a few factors that determine the coupling coefficient of modes, including the integral overlap of core and cladding modes as well as the amplitude of the periodic modulation of the mode propagation constants (Erdogan *et al.*, 1997).

Moreover, the radius of the fiber cladding determines the number of cladding modes available. In a single mode fiber, the radius of cladding is much larger if compared to the fiber core, therefore a large number of cladding modes can be supported. According to the theoretical analysis, efficient coupling will occur only between modes with a large overlap integral, which means that coupling is possible only between core and cladding modes that possess similar electric field profiles. In LPFG, coupling is often observed between the core and cladding with odd number of modes as the electric field of modes with an odd number is peak within the core. On the contrary, coupling is limited in modes with an even number due to the low electric field amplitude within the fiber core (Erdogan *et al.*, 1999).

## 2.6 Development of Fabrication Techniques of LPFG

As mentioned in the section of coupled-mode theory, the formation of LPFG is mainly based on the creation of periodic perturbations along the structure of the optical fiber which facilitates the coupling of light from the guided core mode to the forward propagating cladding modes. The perturbation is induced by utilizing either refractive index modification of the core and cladding modes or the physical deformation mechanism. Initially, LPFG was first introduced by Poole *et al.* in 1994 where the LPFG was demonstrated as a device for mode conversion purposes (Poole *et al.*, 1994). The presented LPFG was fabricated by using a two-step process, which included the process of periodic cuts of the fiber surface by a focused CO<sub>2</sub> laser radiation, followed by the annealing of the fiber structure periodically by using electric arc discharged from the fusion splicer. In 1996, LPFG was again fabricated with different technique which involved the usage of ultra-violet (UV) radiation to induce a periodic index change of the fiber core (Vengsarkar *et al.*, 1996). The concept of the LPFG produced was investigated thoroughly and the application of LPFG was further demonstrated as a band-rejection filter. UV-based fabrication technique was one of the widely utilized methods in fabricating LPFGs. However, it was discovered that this well-established technique might have some shortcomings. For example, the requirement of a large number of photomasks as well as the complicated and time-consuming pre-treatment procedures have become a concern. The optical fiber used in UV radiation fabrication technique was required to be photosensitive. Also, the challenge faced in controlling the filter parameters such as the grating period

is another limitations (Hwang *et al.*, 1999, Tan *et al.*, 2015). Due to these reasons, different fabrication techniques such as femtosecond laser exposure, ion beam implantation, CO<sub>2</sub> laser irradiation as well as electric arc discharge techniques had been proposed to overcome some of the limitations found in the UV radiation method (Kondo *et al.*, 1999; Fujimaki *et al.*, 2000; Davis *et al.*, 1998; Georges *et al.*, 2002). For instance, the electric arc discharge and CO<sub>2</sub> laser irradiation fabrication technique do not require extra treatment procedures as in the UV radiation technique (Tan *et al.*, 2015). Among these fabrication techniques, electric arc discharge technique offered higher flexibility and simpler fabrication processes (Kim *et al.*, 2002). Moreover, it can be applied to various types of optical fibers including single-mode type without the requirement of any prior photosensitization procedures (Humbert *et al.*, 2002). Apart from this, it allows the adjustment of the grating parameters to produce LPFG with the desired resonant wavelength and characteristics. It had been proven that the LPFG produced with the electric arc discharge technique can withstand temperature as high as 1000 °C.

## **2.7 Sensitivity of LPFG towards External Influences**

The sensitivity of LPFG towards external influences is one of the distinct characteristics of this fiber sensor which drives it to become a favourite candidate to be used widely as a sensing device. In the early stage of research after the introduction of LPFG, it had been demonstrated that LPFG is sensitive to different external parameters such as temperature, refractive index as well as strain (Lazaro *et al.*, 2009; Allsop *et al.*, 2006; Huang *et al.*,

2013). The response of LPFG towards such influences can be observed by either the shift in the resonant wavelength, or the variation in its minimum transmission power. It has been reported that the sensitivity of LPFG will increase in accordance to the increment in the fiber coupled cladding mode order. The order of the cladding mode can be increased by altering either the effective refractive indices, or the grating period of the LPFG (Gouveia *et al.*, 2013). The sensing mechanism of LPFG is based on the phase matching condition which results in a coupling wavelength  $\lambda$ , that can be expressed as:

$$\lambda = (\delta n_{eff})\Lambda \quad (2.39)$$

where  $\delta n_{eff}$  indicates the difference in the effective refractive indices of core and cladding mode,  $n_{eff}^{co} - n_{eff}^{cl,m}$ . On the other hand,  $\Lambda$  represents the grating period LPFG.

Generally, the sensitivity of LPFG can be expressed as:

$$\frac{\partial \lambda}{\partial X} = \gamma \left( \frac{\partial \Lambda}{\partial X} \delta n_{eff} + \frac{\partial \delta n_{eff}}{\partial n} \frac{\partial n}{\partial X} \Lambda \right) \quad (2.40)$$

where the general sensing parameter is represented as  $\gamma$ , and can be expressed as:

$$\gamma = \frac{1}{1 - \frac{d\delta n_{eff}}{d\lambda} \Lambda} = \frac{1}{\delta n_{eff}} \frac{d\lambda}{d\Lambda} \quad (2.41)$$

### 2.7.1 Temperature Sensitivity

Over the years, the thermal behaviour of the LPFG gratings had been investigated (Humbert *et al.*, 2002; Rego *et al.*, 2004; Yamamoto *et al.*, 2010). The effect of changes in temperature on LPFG was mainly observed in the shifting of the resonant wavelength. This temperature dependence characteristic of LPFGs enabled them to become an important device in temperature sensing applications.

As mentioned earlier, the resonant wavelength of LPFG was determined by the phase-matching condition. Hence, based on the phase-matching condition equation (2.37), the analytical expression of the LPFG temperature sensitivity can be derived by applying the chain rule of differentiation, thus:

$$\frac{d\lambda_{res}}{dT} = \frac{\Lambda \left[ \frac{\delta n_{eff}^{co}}{\partial T} - \frac{\delta n_{eff}^{cl,m}}{\partial T} \right] + \frac{\lambda d\Lambda}{\Lambda dT}}{1 - \Lambda \left[ \frac{\partial n_{eff}^{co}}{\partial \lambda} - \frac{\partial n_{eff}^{cl,m}}{\partial \lambda} \right]} \quad (2.42)$$

where  $\frac{\lambda}{\Lambda} \frac{d\Lambda}{dT}$  represents the thermal expansion coefficients of the fiber. According to the expression obtained, it had been proven that LPFG was inherently sensitive to the variations in the surrounding temperature. Since LPFG is made up of silica glass and that the expansion coefficient of glass is small, therefore it can be neglected. Thus, as observed from the equation, the

LPFG sensitivity towards temperature is mainly induced by two factors. The first is the temperature sensitivity of the refractive indices of both core and cladding modes. The second is the waveguide properties of the fiber that contributes to the temperature sensitivity of LPFG (Dianov *et al.*, 1996). Higher temperature sensitivity of LPFG can be achieved by decreasing the waveguide term in the equation. This can be achieved by either decrement in the diameter of cladding or coating of extra outer layer of material with lower refractive index (Du *et al.*, 2017; Smietana *et al.*, 2011).

### 2.7.2 Refractive Index Sensitivity

The sensitivity of LPFGs towards the external index is one of the most significant characteristics that had inspired most of the research regarding which LPFGs were used as sensors to detect different elements. The investigations of LPFG response towards external index had begun since 1998 (Patrick *et al.*) and the influence of the external index on the cladding of LPFG was analyzed in 1999 (Bhatia, 1999). Again, by rearranging the phase matching condition equation, its sensitivity towards the external RI can be represented as:

$$\frac{d\lambda_{res}}{dn_3} = \frac{d\lambda}{dn_{cl,m}} \frac{dn_{cl,m}}{dn_3} \quad (2.43)$$

where  $n_3$  indicates the refractive index of the surrounding medium whereas the shifting of the resonant wavelength of LPFG is expressed as  $d\lambda_{res}$ . On the other hand,  $n_{cl,m}$  represents the effective refractive index of  $m^{\text{th}}$  cladding

mode. From the equation, it is shown that the propagation constant of LPFG cladding mode depends not only on the fiber parameters, but also on the surrounding refractive index. Furthermore, the term of  $\frac{dn_{cl,m}}{dn_3}$  will be different for each cladding mode present within LPFG. Therefore, it can be concluded that the response of LPFG is highly affected by the order of the coupled cladding mode as the refractive index of external medium varies (Yin *et al.*, 2012). The interaction between cladding modes and external medium is prompted by the penetration of evanescent fields of these modes beyond the cladding surround interface, hence the response of LPFG will be affected by the difference in external index (Bhatia *et al.*, 1999).

According to research conducted, the increment in the external RI will lead to a larger shift of LPFG resonant notch. When the refractive index of external medium is lower than the cladding index ( $n_3 < n_2$ ), the sensitivity of LPFG towards the increasing external index can be observed as the shifting of LPFG attenuation band towards a shorter wavelength. Also, the peak depth of the attenuation band will decrease in accordance to higher external index (Silva *et al.*, 2012). The latter effect is due to the decrease in overlap integral between core and cladding modes, which leads to successively smaller coupling coefficients. As the external index approaches the index of cladding ( $n_3 \cong n_2$ ), the resonant notch of LPFG is close to disappearance. This is because the cladding has an infinitely large radius and becomes an infinite medium. As a result, the discrete cladding modes are no longer guided along the LPFG as total internal reflection does not occur at the cladding boundary anymore. In this case, the cladding modes are converted into radiation modes

and light is lost through this continuum of radiation modes (Khadri *et al.*, 2012). The sensitivity of LPFG towards external RI changes is found to be highest in this region where index matching occurs between the cladding and surrounding medium (Villar *et al.*, 2005). As the refractive index of external medium exceeds cladding ( $n_3 > n_2$ ), leaky modes are present in the cladding. The resonant notch of LPFG re-appears at a higher wavelength and the shifting of the resonance wavelength becomes very small when the surrounding refractive index changes. Instead, a variation of the depth of the resonant band is expected (Stegall *et al.*, 1999; Akki *et al.*, 2013).

### 2.7.3 Strain Sensitivity

Investigations have been conducted to prove that LPFG is also sensitive to strain because the axial strain,  $\varepsilon$  is one of the essential features of LPFG. By expanding and rearranging the phase matching condition, the sensitivity of LPFG towards strain can be derived as (James *et al.*, 2003):

$$\frac{d\lambda_{res}}{d\varepsilon} = \frac{d\lambda}{d(\delta n_{eff})} \left( \frac{dn_{eff}^{co}}{d\varepsilon} - \frac{dn_{eff}^{cl}}{d\varepsilon} \right) + \Lambda \frac{d\lambda}{d\Lambda} \quad (2.44)$$

where  $\varepsilon$  represents the axial strain of LPFG. As observed from the equation, the resonant wavelength of LPFG can be influenced by both material and waveguide effects. The material effect is mainly induced by a variation in the differential refractive index of core and cladding. On the contrary, the waveguide effect is mainly related to the function of the local slope,  $\frac{d\lambda}{d\Lambda}$ , i.e. the

grating period of LPFG. Both material and waveguide contributions can have either polarity, and relies either on the period of the grating or the order of the cladding mode.

## **2.8 Modifications of LPFG Sensitivity**

Since the discovery of the sensitivity of LPFG, numerous research works were conducted to modify and enhance its sensitivity. The idea of modifying their sensitivity as mainly inspired by the challenges induced in some of the sensing applications, where the wavelength shift of conventional LPFG was found to be relatively small. Different enhancement techniques were investigated so that the sensitivity of LPFG can be adjusted to suit different sensing applications. The bending and etching of the fiber cladding as well as the optimization of the grating period are examples of common sensitivity modification techniques that have been proposed for the purpose of enhancing LPFG sensitivity.

### **2.8.1 Bending**

The effect of bending on the performance of LPFG was first investigated in 2005 (Frazao *et al.*). Observations showed that the transmission loss of the resonant wavelength increased in accordance to the increment in the curvature of the fiber bending. In other words, the amount of power loss was dependent on the bend radius, *i.e.* the lower the bend radius, the higher the transmission loss. By applying bending effect, the flat and smooth surface of

the LPFG sensing zone no longer occurred, causing the waveguide to become distorted and affected the surface scattering loss. As a result, the transmission loss of the resonant wavelength was affected (Zhang *et al.*, 2009). In 2014, the influence of bending effects on the sensitivity of LPFG towards external RI was further experimented (Szymańska *et al.*, 2014). The results showed that the LPFG with applied bending was more sensitive towards external RI if compared to normal LPFG.

### **2.8.2 Etching**

Etching was one of the approaches that was demonstrated to remarkably improve the sensitivity of LPFG. The etching of the LPFG cladding was utilised as a post-fabrication method with the purpose to reposition the resonant notch of LPFG, therefore enhancing its sensitivity towards the external RI (Zulkifly *et al.*, 2010; Mysliwiec *et al.*, 2013). An analysis of the effect of cladding etching on the LPFG resonant wavelength was conducted in 2010 (Zulkifly *et al.*). In the experiment, the LPFG fabricated was etched by buffered hydrofluoric (HF) solution and it was observed that the resonant wavelength of LPFG had shifted to a longer wavelength and the notch depth of the resonant wavelength had increased after the etching process. By etching the fiber, the diameter of cladding was reduced, causing the differential effective refractive index between core and cladding modes to increase. According to the phase matching condition, an increment in the effective refractive index difference caused the resonant wavelength to shift to a longer wavelength, thus being more evident for the higher order

cladding modes (Vasiliev *et al.*, 1996). In 2000, the effect of cladding etching on the sensitivity of LPFG was investigated as well. Results showed that the wavelength shift of the etched LPFG was larger if compared with non-etched LPFG due to the existence of higher order cladding modes in the etched LPFG (Chiang *et al.*).

### **2.8.3 Grating Period Optimization**

In the phase matching condition equation shown in equation 2.37, it was shown that the resonant wavelength can be affected by two factors, *i.e.* the differential in effective refractive indices between the core and cladding mode as well as the grating length. The resonant wavelength of a LPFG is highly dependent on the period of the gratings drawn within the fiber. In other words, the sensitivity of a LPFG can be affected by the grating period of the LPFG. In one of the research conducted by Patrick *et al.*, it was observed that by decreasing the grating period, the order of the coupled cladding mode is increased. Therefore higher sensitivity can be achieved with the higher order of coupled cladding mode. With this findings, some research have been conducted in the past to investigate the influence of the grating period on the sensitivity of LPFG towards external perturbations. One of the example where the effect of grating period was investigate was conducted in 2012, where the sensitivities of LPFGs with different grating periods were compared. Results showed that the sensitivity of the LPFG with shorter period has higher sensitivity towards the external refractive index.

## 2.9 Influence of Coupled Cladding Mode on the sensitivity of LPFG

As discussed in previous section, it is known that the LPFG is sensitive to the changes in physical parameters like temperature, bending as well as strain. The sensitivity characteristics of LPFGs were investigated by several authors, in which it was then realised that the increase in the order of the coupled cladding mode will lead to the increment in the LPFG sensitivity. Also, research has been conducted to show that the order of coupled cladding modes can be increased by decreasing the grating period of LPFG (Gouveia *et al.*, 2013). However, this has become one of the drawbacks in modifying the sensitivity of arc-induced LPFG due to the width of the arc, which produces the overlapping of the refractive index modulations when the period is reduced to too short.

## 2.10 LPFGs in the Turning Point

As discussed in previous section, it is known that the sensitivity of LPFG depends on the order of cladding modes. Nonetheless, there will be a point where the sensitivity of the LPFG reaches to its maximum, which is called as the turning point of the LPFG. It was reported that, at each turning point,  $|d\lambda_{res}/d\lambda|$  will be close to infinity,  $\infty$ . Hence, by applying this into Equation 2.41, the sensing parameter of LPFG,  $\gamma$  will be  $\infty$  as well. Therefore, the turning point operation of the LPFG determines the condition for maximum sensitivity. As a result, LPFG can be designed to exhibit high

sensitivity by selecting fabrication parameters or sensitization method that can push the LPFG towards turning operation.

## **2.11 Applications of LPFG**

In Section 2.5, it was discussed that the sensitivity of LPFG towards external parameters such as strain and refractive index was one of the important properties of LPFG. Therefore, LPFG had attracted increasing research interests and had been adopted as an optical fiber sensor in a variety of applications over the years. Some of the applications that were demonstrated included pressure sensing, refractive index sensing and bio- or chemical detection (Smietana *et al.*, 2011; Smietana *et al.*, 2013; Lee *et al.*, 2001).

### **2.11.1 Pressure Sensor**

One of the sensing applications of LPFG that was proposed was the pressure sensor. It was reported that the resonant wavelength of LPFG shifted linearly when pressure was applied to the fiber. According to the investigation done in 2007, LPFG fabricated using arc discharge technique was used to conduct a direct measurement of hydrostatic pressure up to 450 bars (Bock *et al.*). The findings from the research showed that the resonant notch of the LPFG shifted linearly to a longer wavelength as the applied pressure increased. The presence of pressure along the fiber radial direction caused the diameter of the fiber cladding to decrease, but the diameter of fiber core was not greatly

affected because its diameter was much smaller if compared to the fiber cladding. The decrement in the cladding diameter led to the diminishing of the effective refractive index of cladding modes. According to the phase matching condition, the changes in the effective index shifted the resonant wavelength of the LPFG. On the other hand, another investigation was conducted in 2010 for pressure sensing using LPFG. Similar findings were obtained in the experiment, where the resonant notch of LPFG shifted to a longer wavelength when the pressure increased from 1 bar up to 240 bars (Smietana *et al.*, 2010).

### **2.11.2 Refractive Index Sensor**

LPFG had been widely demonstrated as a refractometer since its sensitivity towards external index was discovered. One of the investigations was conducted in 2010, in which the LPFG adopted was fabricated by using a fusion splicer, with grating period of 500  $\mu\text{m}$  and a total of 40 gratings (Rios *et al.*). The LPFG was then sensitized by the process of etching with hydrofluoric acid solution before it was experimented with different refractive indices. The results of the sensitized LPFG was then compared with non-etched LPFG. It was discovered that the sensitivity of the etched LPFG was higher than that of non-etched LPFG, due to the existence of higher order cladding modes in the etched LPFG. The coupling between core mode to higher order cladding modes led to higher sensitivity towards the refractive index. Hence, it was then concluded that the reduction in diameter of fiber cladding can lead to higher sensitivity of LPFG towards the external RI.

Another investigation that employed LPFG as a refractive index sensor was conducted in 2013 by Smietana *et. al.*, in which the arc-induced LPFG was tested with refractive indices ranging from 1.33 to 1.40. A thin nano-thick layer of silicon nitride was coated onto the surface of LPFG to tune its sensitivity towards the external RI. Results showed that the resonance wavelength of LPFG encountered blue-shift to shorter wavelength when the external index increased from 1.33 to 1.40. The performance of the coated LPFG was then compared with uncoated LPFG and the comparison concluded that the deposition of coating strongly enlarged the wavelength shift of the LPFG in response to the changes in external RI.

### **2.11.3 Biosensor**

Due to the sensitivity dependence of the LPFG resonance wavelength towards the changes in the external RI, LPFG had been widely used as a biological sensor in different fields, especially in the medical industry. For instance, Chan *et al.* demonstrated the potential of LPFG as a dengue detection device in 2010. Observations showed that the wavelength shift of LPFG was greater in the serum of a positive dengue patient than the serum extracted from a healthy person. Due to the presence of dengue virus, antibody was produced by the human body to control the spreading of the virus in the body. Hence, the refractive index of the serum extracted from a positive dengue patient was higher if compared to a healthy serum due to the presence of the antibody. As a result, the response of LPFG was more prominent in the serum of a positive dengue patient.

On the other hand, LPFG was proposed to be used as an immunosensor in 2010 (Wang *et al.*). The purpose of the research was to measure the interaction between an immobilized antibody, Immunoglobulin G (IgG) and the corresponding antigen. The LPFG was pre-coated with a layer of nanothick polymer before being immersed in IgG solution, followed by a binding block solution. Investigations showed that LPFG was able to detect the bind between the antigen and antibody.

## **2.12 Advantages of LPFG as a Sensor**

As emphasized, LPFGs have become a favourite device for different sensing applications due to the variety of advantages that they offer. The first advantage is that they are immune to electromagnetic interference (EMI) (Medlock *et al.*, 1989). Unlike some other sensors which are susceptible to EMI, the immunity of fiber sensor is due to the fact that fiber does not conduct electricity. Instead, they used light to transmit signals, thus no magnetic field is produced. Also, fiber sensors provide remote sensing ability, in which the signal transmission loss is significantly lower than other sensors. As reported in 2017, LPFG can be deployed in the real environment that is kilometres away and no electricity sources are needed at the sensing site (Yong *et al.*). Furthermore, LPFGs are small and lightweight. As we all know, optical fibers are intrinsically small-sized, hence providing higher convenience if it is required to be embedded or installed into compact structures. Moreover, LPFGs have been proven to be able to withstand certain extreme conditions such as high temperatures and pressure as well as corrosive environments

(Huang *et al.*, 2014). Hence, LPFGs are suitable to be used as a sensor in the real environment. Most importantly, LPFG is sensitive to small perturbations in the surrounding near its surface, and its surface can be modified so that it can respond to different targeted elements. This is the main reason why LPFG has become a commonly used sensor for research purposes. Lastly, LPFGs allow multiple sensing over multiple points. In other words, LPFGs support simultaneous sensing of more than one measurand with the help of the multiplexing technique (Lin *et al.*, 2009).

### **2.13 Summary**

In this chapter, the basic theory of LPFG was discussed and presented in detail. The description of LPFG concept started with the wave model of light, coupled mode theory and phase matching condition. The content was then followed by the development of different fabrication techniques for producing LPFG.

The sensitivity of LPFG towards different external parameters such as temperature, refractive index and strain was discussed in this chapter as well. Furthermore, some of the enhancement methods that can be employed to improve the sensitivity and performance of LPFG have been discussed. Last but not least, some of the advantages and applications of LPFG that have been demonstrated over the years have been reviewed in the last section of this chapter.

## **CHAPTER 3**

### **FABRICATION OF ARC-INDUCED LPFG**

#### **3.1 Introduction**

The research proposed in this thesis is divided into four phases. In this chapter, the first phase of the research is presented, which includes the descriptions and details about the fabrication of LPFG. Among the proposed fabrication techniques, electric arc discharge was chosen as the technique to produce LPFGs in this research. The chapter begins with the discussion of the advantages and disadvantages of the electric arc discharge fabrication technique. Also, the history of arc-induced LPFG will be briefly discussed, followed by the details of the gratings formation mechanisms and fabrication setup of this research. Finally, the properties and performances of the LPFG fabricated will be investigated and observed by conducting experiments with sucrose solutions and refractive index matching oils.

##### **3.1.1 Advantages of Arc-Induced LPFG**

Among the techniques that have been demonstrated for fabricating LPFGs in the past, the electric arc discharge technique is probably the one that offers more advantages than the others. First and foremost, the simplicity of this technique is the first reason that makes it a commonly used and popular

fabrication technique. In the fabrication setup of the electric arc discharge technique, it does not involve complicated procedures as in other fabrication techniques (Kim *et al.*, 2002; Humbert *et al.*, 2002). For instance, the pre-treatment process and the large number of photomasks that are required in the UV-based fabrication technique are not needed in the electric arc discharge technique. This leads to a lower fabrication cost. On the other hand, the gratings produced by this technique possess high thermal stability due to the formation mechanisms of arc discharge technique, which rely mainly on thermal effects caused by the electrodes (Ayala *et al.*, 2012). In other words, the LPFG produced by the electric arc discharge technique offered the best performances to be used as temperature sensor due to its high temperature stability. It has been proven that LPFGs produced by arc discharge technique can withstand temperatures as high as 800 °C, even up to 1000 °C, without significant degradation in their properties and performances (Hwang *et al.*, Rego *et al.*, 2009). This advantage helps to overcome the limitation found in other techniques such as UV radiation, where the LPFG transmission starts to experience decay at few hundred of degrees Celsius (Dianov *et al.*, 1997). Furthermore, this fabrication method offers higher flexibility because it allows the formation of gratings on various kinds of fibers, which includes single-mode, photonic crystal, non-photosensitive and so on (Rego *et al.*, 2016). Also, the fabrication of arc-induced LPFG using the electric arc discharge technique does not require extra time-consuming processes such as post-fabrication annealing or hydrogenation. Due to the advantages offered, the arc discharge technique became a widely used method in fabricating LPFG for different applications.

### 3.1.2 Disadvantages of Arc-Induced LPFG

On the contrary, there are a few drawbacks that can be observed from the electric arc discharge technique. The asymmetric changes caused by the electric arc that may vary in every single discharge from the electrodes has led to one of the main drawbacks of arc-induced LPFG, *i.e.* lacking duplicability and reproducibility (Rego *et al.*, 2006). The coupling strength of the LPFG produced may be significantly influenced by the inconsistency caused by the electric arc discharge. Moreover, a slight misalignment of the fiber in between both electrodes caused by the movement of translation stage after each discharge has become one of the factors which limits the duplicability of the LPFG. In addition, another limitation found with this fabrication technique is that it is difficult to achieve shortest grating period on the fiber. This limitation is mainly induced by the width of electric arc produced. If the grating period is too small, overlapping of the refractive index modulations between gratings may occur as each grating is too close to one another (Smietana *et al.*, 2011). As mentioned earlier, the grating period is one of the parameters which will affect the resonant wavelength and sensitivity of LPFG according to the phase matching condition. Hence, investigations and hard work have been proceeded in recent years to determine the shortest grating period that can be achieved despite the challenges induced by the overlap effect of the adjacent arc discharges (Smietana *et al.*, 2013; Colaco *et al.*, 2015). It was analyzed that a grating period of around 200  $\mu\text{m}$  and below is required to allow LPFG to achieve highest sensitivity.

### 3.1.3 History of Arc-Induced LPFG

Arc-induced LPFG fabricated by the electric arc discharge technique was first introduced in 1994, where a two-step point-by-point fabricating process was implemented (Poole *et al.*, 1994). The first step of the process involved the exposure of fiber surface to a focused CO<sub>2</sub> laser beam to produce a v-groove cut on the surface. The v-groove cut created led to the periodic modulations of the fiber. The second step of the fabrication process required a fusion splicer to produce an electric arc, which was then applied to each v-groove cut created previously to heat them and transform the fiber surface into sinusoidal deformation.

In 1997, a simpler fabrication methodology which required only either one of the two steps was proposed, where a step-index nitrogen-doped silica fiber was used in the experiment (Dianov *et al.*). Either the CO<sub>2</sub> laser beam or the electric arc produced by the fusion splicer was used to anneal the fiber to a point where the diffusion of nitrogen occurred efficiently and produced a periodic perturbation on the fiber. This proposed methodology allows the fabrication of LPFG with a grating period of more than 200  $\mu\text{m}$ . A year later, this technique was applied to pure-silica-core fiber as well, where the gratings were induced by the electric arc discharge technique (Enomoto *et al.*, 1998).

In the same year, the methodology and setup of arc discharge technique had been further modified (Kosinski *et al.*, 1998). A one-step fabrication process was introduced with the addition of a pair of electrodes to

produce electric arcs. On the other hand, a motorized stage which enabled the translation of fiber between both electrodes was introduced to the fabrication setup to replace the fiber holding mechanism in a conventional fusion splicer. Three different kinds of gratings including the physical deformation gratings (PDGs), index modulated gratings (IMGs) as well as mode-field modified gratings (MFGs) were successfully fabricated using this setup, where the spectra of IMGs were sharper than standard UV-induced LPFGs. Moreover, a new fabrication methodology which focus on periodic microbends technique was demonstrated in 1999 (Hwang *et al.*, 1999). In order to induce a lateral stress on the fiber, one of the fiber holders was placed in an orthogonal direction to the fiber axis so that the fiber was slightly deformed and a microbend was created when the fiber was heated by electric arc. The electrodes were then moved along the fiber axis with a distance similar to the predefined grating period and the fiber was again heated to produce the next grating. Without the translation of both the fiber holders, the misalignment of fiber in between both electrodes caused by the movement of fiber can be avoided as well.

Three years later, improvement was done to the fabrication setup demonstrated by Hwang *et al.* (Kim *et al.*, 2002). Similar to the previously discussed method, this proposed fabrication system consisted the use of the translation stage to move the fiber in between the electrodes. However, the attachment of one end of the fiber to an extra weight was the main difference between this proposed method and the traditional arc discharge technique. The main purpose in introducing the weight to one end of the fiber was to create a

constant axial to the fiber. The longitudinal tension caused by the extra weight attached caused the fiber to become merely tapered as the fiber was annealed by the electric arc.

Most of the fabrication methodology discussed earlier focused on the change of the fiber diameter due to physical deformation. In 2008, another arc discharge method was proposed where the fiber diameter was not altered, but the fiber gratings were induced due to the direct change of the fiber glass structure (Chávez *et al.*, 2008). Instead of producing gratings by thinning or tapering of fiber, hot push process was introduced in this fabrication setup to heat the fiber up to a softening point and was repeated at the same spot until the fattening of fiber occurred with an achieved desired diameter. Then, the fiber was moved in parallel with the fiber axis to the next gratings point to repeat the hot push process. The benefit of this setup was that it only required a fusion splicer with both light source and OSA but did not required extra equipment such as translation stages.

Also, another fabrication setup was demonstrated by Yin *et al* (2014). The fabrication process proposed required the use of a commercial fusion splicer, a pair of motors and electrodes, fiber holders as well as a SWEEP motor. Similarly, the fiber was fixed by both fiber holders that were placed on the translation stage before the fabrication process started. During the fabrication process, both motors were meant to drive the fiber holders so that both ends of the fiber were stretched synchronously. One of the motors was used for the pulling of the fiber and the other was meant for the feeding of the

fiber after each arc discharge. On the other hand, the SWEEP motor was used to control the translation stage in moving the fiber with a maximum moving distance of 18 mm along the fiber axis after every discharge. In this setup, the tapering ratio was controlled by the ratio of pulling and feeding of both motors. There was no external weight needed due to the presence of both motors. Hence, the issue of misalignment of fiber and the influence of axial tension on the fiber tapers can be overcome.

Referring to all the fabrication processes discussed earlier, most of them required the use of a fusion splicer to produce the electric arc. A new fabrication setup, which did not require the use of a fusion splicer was proposed (Zulkifly *et al.*, 2010; Lee *et al.*, 2013). In this proposed setup, the fusion splicer was replaced by an ignition coil (Bosch 30KW 12V) and the fabrication system consisted of both light source and OSA, a pair of electrodes which were attached to a translation stage, two different fiber clamps, *i.e.* one with slider and the other without slider, a tension meter attached with weight as well as the ignition coil with an arcing circuit. Before the writings of the gratings, the fiber was fixed by both fiber clamps and positioned in between the electrodes, followed by attaching one end of the fiber to a weight to provide the axial tension. The discharging of the electric arc and the translation of fiber was controlled by the computer. The formation of gratings in this fabrication system was due to the pulling force by the weight attached during every electric arc discharge. After the formation of each grating by a physical deformation mechanism, the pair of electrodes was moved by the motorized stage to the next arcing point to create the next grating. There were

a few parameters that would affect the structure of the tapers produced in this system, including the arcing time, grating period as well as the weight applied to the fiber. One of the benefits of using this fabrication setup was that it required lesser number of gratings and smaller arc current in producing LPFG. Even though the reproducibility of LPFGs with this mechanism might be compromised due to the degradation of both electrodes, the production of LPFGs with similar and precise characteristics can still be achieved by monitoring the arcing parameters as well as controlling the position of fiber between electrodes throughout the fabrication process (Czapla, 2015).

### **3.2 Current Fabrication Setup for Arc-Induced LPFG**

The fabrication setup used to produce LPFGs in this research is described in this section. Electric arc discharge was chosen as the fabrication technique of LPFGs because of its simpler setup and higher flexibility offers, in which extra pre-treatment of the fiber was not required. The fabrication setup was relatively similar to the one introduced by Zulkifly *et al.* (2010) and Lee *et al.* (2013). One major difference of this setup was that it did not require a fusion splicer if compared to most other electric arc discharge techniques. The fusion splicer was replaced by an ignition coil with an arcing circuit. Furthermore, the fabrication setup used in this research consisted of different components including two electrodes which were attached on the motorized translation stage, light source, an optical spectrum analyser, as well as a tension meter with weight and two fiber clamps (one with slider and one without). Both motorized translation stages and discharging of electrical arc

were controlled by a computer program called LabVIEW. The main mechanism of gratings formation in this fabrication setup was physical deformation in which periodic reductions in the fiber diameter was induced by the arc discharged by both electrodes. The experimental configuration of this fabrication system is shown in Figure 3.1.

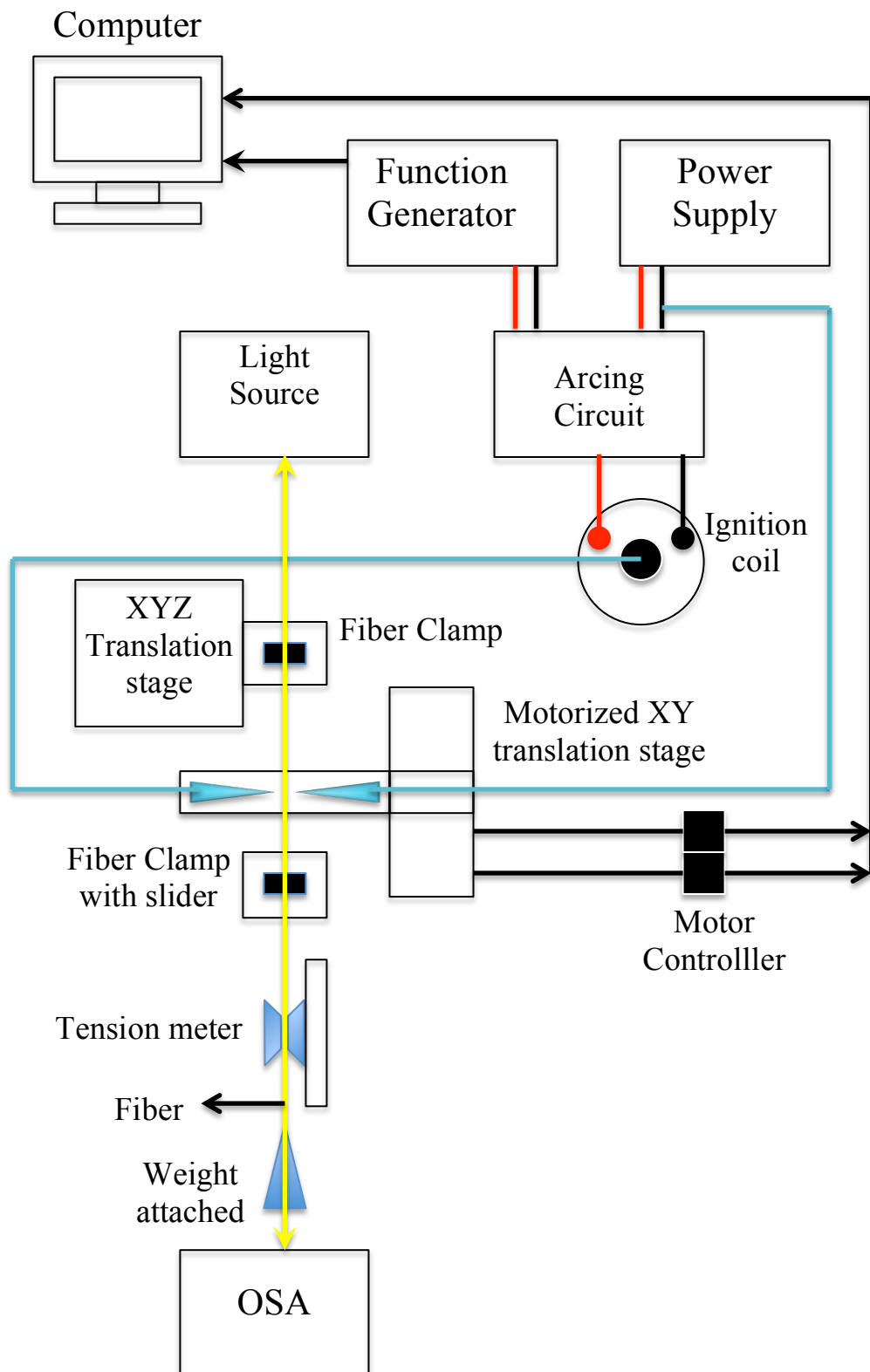


Figure 3.1 Current fabrication setup for producing arc-induced LPFGs

### **3.3 Fabrication of Arc-induced LPFGs**

#### **3.3.1 Preparation before Fabrication Process**

In this research, SMF-28 single mode fiber was chosen as the fiber type. The polymer coating jacket of the pre-defined gratings section of the single mode fiber was first carefully removed by a fiber stripper. Then, the stripped section was cleaned with Kimtech wipes which was soaked with Isopropyl alcohol (IPA) beforehand. The main purpose of the cleaning was to decontaminate the fiber surface so that there was no polymer material left on the gratings section to cause the burning of the fiber during arc generation. On the other hand, both electrodes were cleaned with IPA to prevent contamination. Before placing the fiber in between electrodes, a few arc discharges should be conducted first to clean the electrodes from contamination so that the arc generation becomes stable. The process was then followed by the clamping of fiber onto both fiber clamps which were maintained at the same height level. A magnet and a v-groove were embedded on both fiber clamps with the purpose to maintain the position of the fiber. Also, one of the fiber clamps was attached on top of a slider to allow the physical deformation of the fiber caused by the pulling of the axial tension attached to one end of the LPFG.

### 3.3.2 Fabrication Process

The fabrication process of the arc-induced LPFGs began with the placing of an stripped fiber in between two electrodes. Both ends of the fiber were held by two fiber clamps so that the fiber was maintained straight in between electrodes. One end of the fiber was then attached to a weight to provide a constant axial tension to the fiber. A tension meter (Honigmann 137.4 with Digitens 485, 0 cN ~ 100 cN) was used to monitor the axial tension force applied to the fiber. Consequently, an arc discharge was produced at the tips of both electrodes and the stripped fiber section was exposed to the arc generated for a duration to induce a deformation on the fiber, *i.e.* formation of one grating. After the formation of the first grating, the electrodes were moved by the translation stage for a distance similar to the pre-set grating period, and the arc was regenerated to form second grating on the fiber surface. This process was repeated several times until a desired attenuation of the LPFG resonant wavelength was achieved. The spectrum of the LPFG was monitored in the spectral range from 1520 nm to 1580 nm by a Yokogawa AQ6370C optical spectrum analyser (OSA) throughout the fabrication process. The arcing profile of the system used in this research is as shown in Table 3.1.

Table 3.1 Arcing profile of LPFG fabrication process

|                 |                   |
|-----------------|-------------------|
| Grating Period  | 650 $\mu\text{m}$ |
| Arc Duration    | 1 s               |
| Weight Attached | 18 cN             |

As mentioned in the previous section, the arcing generation and motorized translation stages were controlled by a computer program called “LabVIEW”. The parameters of the fabrication process including the grating period, arc duration as well as the number of arc generation could be predefined and modified accordingly in the LabVIEW program. After the fabrication of every LPFG, the translation stage moved the electrodes back to the initial “Home” position (first grating point) before the fabrication of next LPFG. The whole fabrication process of LPFG was simplified and portrayed in the flowchart as shown in Figure 3.2.

### 3.3.3 Flowchart of the Fabrication Process

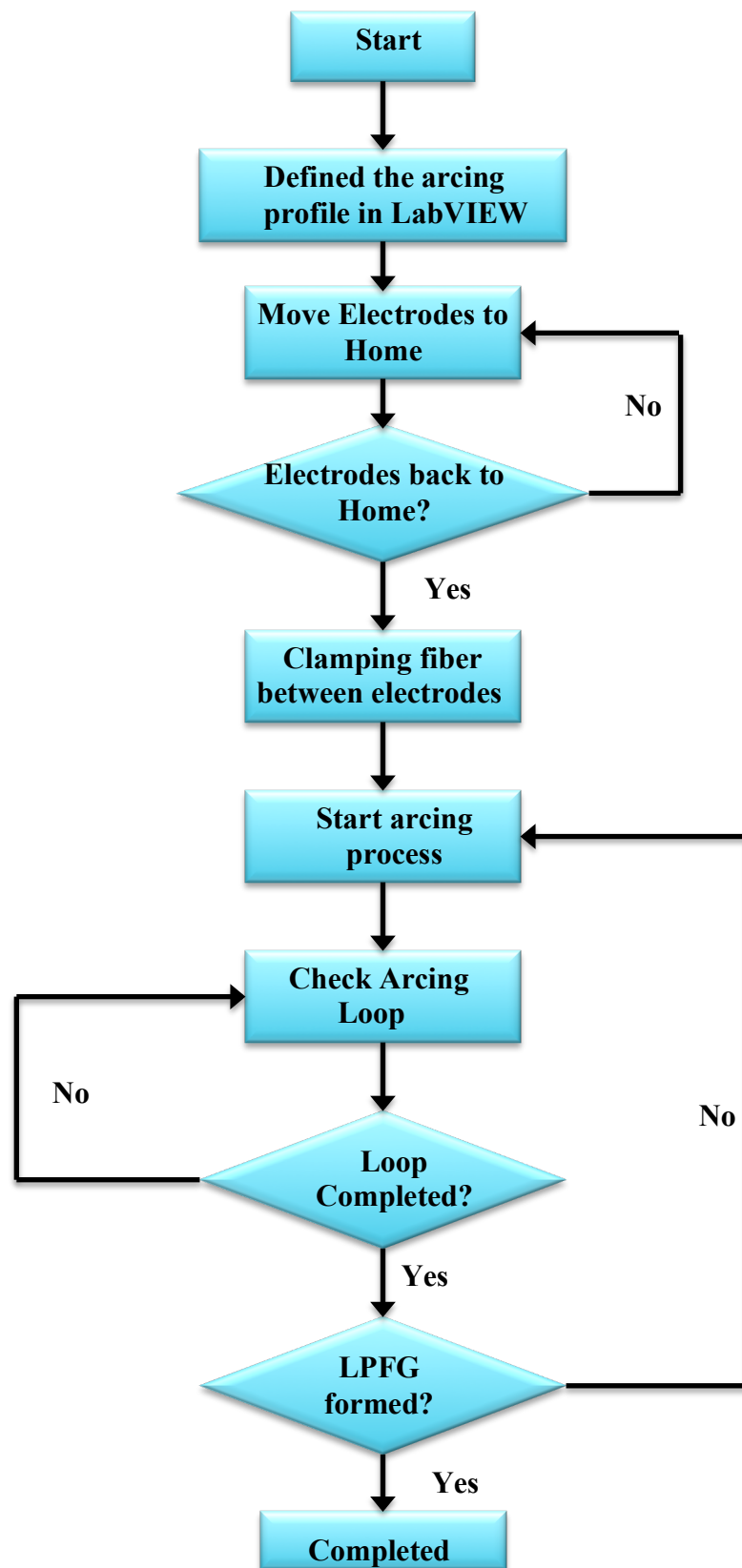


Figure 3.2 Flow chart of the fabrication process

### 3.3.4 Arc Generation and Gratings Formation on LPFG

As mentioned earlier, the formation of the gratings on arc-induced LPFGs was mainly caused by the discharge of electric arc from both electrodes. Basically, arc discharge is a self-sustained discharge that occurs in between two electrodes (Ushio *et al.*, 1988). The high intensity electric field generated at the tips of the electrodes causes electrons to be emitted from one of the electrodes which functions as the cathode. The other electrode, anode works as the electrons collector. The transition of electrons from cathode to anode causes the surrounding gas atoms to ionize. Subsequently, the ionization of gas atoms leads to the creation of high temperature plasma which consists of both ions and electrons, and as a result, an arc is generated (Correy, 1982).

There are a few possible mechanisms that have been proposed for the formation of arc-induced LPFGs. The main mechanism that occurred with the fabrication system used in this research was physical deformation. When one of the fiber section was exposed to the electric arc, a periodic reduction of the fiber diameter (one grating) occurred, which in the end caused a physical deformation of the fiber (Kosinski *et al.*, 2010). Physical deformation of fiber can be divided into two types, *i.e.* fiber tapering as well as microbending (Shao *et al.*, 2008; Ivanov *et al.*, 2004). The type of physical deformation induced by this fabrication setup was fiber tapering. Throughout the fabrication process, the fiber was placed under slight tension due to the weight attached to one end of the fiber. In this case, the tension applied was 18cN. During the arc discharge, the high temperature produced heated the fiber and

softened its silica structure until the fiber became pliable (Ayala *et al.*, 2012). Then the pulling tension formed by the weight attached decreased the diameter of the fiber and resulted in a fiber taper. Consequently, it caused the mode coupling coefficients to increase as the tapering process continued (number of fiber taper increases) until a point where a desired attenuation band was formed at the transmission spectra. One of the examples of LPFG spectrum is shown in Figure 3.3. Referring to the spectrum, an attenuation band was created after the formation of 33 gratings on the surface of the fiber. The attenuation notch observed in the LPFG spectra indicates the transmission loss caused by the coupling of light from the fundamental core mode to several propagating cladding modes of fiber (Yoon *et al.*, 2012).

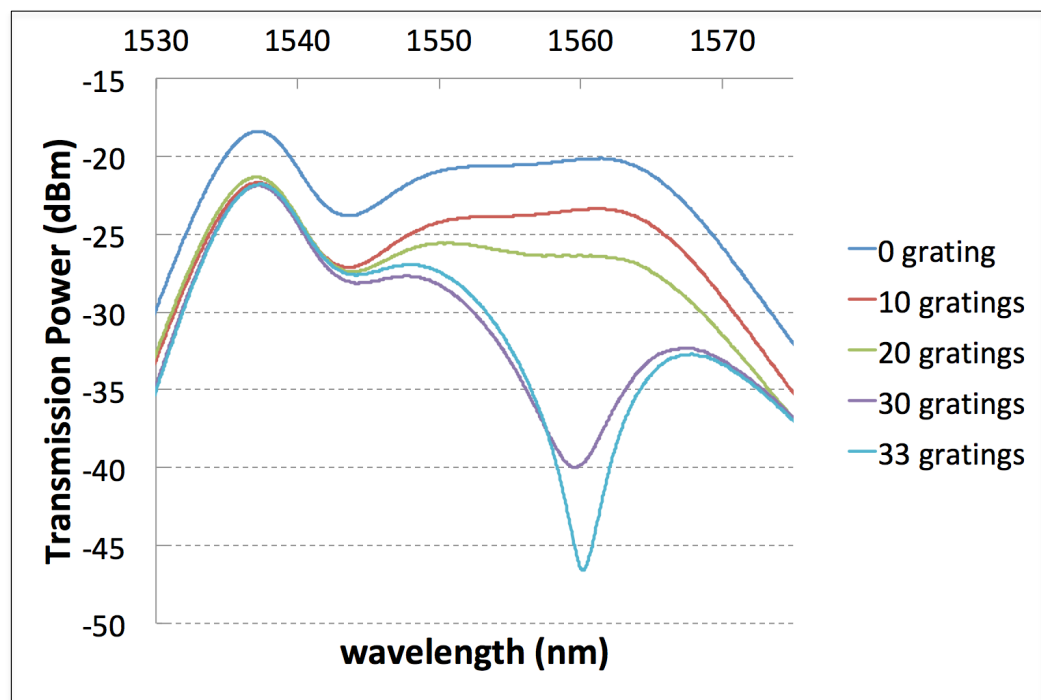


Figure 3.3 Formation of arc-induced LPFG after 33 gratings

### 3.3.5 The Reproducibility of LPFGs Fabricated

As discussed, one of the limitations found in LPFGs fabricated by the electric arc discharge technique was the lack of reproducibility, so the evaluation of the system duplicability is crucial. In the arc-induced fabrication technique, the reproducibility of the LPFG can be limited by the degradation of electrodes and the inconsistency of every arc produced. Nonetheless, it was discovered that LPFGs with reproducible characteristics were still able to be produced with careful control and adjustment of the position of fiber in between electrodes as well as the fabrication parameters (Ivanov *et al.*, 2007).

In order to investigate the reproducibility of the fabrication system used in this research, the whole fabrication process was repeated with four different fibers. The fabrication parameters remained with the same arcing profile, where the arc duration was maintained at 1 second, grating period was preset at  $650\ \mu\text{m}$  and the axial tension applied remained at 18 cN. After the fabrication, the resonant wavelength and the transmission power of the fibers were compared to evaluate the similarity among different fibers. The resonant attenuation of all fibers are shown in Figure 3.4, and their grating properties are summarized in Table 3.2. As can be observed from the table and spectra obtained, the grating properties and the transmission spectra of all LPFGs fabricated with the same arcing profile were very similar to each other. The transmission depth of all four LPFGs were very close to each other, *i.e.* near to  $-20\ \text{dB}$ . On the other hand, the resonant wavelengths of all four LPFGs were in the range from 1560 nm to 1562 nm, which indicates that their resonant

wavelengths were very close to 1560 nm despite the small variations found. In the investigations reported in 2013 and 2014, it was explained that if a large number of gratings are formed on the fiber, the cumulative effect of the local diameter decrease at the grating region will cause the diameter of the fiber in the whole grating section to reduce (Yoon *et al.*, 2013; Yin *et al.*, 2014) Hence, the differential effective indices between core and cladding mode is increased due to the reduction in fiber diameter. As a result, the resonant wavelength of LPFG is shifted towards a longer wavelength instead of a shorter wavelength after a certain number of gratings is achieved. It is believed that this is the main reason which causes the variation in resonant wavelengths of different LPFGs.

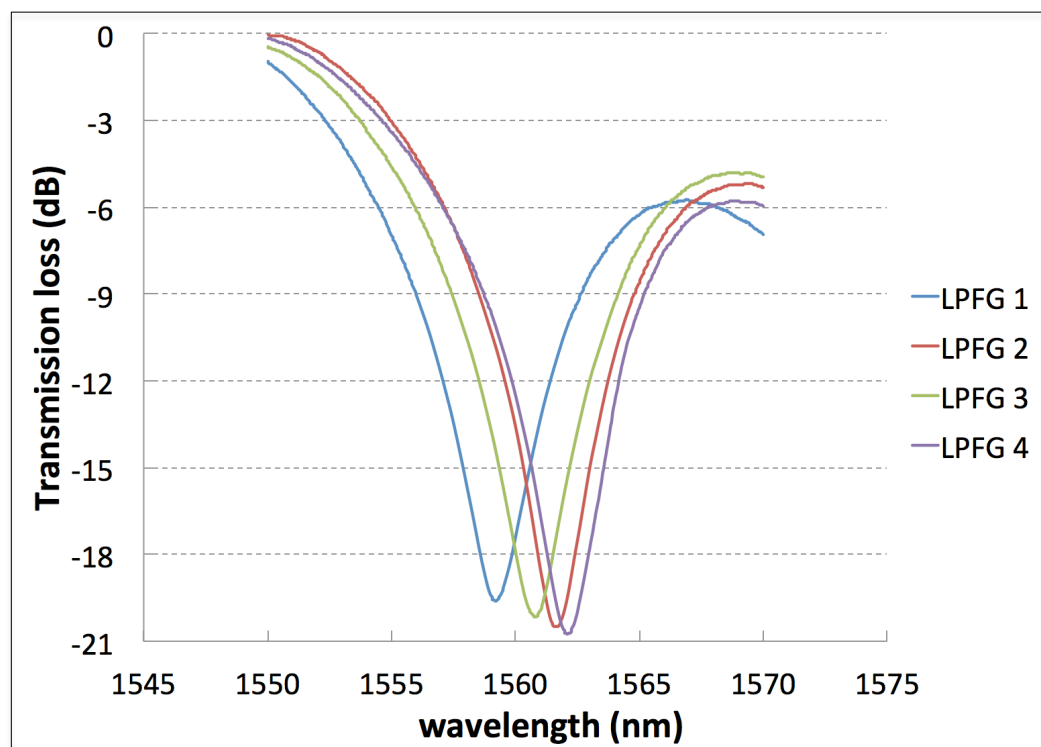


Figure 3.4 Transmission spectra of four different LPFGs fabricated with the same arcing profile

Table 3.2 Comparison of the properties of four different LPFGs

| LPFG Properties          | LPFG 1  | LPFG 2  | LPFG 3  | LPFG 4  | Mean value |
|--------------------------|---------|---------|---------|---------|------------|
| Grating length (mm)      | 21.45   | 21.45   | 20.80   | 22.75   | 22.10      |
| Resonant wavelength (nm) | 1560.12 | 1561.64 | 1560.76 | 1562.12 | 1561.16    |
| Transmission Loss (dB)   | -19.621 | -20.513 | -20.157 | -20.755 | -20.262    |

### 3.4 Characterization of LPFGs Fabricated with Current Fabrication

#### System

In this section, the performances of the arc-induced LPFGs fabricated with the setup discussed earlier is evaluated. As mentioned in the previous section, the sensitivities of LPFGs towards the external index is the main reason that drives them to become a favourite candidate to be used as different sensors. Hence, the sensitivities of the LPFGs fabricated towards the external RI must be investigated before modifying them further for desired sensing applications.

#### 3.4.1 Sensing of Cargille Oils

##### 3.4.1.1 Experimental Setup

Before the refractive index experiment was conducted, LPFGs were fabricated with the same arcing profile as discussed in Section 3.3. Consequently, the sensitivities of the fabricated LPFGs towards different

refractive indices were tested. An experiment with a set of liquid oils (Cargille oil Series AA and A, standardized at 5893 angstroms under 25 °C) was conducted with eleven oils of different refractive indices, ranging from 1.4000 to 1.5000. Before the experiment, the LPFG was positioned in the middle of a glass fixture groove and held straight in between two fiber clamps. A constant tension of 18 cN was applied to one side of the LPFG to ensure that the LPFG was kept straight in between the clamps and to avoid any bending effects on the LPFG. Measurand was dropped into the groove of the glass fixture where the gratings part of the fiber was placed to allow the whole gratings to be fully soaked in the solution. Before the experiment started, the spectrum of the LPFG in air was first recorded as the reference for comparison.

Consequently, the gratings section of the LPFG was then immersed in Cargille liquid oils with refractive indices (from lowest to highest refractive index) ranging from 1.40 to 1.50, with 0.01 as the intervals of each refractive index. In between every oil with different refractive indices, the previous liquid oil was removed and the fixture was cleaned with acetone and isopropyl alcohol to remove any residue. Also, the grating parts of the LPFG were fully cleaned and wiped with acetone as well as isopropyl alcohol to remove the oil. Finally, the LPFG was left to air dry until its response goes back to the reference point (as in air) before the immersion in Cargille oil with higher refractive index. The exact same experiment was repeated with another LPFG to observe the consistency of their performances. These experiments were conducted in a controlled room with a constant temperature of  $24.2\text{ °C} \pm 0.2\text{ °C}$ . Also, the power fluctuation of the broadband light source was recorded

to be within the range of  $\pm 0.01$  dBm. The experiment setup of this section is shown in Figure 3.5.

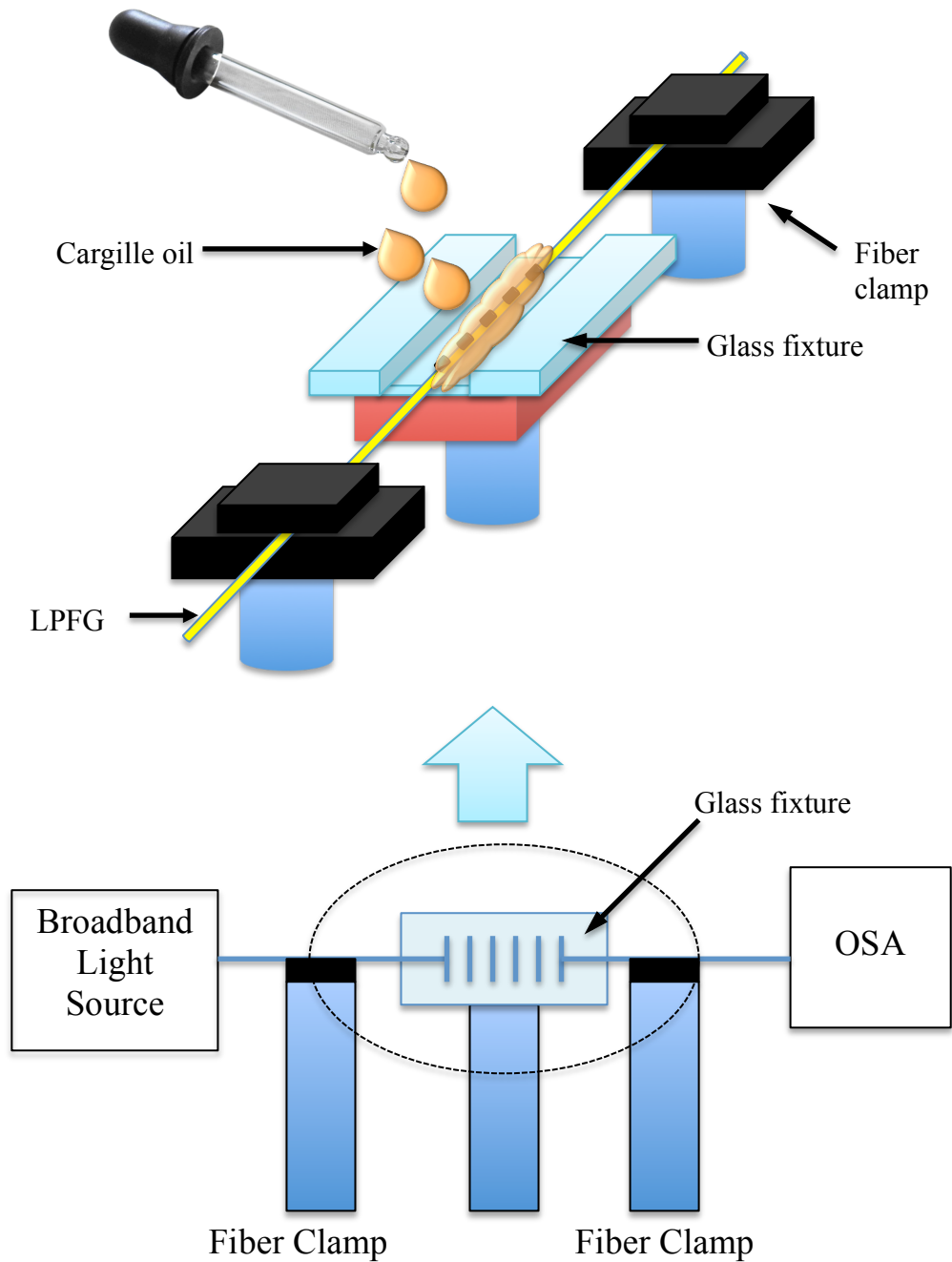


Figure 3.5 Experimental setup for testing with refractive index matching oils

### 3.4.1.2 Results and Discussion

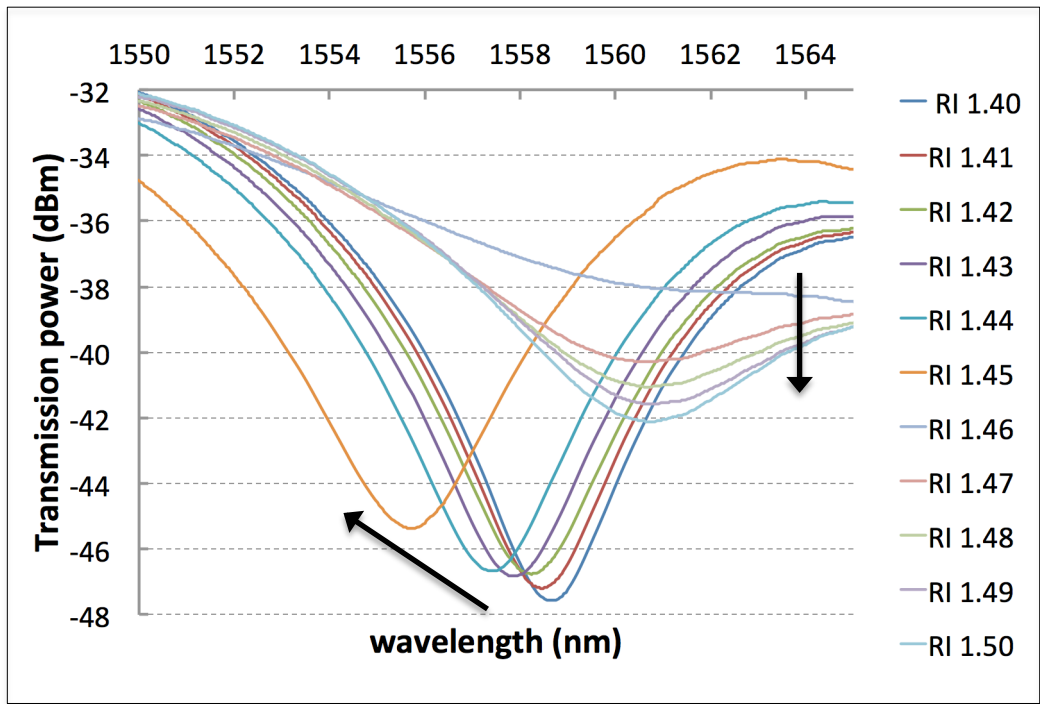
Figure 3.6 shows the spectra responses of both LPFGs in accordance to the increment in refractive indices. As expected, the variation in the external index (refractive index of the surrounding medium) has led to the shifting of the LPFG resonant wavelength due to its unique property, *i.e.* refractive index sensitivity. The sensitivity of LPFG towards the external index relies on the differential refractive indices between both external medium and cladding mode, which leads to the changes in the effective refractive index of LPFG cladding mode in the phase matching condition, therefore causing the resonant wavelength to shift (Korposh *et al.*, 2013). In this experiment, it can be observed that responses of both LPFGs towards different refractive indices are similar.

As observed from the results, the resonant wavelength of both LPFGs encountered blue shift when the refractive index of liquid oil increased from 1.40 to 1.45. This phenomenon can be explained by the first case of LPFG refractive index sensitivity, where the refractive index of the surrounding medium was lower than that of the cladding index ( $n_3 < n_2$ ). In this case, the mode guidance within LPFG was explained by total internal reflection (TIR). As the refractive index of external medium increased towards the cladding index, the resonant wavelength shifted towards a shorter wavelength. The shifting of the resonant wavelength was due to the decrement of the differential refractive indices between fiber core and cladding modes when the external index slowly approached the cladding index, thereby affecting the

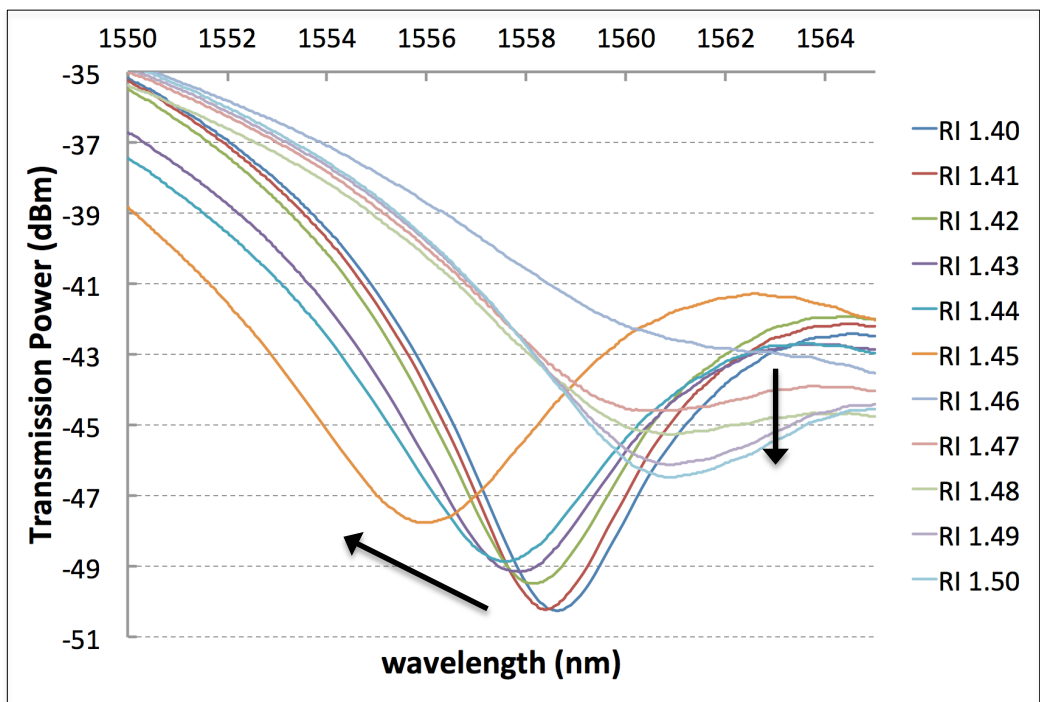
resonant notch as according to the phase matching condition equation (Lee *et al.*, 1997; Shu *et al.*, 2002; Libish *et al.*, 2011).

In addition, the resonant notches of both LPFGs almost disappeared as the surrounding refractive index exceeded 1.45 and approached 1.46. This scenario occurred when the surrounding refractive index was approximately similar to the index of fiber cladding mode ( $n_3 \cong n_2$ ). In this case, the cladding had an infinitely large radius, thus becoming an infinite medium. There was no discrete guided mode encountered at this moment, therefore there was no cladding mode which was coupled to the core mode. A broadband radiation mode coupling will occur instead, with no distinct transmission band observed at the output due to the lack of TIR at the cladding interface (Villa *et al.*, 2005).

By further increasing the surrounding refractive index from 1.46 to 1.50, the resonant notch of both LPFGs reappear at a longer wavelength as the surrounding refractive index exceeds the cladding index ( $n_3 > n_2$ ). In this case, the cladding modes are no longer experiencing TIR, but they are guided by Fresnel reflection, and is referred to as leaky modes (Stegall *et al.*, 1999).



(a)



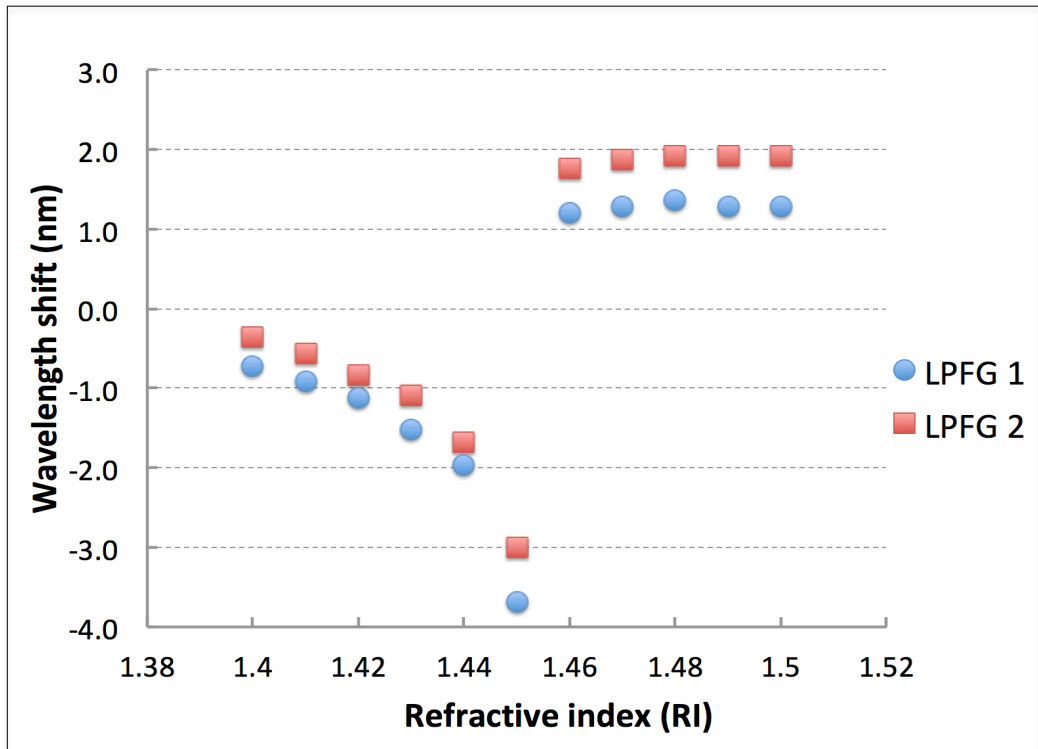
(b)

Figure 3.6 Spectra response of (a) LPFG 1; and (b) LPFG 2 in accordance to difference refractive indices

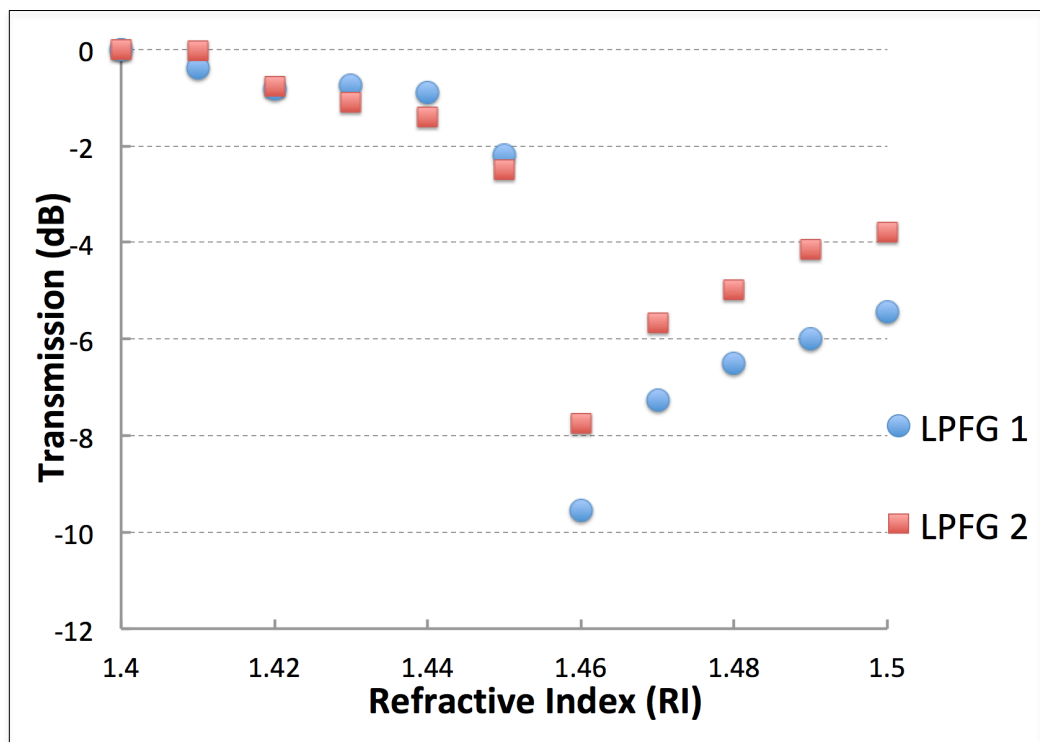
A comparison of the LPFG response over RI in terms of wavelength shift as well as transmission power was plotted for both LPFGs. Referring to the comparison shown in Figure 3.7(a), the refractive index sensitivity of both LPFG 1 and LPFG 2 were  $-31.0$  nm/RI and  $-33.0$  nm/RI respectively as the external RI increased from 1.40 to 1.44. As the external index raised from 1.44 to 1.45, the shortest resonant wavelength was obtained for both LPFGs, where the refractive index sensitivity of LPFG 1 was found to be  $-172.0$  nm/RI, whereas LPFG 2 was measured to be  $-134.0$  nm/RI. The closer the external RI to the cladding index, the higher the LPFG sensitivity, hence causing the resonant notch to encounter a larger wavelength shift (Libish *et al.*, 2011). As the surrounding refractive index exceeds 1.45 and approaches 1.46, the resonant wavelength of both LPFGs encountered a sudden jump to a longer wavelength in this range of refractive index due to the mode transition effect. This indicates that both LPFGs were most sensitive between refractive indices of 1.45 and 1.46. From the results, it can be obtained that the sensitivity of both LPFG 1 and LPFG 2 was highest in this region, *i.e.* 495.0 nm/RI and 480.0 nm/RI respectively. The shifting of resonant wavelength became very small for both LPFGs when the external RI increased from 1.46 to 1.50. The refractive index sensitivity of LPFG 1 dropped to 3.0 nm/RI whereas the sensitivity of LPFG 3 was 1.5nm/RI. As the refractive index of external medium exceeds that of the cladding index ( $n_3 > n_2$ ), the shift of LPFG resonant wavelength became non-prominent. In this case, the cladding modes will no longer undergo TIR, and the resonant wavelength shift becomes very small in accordance to the increment in the surrounding refractive index. The

slight wavelength shift occurred in this case was mainly due to the coupling to the leaky modes at the interface between external medium and fiber cladding.

On the other hand, the transmission power of the LPFG resonant notch in response to different refractive indices is shown in Figure 3.7(b). The comparison showed that the response trends of both LPFGs towards refractive index are relatively similar to one another. Furthermore, both LPFGs are most sensitive to RI range from 1.45 to 1.46. As observed, the transmission power of both LPFG notch increased when the surrounding refractive index increased from 1.40 to 1.45. This is due to the successively smaller coupling coefficients caused by the decrement in overlap integral between core and cladding mode as the surrounding refractive index slowly approached the cladding index (Laffont *et al.*, 2000). The gradient of transmission power for LPFG 1 and LPFG 2 in the RI range from 1.40 to 1.44 were  $-22.3$  dB/RI and  $34.8$  dB/RI, respectively. Moreover, the gradient of LPFG 1 and LPFG 2 in RI range from 1.44 to 1.45 were  $-129.7$  dB/RI and  $-109.0$  dB/RI. The transmission power gradient for both LPFGs were highest in the RI range between 1.45 to 1.46, *i.e.* LPFG 1 was  $-735.2$  dB/RI, while LPFG 2 was  $-525.3$  dB/RI. Lastly, the gradient for both LPFGs in the RI range from 1.46 to 1.50 were  $102.3$  dB/RI and  $99.1$  dB/RI respectively. The refractive index sensitivities of both LPFGs are summarised in Table 3.3.



(a)



(b)

Figure 3.7 (a) Wavelength shift and (b) Transmission power of both LPFG 1 and LPFG 2 in accordance to the increment in the surrounding refractive index

Table 3.3 Comparison of refractive index sensitivity of LPFG 1 and LPFG 2

| RI        | LPFG 1                |                         | LPFG 2                |                         |
|-----------|-----------------------|-------------------------|-----------------------|-------------------------|
|           | Wavelength<br>(nm/RI) | Transmission<br>(dB/RI) | Wavelength<br>(nm/RI) | Transmission<br>(dB/RI) |
| 1.40-1.44 | -31.0                 | -22.3                   | -33.0                 | -34.8                   |
| 1.44-1.45 | -172.0                | -129.7                  | -134.0                | -109.0                  |
| 1.45-1.46 | 495.0                 | -735.2                  | 480.0                 | -525.3                  |
| 1.46-1.50 | 3.0                   | 102.3                   | 1.5                   | 99.1                    |

### 3.4.2 Sensing of Sucrose Solutions

#### 3.4.2.1 Experimental Setup

To further evaluate the performance of the fabricated LPFG as a chemical sensor, another experiment was conducted. Sucrose solutions with six different concentrations were tested in this experiment, ranging from 10% to 60%, with 10% as intervals of each concentration. On the other hand, two different arc-induced LPFGs were used in this experiment to verify the consistency of the results.

The experimental setup to test the responses of arc-induced LPFG fabricated towards sucrose solutions was similar to the setup discussed earlier in Section 3.4.1. Sucrose solution (Acros Organics, AR sucrose) with different concentrations, from 10 % to 60% were prepared according to the weight of

sucrose and volume of deionised water stated in Table 3.4. Initially, the gratings section of the LPFG was fully immersed in deionised water to obtain the spectrum in water as a reference. Then, sucrose solution was dropped to the v-groove of the fixture until the LPFG was fully soaked in the solution. The response and transmission power of the arc-induced LPFG was recorded by OSA. Consequently, the experiment was carried on with other concentrations of sucrose, from the lowest to the highest concentrations. In between the immersion of different concentrations of sucrose solutions, the previous measurand was removed from the glass fixture and the LPFG was rinsed thoroughly with deionised water to remove the residue from the previous solution.

Table 3.4 Weight of sucrose and volume of deionised water required for the preparation of sucrose solutions with various concentrations

| Concentrations of sucrose solution (wt%) | Sucrose powder (g) | Volume of deionised water (mL) |
|------------------------------------------|--------------------|--------------------------------|
| 10                                       | 10                 | 100                            |
| 20                                       | 20                 | 100                            |
| 30                                       | 30                 | 100                            |
| 40                                       | 40                 | 100                            |
| 50                                       | 50                 | 100                            |
| 60                                       | 60                 | 100                            |

### 3.4.2.2 Results and Discussion

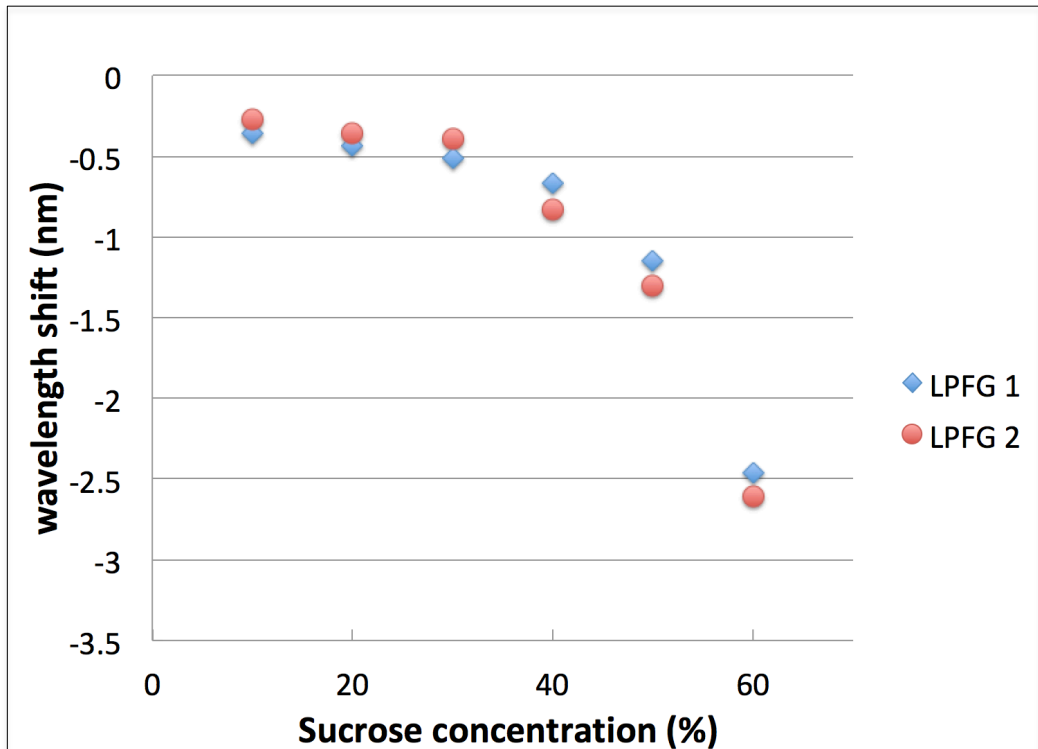
The responses of LPFGs towards sucrose concentrations are shown in Figure 3.8. Referring to Figure 3.8(a), the responses of both LPFGs were similar to each other. The resonant wavelength of both LPFGs encountered blue shift to shorter wavelength when the concentration of sucrose solution increased from 10% to 60%. On the other hand, the minimum transmission power of LPFG increased as the concentration increased from 10% to 60%. As discussed earlier, the effective refractive index of the cladding mode was affected by the surrounding solutions. In this case, the increment of the sucrose concentration increased the effective refractive index of cladding mode, thus reducing the differential effective indices between core and cladding mode. As a result, the resonant wavelength was shifted to shorter wavelength (Lee *et al.*, 1997; Shu *et al.*, 2002; Libish *et al.*, 2011).

In this experiment, the results showed that the sensitivities of both LPFGs towards refractive index were highest in 60% of sucrose solution as the refractive index of 60% of sucrose solution was the one closest to that of the cladding index compared to a lower percentage of sucrose (Patrick *et al.*, 1998). This finding was in good agreement with the results obtained from the investigations done in 2011, where the resonant wavelength of LPFG encountered the largest shift in 60% of sucrose solution (Li *et al.*, 2011).

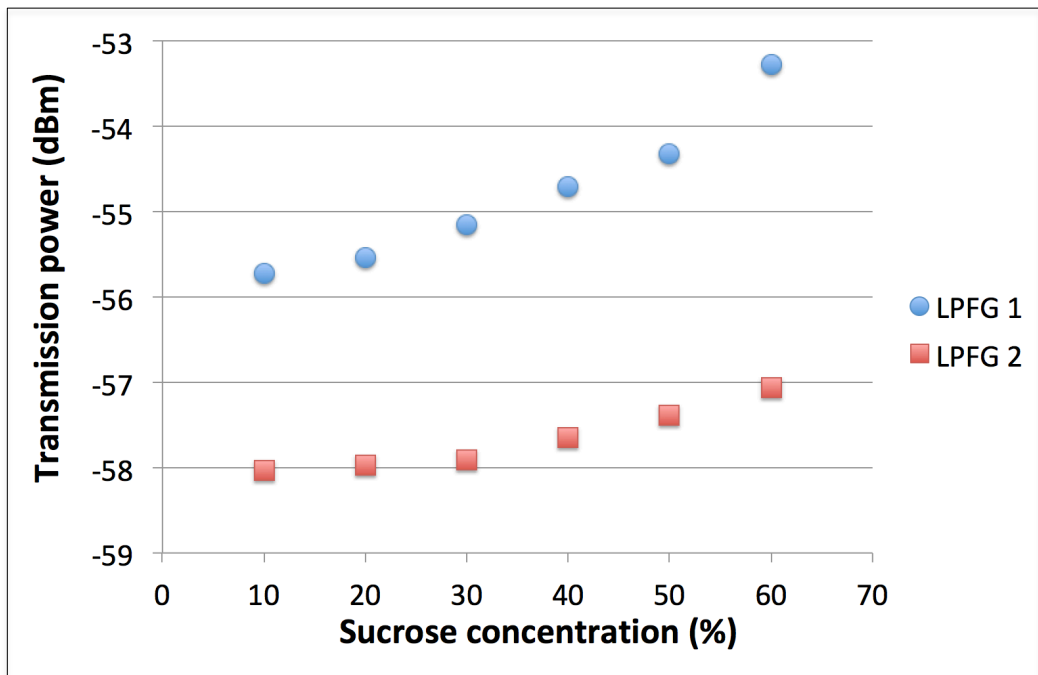
On the other hand, the minimum transmission power of the resonant notch increased in accordance to the increment in sucrose solution. The

minimum transmission power of LPFG 1 encountered a total increase of 5.226 dBm as the concentration increased from 10% to 60%, whereas the total increase in minimum transmission power of LPFG 2 was 3.323 dBm. The increment of the minimum transmission power was caused by the changes in the coupling strength between core and cladding modes (Laffont *et al.*, 2000).

Throughout this experiment, it can be concluded that the LPFGs fabricated in this research responded to the changes in external RI. Although both LPFGs had similar trends in different concentrations of sucrose, the changes in the transmission spectra were very small, *i.e.* both wavelength shift and transmission power change were not significant. This indicates that the sensitivity of LPFG was not optimised yet due to the large grating period used in the fabrication of LPFGs. Hence, the sensitivity of LPFG must be improved and optimised before it is further employed in sensing application.



(a)



(b)

Figure 3.8 (a) Wavelength shift and (b) Transmission power of both LPFG 1 and LPFG 2 in accordance to the increment in the concentration of sucrose

### **3.5 Summary**

In this chapter, the arc-induced LPFGs based on electrical arc discharge technique were successfully fabricated. The sensitivity of the fabricated LPFG towards the external RI was investigated and experimented with Cargille oils and sucrose solutions with different concentrations. According to the responses of LPFGs, it was found that there was a need to investigate methods to enhance and improve the sensitivity of LPFG towards RI before applying it to detect targeted elements since the main mechanism in detection using LPFG is based on the changes in the external RI. The following chapter will discuss the methods chosen in this research to improve the sensitivity of LPFG towards the external index.

## **CHAPTER 4**

### **SENSITIZATION OF ARC-INDUCED LPFG TOWARDS SURROUNDING REFRACTIVE INDEX**

The second phase of this research is presented in this chapter, which mainly focused on the sensitization techniques that are adopted in this research to improve the performances of LPFGs before they are further tailored for sensing application. In the previous chapter, the fabrication techniques used for producing arc-induced LPFGs was discussed in detail. Also, the performances of the LPFGs produced were investigated through experiments with measurands of different refractive indices and concentrations. However, it was discovered that there was a limitation in their performances in sensing different refractive indices as only a small shift in the resonance wavelength was encountered in the experiments. This is mainly due to the large grating period used in the fabrication.

Therefore, it is necessary to investigate techniques that can help enhance the existing performance of the arc-induced LPFG. According to past research, the sensitivity of LPFG towards external perturbations can be evaluated through two different interrogation methods. The first method is the wavelength-based interrogation technique, in which the response of the LPFG towards the external RI is observed based on the shifting of the LPFG resonant wavelength. On the other hand, the second technique is the transmission-based

interrogation method, where the sensitivity of LPFG towards different external parameters is investigated through the variation in the minimum transmission power of the LPFG resonant notch. Hence, two different enhancement techniques were adopted in this research to sensitize the LPFG for both interrogation methods. In short, the intention of employing the first enhancement technique, *i.e.* thin film coating, was to make the wavelength shift of LPFG more prominent towards the external index, whereas the second one, double-pass configuration technique helped to increase the transmission loss of the LPFG in response to the refractive index, thus enhancing its sensitivity. The performances of the sensitized LPFG were then tested to evaluate both enhancement techniques.

#### **4.1 Introduction of LPFG Sensitivity Enhancement**

The first ever reported Long Period Fiber Grating (LPFG) fabrication was in 1994 by Poole *et al.*, while the investigation on the concept and details of LPFG were continued by Vengsarkar *et al.* in 1996. Since then, different researches were conducted to analyse the sensitivity of LPFGs towards surrounding parameters such as strain and refractive index (Bhatia *et al.*, 1999; Rego *et al.*, 2006). Also, it was proposed that their sensitivities can be modified towards specific parameters (Bock *et al.*, 2007) so that they can be adopted for sensing different elements. For instance, LPFGs had been demonstrated to work as refractometers, chemical sensors and biosensors (Rios *et al.*, 2010; Linesh *et al.*, 2011; Chan *et al.*, 2010). The main working mechanism of most of the sensors demonstrated were based on the shifting of

LPFG resonant wavelength in accordance to different refractive indices caused by external parameters. However, challenges were induced in the application of LPFGs as different sensors due to the relatively small shift of the resonant wavelength. Due to this limitation, there had been increasing research interests in finding different ways to enlarge the wavelength shift of the LPFG resonant notch and improve its sensitivity towards the external index.

The influence of the external RI on the cladding of the LPFG can be expressed as Equation (4.1) by rearranging the phase-matching condition equation of LPFG (Bhatia *et al.*, 1999):

$$\frac{d\lambda}{dn_3} = \frac{d\lambda}{dn_{cl}} \frac{dn_{cl}}{dn_3} \quad (4.1)$$

where  $\lambda$  represents the resonant wavelength of LPFG. On the other hand,  $n_{cl}$  and  $n_3$  represent the refractive indices of the cladding and surrounding medium. Hence, it can be observed that the propagation constant of LPFG depends not only on the fiber parameters, but also the surrounding refractive index,  $n_3$ . In general, the changes in the surrounding refractive index will alter the effective refractive index of the cladding mode. As a result, the response of LPFG is affected because the differential effective refractive indices between fiber core and cladding mode has changed (Yin *et al.*, 2012).

Most of the research conducted in earlier stage used wavelength shift of the resonant notch as the parameter for measuring the sensitivity of LPFG. Thus, most of the techniques that have been proposed for sensitizing LPFG

such as the turning points of the dispersion mode, fiber tapering as well as etching of fiber cladding techniques focused more on enlarging the wavelength shift of the LPFG. (Shu *et al.*, 2002; Ding *et al.*, 2005; Rios *et al.*, 2009; Mysliwiec *et al.*, 2013). In recent years, the measurements of LPFG sensitivity was extended to focus on transmission-based interrogation, in which the variation in the minimum transmission power of the LPFG attenuation band was used as the parameter to measure LPFG sensitivity instead of investigating the wavelength shift (Loh *et al.*, 2014; Yong *et al.*, 2015). Also, a sensitize method, double-pass configuration was proposed to enlarge the variation in the transmission loss of the LPFG towards external perturbation, thus enhancing its sensitivity towards the external index. The main advantage of this enhancement method is that it is simple and does not require a complicated pre-treatment process.

In this research, it was proposed to employ and combine two enhancement techniques to improve the sensitivity of arc-induced LPFG towards external index for both wavelength-based and transmission-based interrogation methods. The use of the first technique, *i.e.* thin film coating technique was able to increase the shifting of the resonant wavelength of the LPFG and hence improve its sensitivity towards external perturbations. On the other hand, the application of the second enhancement technique, double-pass configuration, aimed to sensitize the LPFG by increasing the transmission loss of its attenuation band in accordance to external perturbations.

## 4.2 Thin Film Coating

Thin film coating was the first technique adopted in this research to enhance the sensitivity of LPFG. This technique was first introduced in 2002 by Rees *et al.*, where the Langmuir-Blodgett (LB) deposition method was used to adsorb a layer of thin film over the gratings section of LPFG. The main mechanism in LB deposition method was based on Van Der Waals interaction. This technique induced one main drawback, in which the thin-film deposited exhibited poor thermal and mechanical stability due to the weak bonding of the Van Der Waals interaction (Yang *et al.*, 2007).

Three years later, another technique was proposed for the coating of thin film on LPFG, which was named the electrostatic self-assembly (ESA) technique (Wang *et al.*, 2005). ESA coating is a layer-by-layer (LbL) deposition technique for the deposition of nano-scale thin-film onto a fiber surface. The process of deposition in ESA technique involves the dipping of the charged substrate (LPFG) into poly-anions or poly-cations aqueous solution to form a layer of nano-thick film onto the substrate surface. The process is then followed by the immersing of the substrate again in polyelectrolytes with opposite charges to induce the attraction between positive and negative charges and form another nano-thick layer of coating (Wang *et al.*, 2005). In the process of forming multilayers of thin films, it requires the charged substrate to be consecutively immersed alternately into solutions that consist of negative and positive charges (Li *et al.*, 2009).

This deposition technique offers a variety of advantages including excellent reliability, film quality as well as better thermal and mechanical stability of the thin film deposited if compared to other techniques of thin-film coating (Decher *et al.*, 1997; Heflin *et al.*, 1999). In addition, this ESA coating technique offers advantages of being a faster coating technique due to the stronger ionic bonding. The simplicity of the coating process in the ESA technique had attracted increasing interest in adopting this technique to enhance the sensitivity of LPFG. On the other hand, the ESA technique provides flexibility as the coating materials are diverse. This means that the coating agents are not only limited to polyelectrolytes, but also includes any nano-objects that consist of positive or negative charges such as colloids and nanoparticles. In other words, it can be tailored to enable multi-material assembly of several compounds onto a charged substrate, without any requirement of chemical modifications (Cheng *et al.*).

In this phase of research, the ESA technique was chosen as the coating method to coat a multilayer of polyelectrolytes onto the fiber gratings surface due to the variety of advantages offered. The surface of LPFG was known to be negatively charged due to the presence of the silanol groups in its silica structure (Behrens *et al.*, 2001). Hence, the first polyelectrolyte layer to be coated was the positively charged poly-dimethyl dially ammonium chloride (PDDA) (polycations). The negative charges of fiber surface would attract the positive charges of PDDA and form a uniform layer of thin film. In order to deposit the second layer of polyelectrolytes onto the LPFG, poly(sodium-p-styrenesulfonate) (PSS) was chosen as the polyanions as the positive charges

of PDDA would attract the negative charges of PSS to form the second PE layer. Apart from sensitizing the LPFG, the polyelectrolytes multilayer coated in this phase was also employed as the preparation for the adsorption of nanoparticles in the next phase of this research, which will be discussed in greater detail in Chapter 5.

#### **4.2.1 Experimental Setup for LPFG Coating Process**

The LPFGs were written on SMF-28 single mode fibers using the electric arc discharge technique discussed in Chapter 3. During the fabrication process, the fiber was held by two fiber clamps and positioned in between two electrodes. One of the fiber holders was attached with a slider and weight was applied to one end of the fiber to create a constant axial tension for the deformation of the fiber cladding. Throughout the whole fabrication process, all LPFGs were fabricated with the same arcing profile, in which the arc discharge time and the grating period were set to 1 s and 650  $\mu\text{m}$ , respectively. Also, a constant tension of 18 cN was applied to the fiber. After each arc discharged, the motorized stage of the setup moved the electrodes along the fiber to the next grating point for the formation of the following gratings. After the fabrication process, the experiment proceeded with the coating process.

Before the coating process, the gratings section of LPFG was wiped and cleaned with isopropyl alcohol, followed by de-ionized water to eliminate contaminants and dust on the fiber gratings section that might affect the deposition of thin film layers. Also, both the PE coating agents were prepared.

The decontaminated gratings section was then coated with the PE coating agents by using the ESA technique, in which the coating mechanism was based on the bonding between cations and anions that were attracted to one another. The coating process began with the immersion of the fiber gratings section in 5 wt% poly-dimethyl diallyl ammonium chloride (PDDA, Mw of 100,000 – 200,000, Sigma Aldrich) solution for a duration of 10 minutes. Then, the gratings section was rinsed with DI water for around 3 minutes. After this process, a monolayer of PDDA was adsorbed onto the surface of the gratings section and formed a layer of positive charges. Consequently, the monolayer-coated LPFG was soaked in 5 wt % of poly(sodium-p-styrenesulfonate) (PSS, Mw of 70,000, Sigma Aldrich) for another 10 minutes. Again the gratings section was rinsed with DI water for another 3 minutes to remove the residue after the coating process. Another layer of negatively-charged PSS was adsorbed onto the gratings surface and formed a bilayer of (PDDA/PSS). The coating process was then repeated n times until a desired number of bilayers (PDDA/PSS)<sub>n</sub> was coated onto the gratings surface. The spectral response of the LPFG was monitored throughout the whole coating process with the help of a Yokogawa AQ7370C OSA. The schematic of the LPFG coated with bilayer of polyelectrolytes (PDDA/PSS)<sub>1</sub> is shown in Figure 4.1.

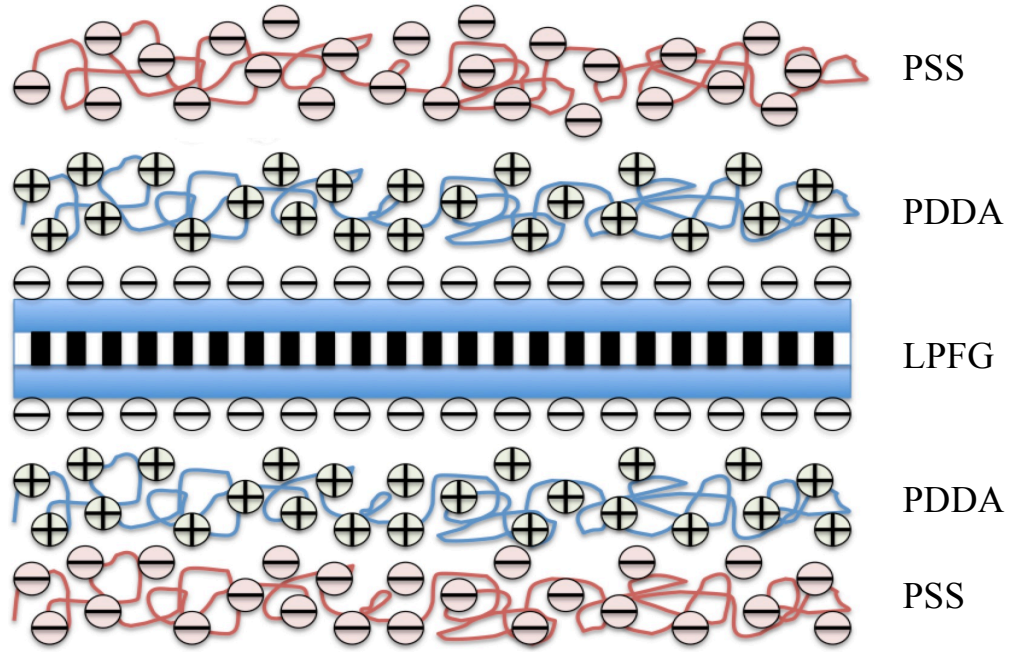


Figure 4.1 Schematic of the LPFG coated with bilayer of polyelectrolytes (PDDA/PSS)<sub>1</sub>

#### 4.2.1.1 Results and Discussions

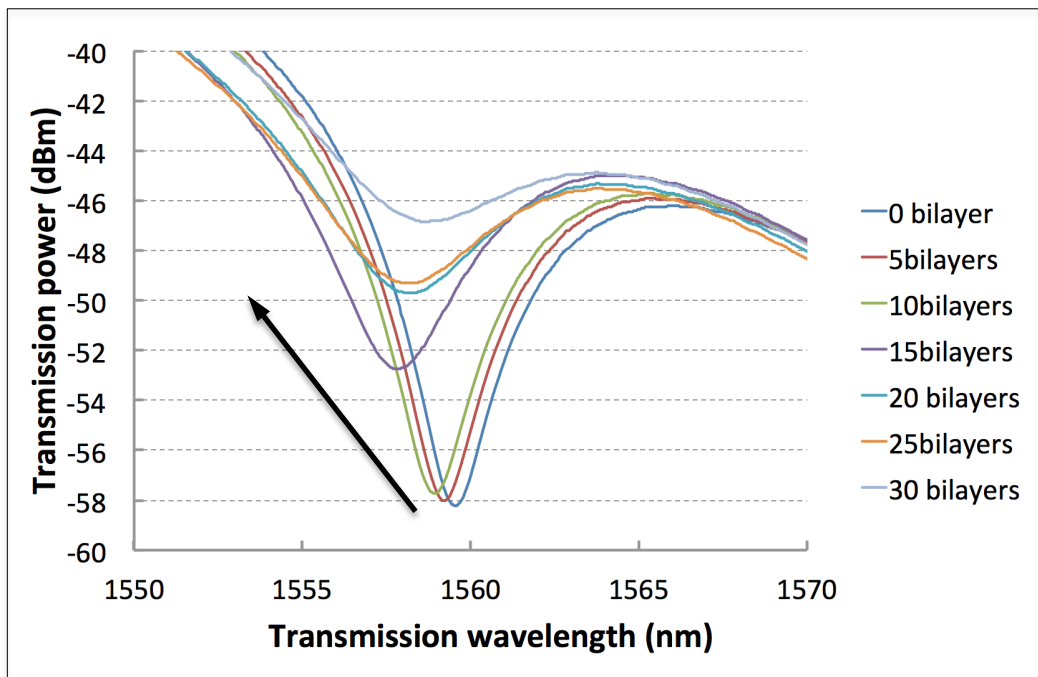
The main purpose of coating PE layers onto the LPFG gratings was to improve its sensitivity towards the external index. The spectra shown in Figure 4.2 represents the transmission power responses of both LPFGs in water, before and after they were coated with the increasing number of PDDA/PSS bilayers. In the experiment, the output spectra of the LPFGs were recorded after the deposition of every five bilayers (10 layers of PE) to investigate the effect of film thickness on the resonant wavelength of LPFG. As can be seen, the responses of both LPFGs encountered similar trends, in which their resonant wavelengths encountered blue-shift after every five bilayers of coating. This indicates that the increasing of the thin film thickness causes the resonant wavelength of LPFG to shift towards a shorter wavelength.

By increasing the thickness of the PE bilayers, the effective refractive index of cladding is increased, therefore decreasing the differential effective indices between core and cladding mode. According to the phase matching condition as shown in Equation (2.37), a decrement in the differential effective indices will lead to lower resonant wavelength (Rego *et al.*, 2013). This observation is in good agreement with the investigations done in 2009 and 2015, where the resonant wavelengths of LPFGs shifted to a lower wavelength after the deposition of thin film material (Li *et al.*, 2014; Loh *et al.*, 2015).

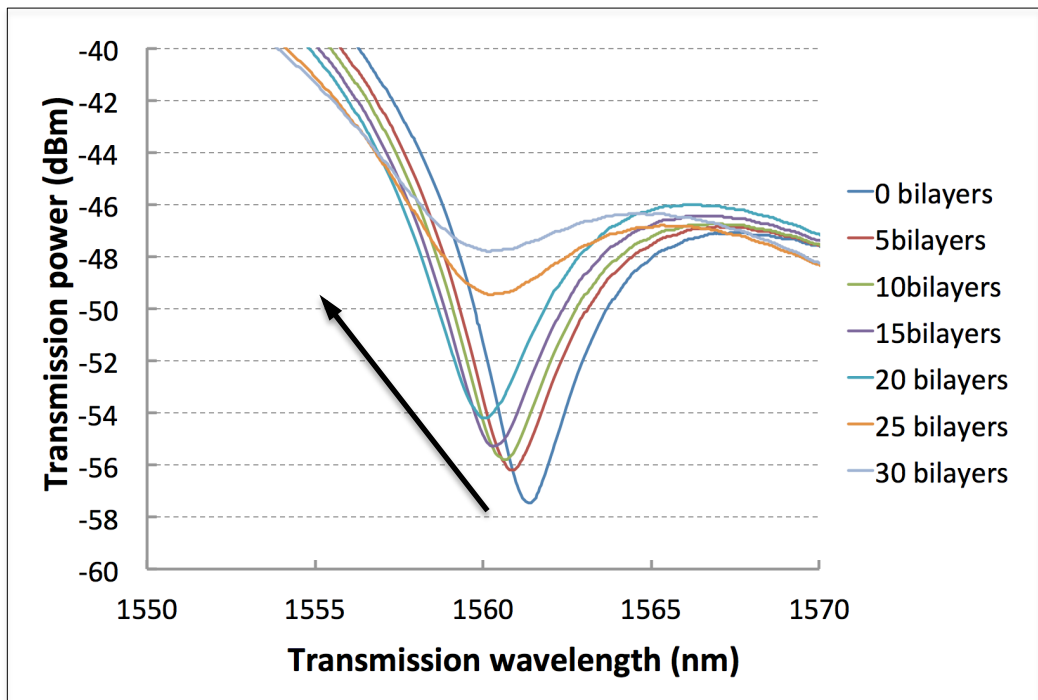
According to the research reported by Rees *et al.*, the continuous deposition of thin film materials caused the external index to approach to the refractive index of fiber cladding. The closer the refractive index of external medium to the cladding index, the higher the grating sensitivity which leads to larger wavelength shift. However, there will be a point where the further deposition of PE layers will match the external RI to the cladding index ( $n_3 \cong n_{cl}$ ). In this case, the cladding will act as an infinitely extended medium as its radius is infinitely large. The discrete guided mode will no longer be supported at this moment. Instead, broadband radiation mode coupling will occur with no distinct transmission band observed (Venugopalan *et al.*, 2008; Czaplá *et al.*, 2015). In other words, the transmission notch of the LPFG will disappear as the average refractive index of external medium equals to the cladding index. The disappearance of the resonance notch makes it impossible to follow and observe the resonance change of LPFG (Rego *et al.*, 2013). Due to this, care must be taken to stop the deposition process before reaching this

particular point to maximise the sensitivity of LPFG and avoid the disappearance of the LPFG notch.

According to the spectra obtained in this experiment, the resonance wavelengths of both LPFGs are close to disappearance when the coating reached 30 bilayers. Hence, the deposition process was stopped after this and it can be concluded that the optimum number of PE bilayers for both LPFGs is 30 bilayers (60 layers of coating).



(a)



(b)

Figure 4.2 Transmission spectra of (a) LPFG 1 and (b) LPFG 2 in water in accordance to the increment number of bilayers

#### 4.2.2 Characterization of PE-coated LPFG towards Refractive Index

It is well-known that the sensitivity of gratings increases as the average refractive index of external medium approaches the index of cladding (Ishaq *et al.*, 2005). In order to evaluate the influence of coated PE bilayers towards the sensitivity of LPFG, an experiment was carried out with different concentrations of sucrose solutions. The experiment setup was similar as the one demonstrated in Chapter 3, where the measurand was dripped onto the groove of the glass cell fixture until the gratings section was fully soaked in the solution. After the deposition of the first five bilayers of PE onto the LPFG gratings, the PE-coated LPFG was tested with different concentrations of sucrose solutions ranging from 0% to 60% to observe their sensitivity towards different refractive indices. The spectral responses of LPFG in different concentrations were recorded throughout the whole experiment. In between the testing with different concentrations of sucrose solution, the previous measurand was removed from the fixture, followed by cleaning and rinsing both LPFG and fixture with DI water to remove residue. After testing every concentration of sucrose solution, the deposition process of PE bilayers proceeded for another five bilayers. A similar experiment was repeated after every deposition of five bilayers, *i.e.* from (PDDA/PSS)<sub>5</sub>, (PDDA/PSS)<sub>10</sub>, up to (PDDA/PSS)<sub>30</sub>. Also, the exact same experiment was repeated with another arc-induced LPFG to evaluate the consistency of the LPFGs' performances.

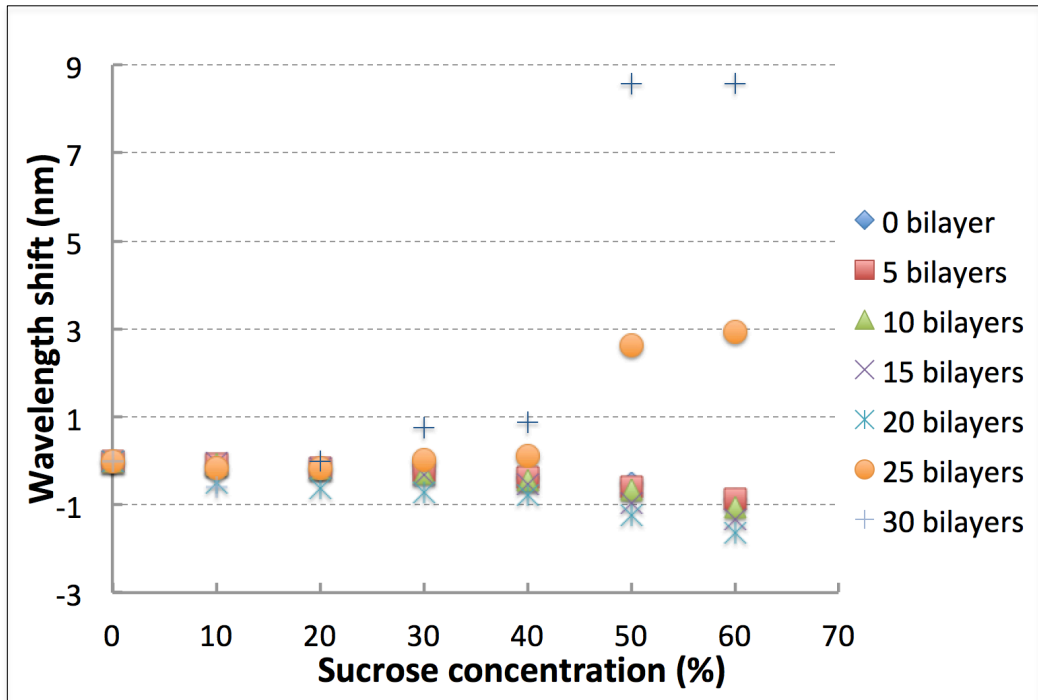
#### 4.2.2.1 Results and Discussions

This experiment was conducted to investigate the effect of increasing the number of PE bilayers deposition to the sensitivity of LPFGs towards different concentrations. When LPFG was coated with a certain material, there was a small amount of optical power which radiated within the coated material and caused the shifting of the LPFG resonant wavelength. The amount of the shifting relied highly on the thickness of the coating film. As the thickness of the coating approached a certain thickness, the optical power in the coated material reached a higher value, and a similar situation goes to the evanescent wave that interacted with the surrounding medium. As a result, higher sensitivity towards the surrounding refractive index was achieved. (Villar *et al.*, 2005).

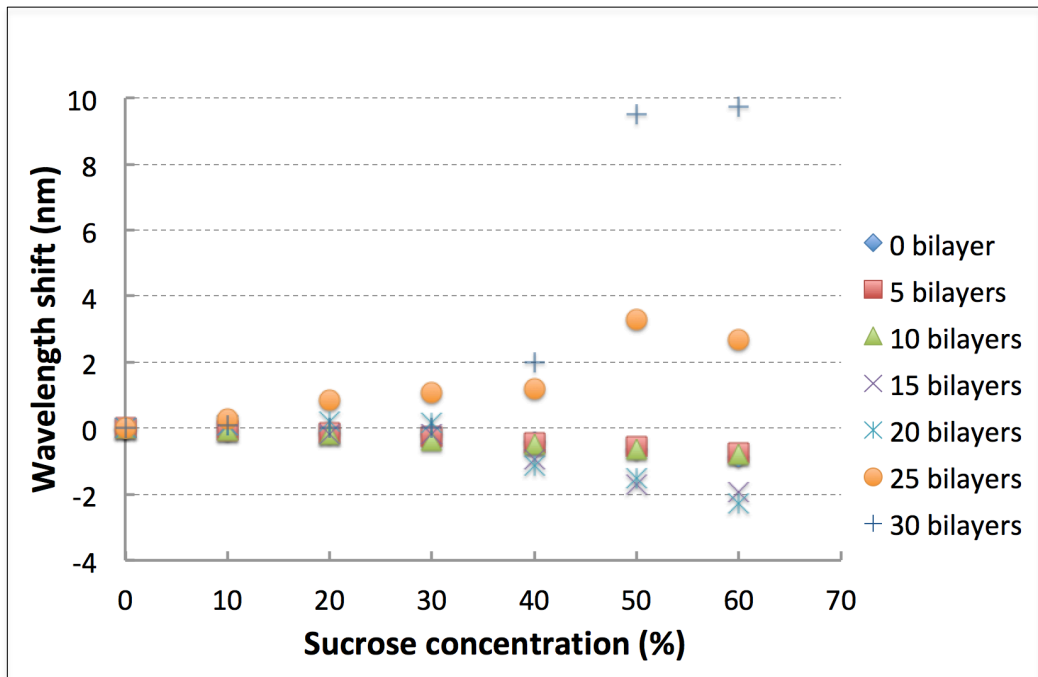
The comparison of LPFG performances in accordance to the increment number of bilayers are shown in Figure 4.3. For the deposition of PE from 0 bilayer to 20 bilayers, the resonance wavelength of both LPFGs encountered blue shift to a shorter wavelength as the sucrose concentration increased from 0 % to 60 %. The downshift of the resonance wavelength was caused by the increment in refractive index when the sucrose solutions became more concentrated (Li *et al.*, 2011). As the deposition on LPFG became thicker (number of bilayers increased), the wavelength shift of LPFG in accordance to different concentrations was slightly increased as well. This is because the increment in the number of bilayers increased the thickness of the thin film on the grating surface, thus increasing the effective index of the LPFG cladding

modes and led to larger wavelength shift, *i.e.* higher sensitivity (Alwis *et al.*, 2013). Although the sensitivity improved, the difference in wavelength shifts was still not significant as the deposition of PE reached to 20 bilayers. The maximum wavelength shift observed was only near to 1.65nm for first LPFG and 2.28 nm for the second LPFG.

The wavelength shifts of both LPFGs were most prominent towards changes in refractive index when the coating went up to 30 bilayers (60 layers). As observed, there was a drastic increase in the wavelength shift between 40 % and 50 % of sucrose solutions. For LPFG 1, the resonance wavelength encountered a maximum of 8.5658 nm, whereas LPFG 2 shifted a maximum of 9.5262 nm to longer wavelength when immersing in 50 % of sucrose solution. Referring to the previous section, the resonance wavelengths of both LPFGs almost disappeared as the coating reached 30 bilayers. According to Rego *et al.* (2013), the performance of LPFG was optimized in this region, in which the sensitivity was significantly improved and it was still possible to trace the resonant change of LPFG. The results obtained in this experiment proved that 30 bilayers was the optimum number of coating for these two LPFGs as the wavelength shift was found to be highest if compared to a lower number of bilayers. On the other hand, it was proven that the thin film coating technique was suitable to be employed to enlarge the wavelength shift of LPFG, hence achieving higher sensitivity for the wavelength-based interrogation method.



(a)



(b)

Figure 4.3 Wavelength shift of (a) LPFG 1; (b) LPFG 2 coated with increasing number of PE bilayers in accordance to different concentrations of sucrose solution

### 4.3 Double-Pass Configuration

It had been reported that the interrogation of the sensitivity of LPFG towards external perturbation had extended in recent years to focus on the variation in the minimum transmission power of LPFG resonant notch, *i.e.* transmission-based interrogation. In this research, the second enhancement technique that was employed to improve LPFG sensitivity was the double-pass configuration. This configuration was proposed in 2014 by Loh *et al.* to increase the transmission loss at resonant wavelength of LPFG and enhance the sensitivity of LPFG towards the external index for transmission-based interrogation. The mechanism of double-pass configuration was based on the minimum transmission power equation of the LPFG attenuation band, which can be expressed as (Kashyap *et al.*, 1999):

$$T_m = \cos^2(\kappa_m)L \quad (4.1)$$

where  $T_m$  indicates the minimum transmission power of the LPFG resonant notch while  $\kappa_m$  represents the coupling coefficient for the  $m^{th}$  mode of fiber cladding. In addition, the length of the LPFG is indicated as  $L$ .

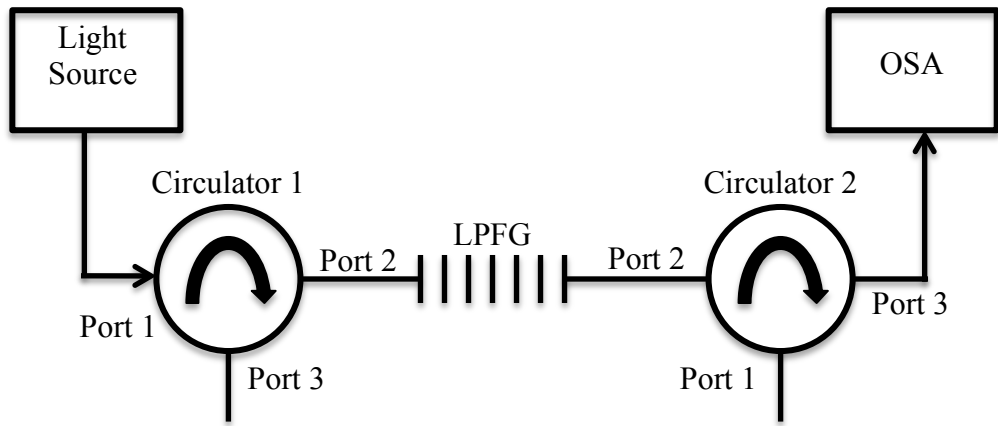
In double-pass configuration, two circulators were introduced to the setup to allow the light to pass through a longer path. The longer the path where the light passes through the LPFG gratings, the more enhanced the coupling in between core and cladding mode, which will hence increase the transmission loss of the LPFG (Loh *et al.*, 2014). With the addition of

circulators, the light will pass through the gratings region twice. According to the minimum transmission power equation, the transmission power of double-pass configuration will be doubled if compared to single-pass due to the recirculation of light:

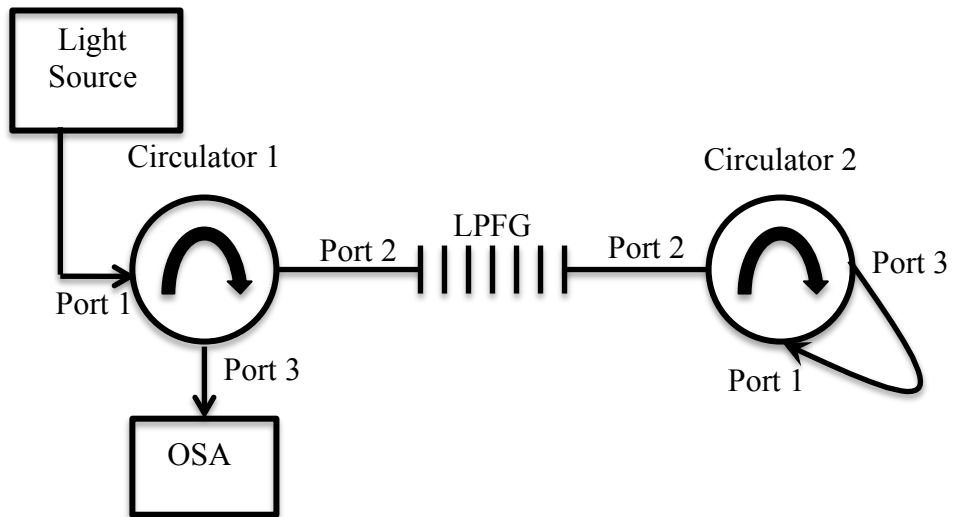
$$T_m = 2 \times \cos^2(\kappa_m)L \quad (4.2)$$

### 4.3.1 Single-Pass Configuration versus Double-Pass Configuration

Figure 4.4 illustrates the configurations for both single- and double-pass systems. From the illustration, the broadband light signal will only pass through LPFG once in a single-pass configuration. The signal from the broadband light source will enter Circulator 1 through Port 1 and pass through LPFG before reaching Circulator 2. Then, it will directly exit to the OSA through Port 2 of the second circulator. The setup for double-pass configuration is rather similar to single-pass configuration, except that Port 3 of Circulator 2 will be connected directly to Port 1, and the light will exit to OSA through Port 3 of Circulator 1 instead. In this setup, the light signal will pass through LPFG twice so that the transmission loss will be doubled. The light first enters through Port 1 of the first circulator and then passes through LPFG and reaches Circulator 2. Consequently, the light will be re-circulated back to the LPFG by Circulator 2 from Port 3 to Port 1. The double-passed light signal will then re-enter Circulator 1 after passing through LPFG and finally exit the OSA through Port 3.



(a)

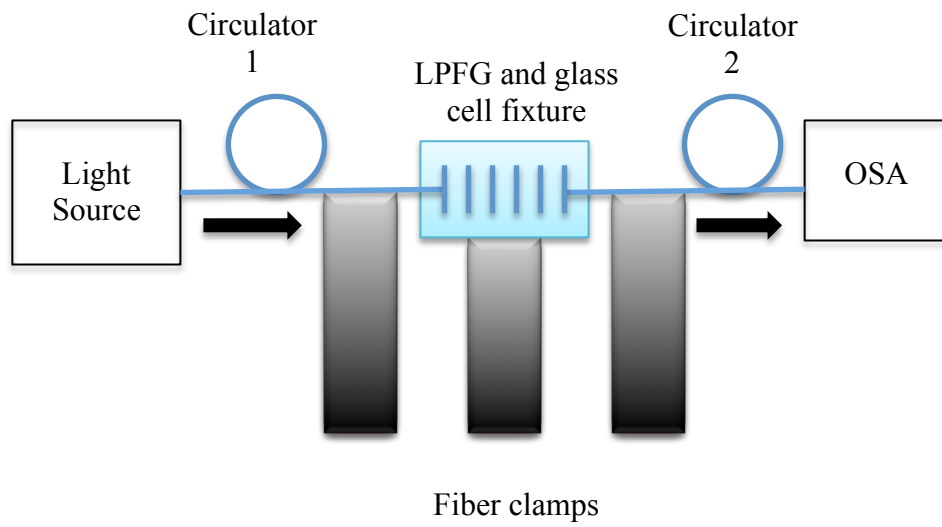


(b)

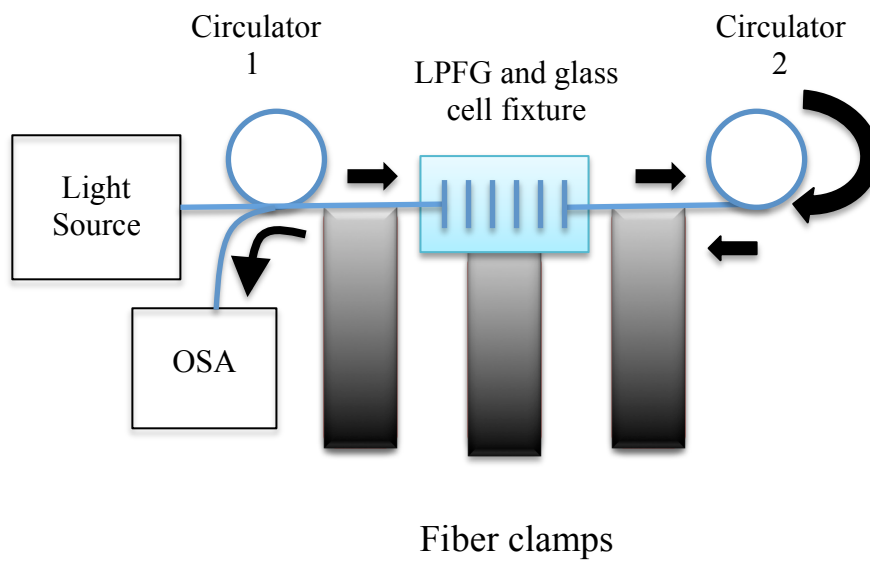
Figure 4.4 Illustration of (a) Single-Pass Configuration; (b) Double-Pass Configuration

### 4.3.2 Characterization of LPFG with Double-Pass Configuration

The sensitivity of LPFG towards the external RI was investigated in this section in order to characterize the influence of double-pass configuration on the performance of LPFG. An experiment was carried out with liquid oils (Cargille oil) of different refractive indices ranging from 1.40 to 1.50, with an interval of 0.01. The experiment setup is shown in Figure 4.5. The gratings section of the arc-induced LPFG was first positioned in the groove of the glass cell fixture, with both fiber ends fixed by fiber clamps. Consequently, a constant axial tension of 18 cN was applied to one end of the LPFG throughout the whole experiment to avoid any bending effects and ensure that the fiber gratings were kept straight on the fixture between the fiber clamps. During the experiment, the initial transmission response of the LPFG was recorded as a reference point. Then, the refractive index matching oil was carefully dropped onto the glass cell fixture until the gratings section was fully soaked in the refractive index oils. Before changing the measurand to different RI matching oils, the gratings section of the LPFG was cleaned by acetone and followed by isopropyl alcohol to remove the residue from the previous measurand until the transmission spectrum of the LPFG was similar with the initial reading. The same cleaning process was applied to the glass cell fixture as well. Throughout the experiment, the output spectra of the LPFG was recorded for both single- and double-pass configurations. Finally, a similar experiment was repeated with another arc-induced LPFG to investigate the consistency of their performances in both single and double-pass configurations.



(a)



(b)

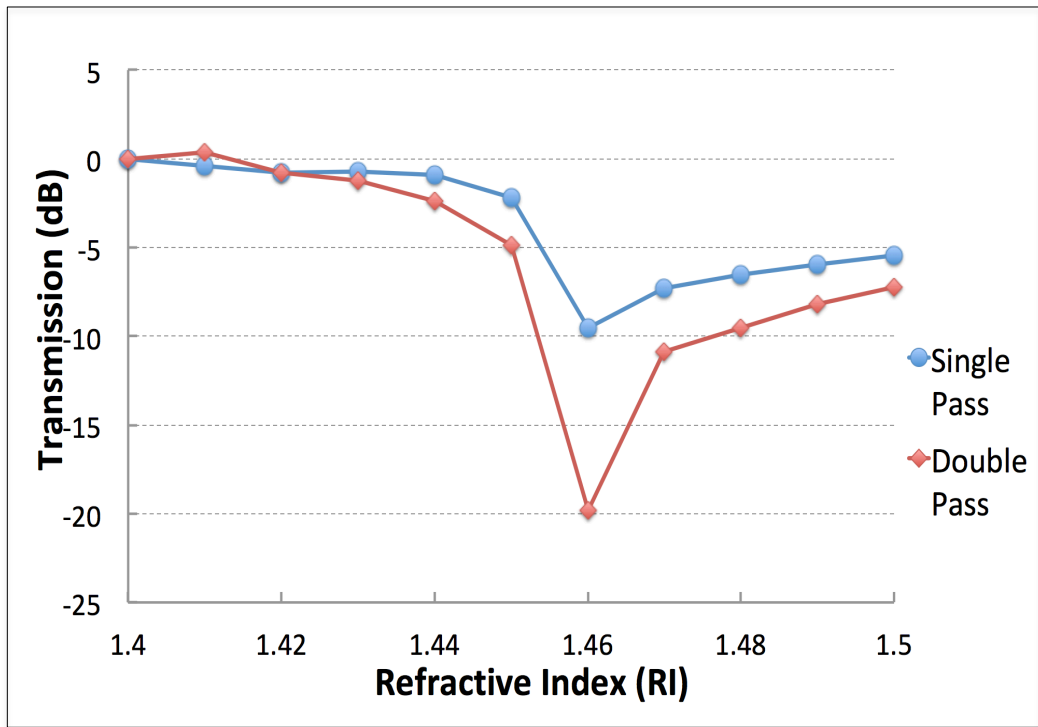
Figure 4.5 Experimental setup for (a) Single-pass configuration;  
(b) Double-pass configuration

#### 4.3.2.1 Results and Discussions

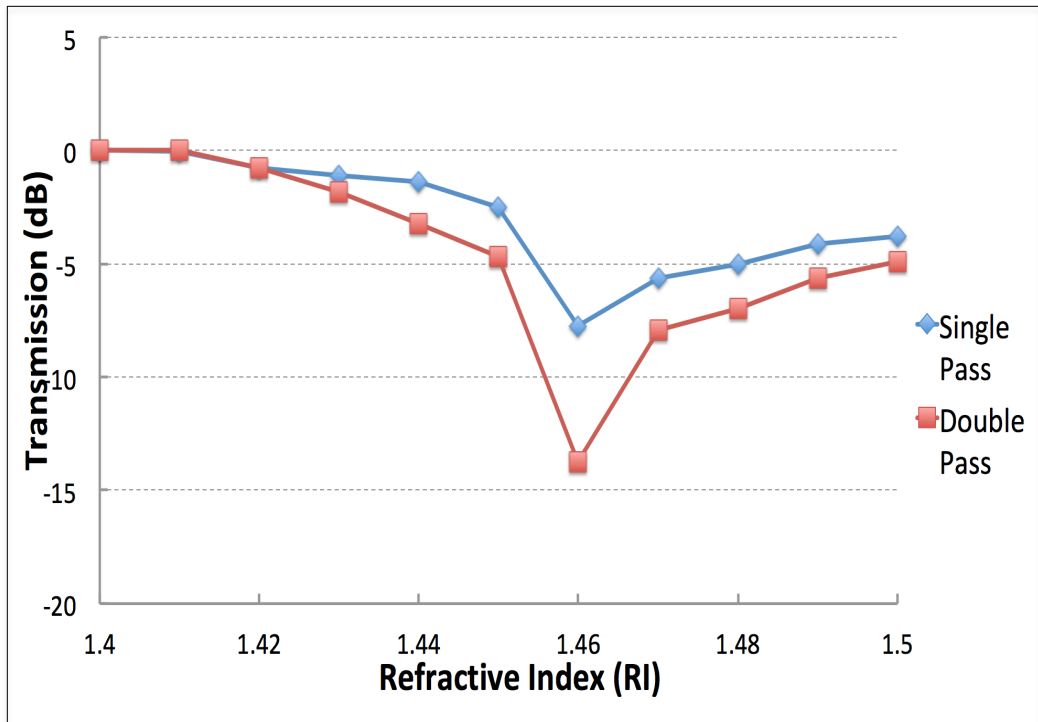
The results shown in Figure 4.6 present the comparison of LPFG responses towards refractive index changes for both single-pass and double-pass configurations. As can be seen from the comparison, both the transmissions of single- and double-pass configurations encountered similar trends. However, the transmission loss of double-pass configuration was nearly twice the transmission loss of single-pass configuration. If referring to the performance of the first LPFG, the gradient of transmission of the double-pass configuration in RI range from 1.40 to 1.45 was around  $-97.26$  dB/RI, whereas for single-pass configuration, the gradient was  $-43.72$  dB/RI. If referring to the LPFG transmission in RI range from 1.45 to 1.46, the gradients of double-pass and single-pass were  $1405.4$  dB/RI and  $735.2$  dB/RI, respectively. On the other hand, the gradient was found to be  $120.03$  dB/RI for double-pass and  $60.8$  dB/RI for single-pass configurations in the RI range from 1.47 to 1.50. By dividing the values of gradients for both single- and double-pass configurations, the gradient of double-pass configuration was approximately twice the gradient of single-pass. On the other hand, the transmission loss was found to be highest in RI of 1.46. This indicates that the LPFG was most sensitive to the RI changes between 1.45 and 1.46 because this refractive index range was very close to the cladding index (Patrick *et al.*, 1998).

Similar findings were obtained from the transmission response of the second LPFG. In the RI range of 1.40 to 1.45, the gradients of single and

double passes were found to be 49.7 dB/RI and 93.96 dB/RI respectively. On the other hand, the gradients of both single and double-pass configurations in RI range from 1.45 to 1.46 were 525.3 dB/RI and 905.1 dB/RI. In addition, the gradient of single-pass when RI increased from 1.47 to 1.50 was 62.7 dB/RI, whereas for double-pass configuration, the gradient was 101.03 dB/RI. From the results obtained, the gradient of double-pass was close to two times of the single-pass configuration. Therefore, it can be concluded that the usage of double-pass configuration can help to improve the overall sensitivity of existing LPFG up to almost double for transmission-based interrogation. In double-pass system, the enhancement in the sensitivity of LPFG was mainly induced by the longer distance where the light passed through the grating sections of the fiber. This led to the improvement in overlap integral, hence, better coupling between core and cladding modes occurred (Loh *et al.*, 2014; Yong *et al.*, 2015). As a result, the transmission loss increased and higher sensitivity towards the refractive index was achieved.



(a)



(b)

Figure 4.6 Comparison of spectra in accordance to external refractive index for (a) first LPFG; (b) second LPFG in both single- and double-pass configurations

### **4.3.3 Characterization of PE-Coated LPFG with Double-Pass Configuration**

The previous experiment proved that the usage of double-pass configuration could increase the variation in minimum transmission power of LPFG in response to different refractive indices. In order to further evaluate the influence of this enhancement technique, a similar experiment was conducted to the first LPFG that was coated with 30 bilayers of PE as discussed in Section 4.2. Again, both single-pass and double-pass configurations were used in the experiment to compare the transmission responses of the coated LPFG in different concentrations of sucrose solutions, ranging from 0% up to 60%. This aimed to increase the variation in transmission power of the PE-coated LPFG towards increasing concentration. By combining both thin-film coating method and double-pass configuration, the wavelength shift and variation in transmission power of LPFG in accordance to the increment in sucrose concentration can be improved.

#### *4.3.3.1 Results and Discussions*

In Figure 4.7, the comparison of the normalized transmission power for the PE-coated LPFG in both single- and double-pass systems is presented. Referring to the figure, the response of LPFG in both configurations present similar trends. For single-pass configuration, the gradient of the normalized transmission power was found to be  $-0.0010$  a.u./% as the concentration of sucrose increased from 0% to 40%. Moreover, the gradient of the normalized transmission power was  $-0.0019$  a.u./% for double-pass configuration. By dividing the gradient of double-pass by the gradient value of single-pass, it was obtained that the double-pass was 1.9 times the value of single-pass. On the other hand, as the concentration of sucrose solution increased from 40% to 50%, the gradients of normalized transmission power for single- and double-pass configurations were  $0.0063$  a.u./% and  $0.0123$  a.u./%, respectively. Again, the gradient of double-pass configuration was almost double that of single-pass configuration. For single-pass configuration, the gradient of normalized transmission power between 50 % and 60 % of sucrose concentrations was  $0.0020$  a.u./%, while the gradient for double-pass configuration was  $0.0030$  a.u./%. This shows that the double-pass system was 1.5 times of the gradient of single-pass.

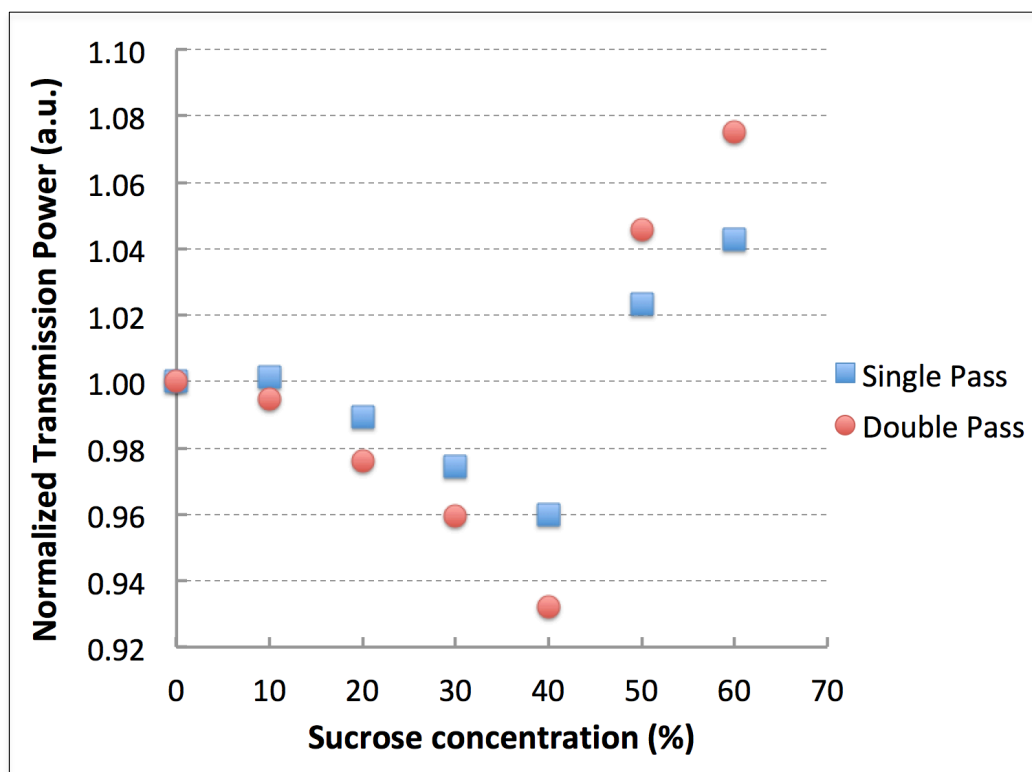


Figure 4.7 Comparison of normalized transmission attenuation for both single- and double-pass configurations in sucrose solutions ranging from 0 % to 60 %

#### 4.4 Summary

It has been proven that the sensitivity of LPFG towards the surrounding refractive index can be evaluated through both wavelength-based and transmission-based interrogation methods. Also, the arc-induced LPFG used in this research had been sensitized with two methods, *i.e.* thin film coating and double-pass configuration. The results showed that the shifting of the resonant wavelength of the sensitized LPFG in sucrose solutions had significantly improved by depositing the optimum number of polyelectrolytes

bilayers onto the fiber grating. The main advantage of this ESA thin film coating is that it provides flexibility in which the coating materials are not limited to only polyelectrolytes, but any charged nano-objects such as gold nanoparticles which can be used as film materials. Hence, apart from improving the LPFG sensitivity, the ESA coating used in this section is also a preparation for the deposition of nanoparticles in the next stage of this research. On the other hand, experiments proved that the usage of a double-pass configuration had increased the transmission attenuation of the LPFG resonant notch, hence improving its sensitivity for transmission-based interrogation. From the results, it can be observed that the variation in the minimum transmission power of the LPFG resonant notch in the double-pass system was nearly doubled compared to the single-pass configuration. The main benefit of this enhancement technique is that it does not require further physical modification on the structure of LPFG such as etching. Also, this sensitization technique can be applied to any LPFG in different sensing applications. By combining these enhancement methods, the sensitivity of arc-induced LPFG was now improved and ready to be further modified for sensing application, which will be discussed in the next chapter.

## CHAPTER 5

### DETECTION OF MERCURY (II) IONS BY POLYELECTROLYTE- GOLD NANOPARTICLES COATED LPFG

In the previous chapter, the sensitivity of arc-induced LPFG was improved by increasing its wavelength shift and transmission variation in response to different refractive indices. In this section, both sensitization methods demonstrated in Chapter 4 were employed and the surface of the sensitized LPFG was further modified for mercury (II) ions detection purposes. A novel combination of coating materials, *i.e.* polyelectrolytes and gold nanoparticles was introduced in this research to modify the surface of the arc-induced LPFG so that it responds to the presence of mercury (II) ions. In short, the first deposition of polyelectrolytes was used to increase the overall sensitivity whereas the deposition of gold nanoparticles was used as the selective agent to detect mercury (II) ions. To evaluate the performance of the modified LPFG, the sensor was experimented with five different concentrations of mercury (II) solutions. With reference to the results obtained, it was proven that the polyelectrolytes-gold nanoparticles coated LPFG was able to detect mercury (II) ions in water. Also, results showed that the proposed sensor was suitable to be used for real-time monitoring purposes.

## 5.1 Introduction

Water is one of the most basic necessities required to sustain life (Hossain *et al.*, 2015). Thus, the purity and quality of water has become a crucial concern in modern civilization as the consumption of contaminated water may lead to serious health risks (Pawari *et al.*, 2015). Recently, the pollution of water bodies has become a severe environmental issue that requires attention, especially when ecosystems and human health are threatened (Halder *et al.*, 2015; Desai *et al.*, 2014). The pollution of water bodies can be defined as the contamination of water due to the presence of certain foreign substances, which may degrade the water quality and bring different health hazards (Myers *et al.*, 2015). It had been suggested that water pollution has become one of the leading worldwide causes of deaths and diseases (Pink *et al.*, 2006), and one of the main culprits that causes the contamination of water bodies is the discharging of waste water that consists of heavy metal elements such as mercury, cadmium and lead (Haseena *et al.*, 2017).

Mercury is one of the most hazardous heavy metals, which can lead to serious health issues affecting the neurological, renal organ and gastrointestinal systems of human bodies (Rice *et al.*, 2014). Due to this, the monitoring of mercury within water sources is extremely important due to its toxicity. A lot of effort had been made throughout the past several decades in identifying different techniques to detect mercury contents. Among the techniques proposed, optical-based sensors were one of the most commonly

proposed devices, which included the Surface Enhanced Raman Scattering sensors, surface plasmon resonance sensors, fluorescent sensors, colourimetric sensors and others (Wang *et al.*, 2009; Fen *et al.*, 2011; Li *et al.*, 2011; Du *et al.*, 2015). There are a few advantages of optical-based sensors which makes them to become favourite devices to be used as sensors, including their immunity to electromagnetic interference, the smaller sizes and lightweight, as well as the ease in signal transmission (Krohn *et al.*, 2015).

Nonetheless, most of the demonstrated optical sensors involved active sampling techniques before conducting the mercury detection process. In other words, solutions to be analyzed were required to be collected from the real site before sent to the laboratory for testing, which means that the sensors were not suitable to be directly deployed in the real environment for detection purposes. Therefore, a limitation was found if the sensing application had to be extended outside laboratory. Due to this, there was a need to identify a sensor which can be used for both laboratory testing and which can be deployed in the real environment.

In this research, the sensor that was proposed for the detection of mercury was Long Period Fiber Grating (LPFG) due to a few advantages that it offers. First and foremost, LPFG can be deployed kilometres away and at multiple points, where an electric source is not needed at the sensing point. This means that it can be deployed outside the laboratory for testing purposes (Lin *et al.*, 2009; Yong *et al.*, 2017). This advantage helps to overcome the limitation found in other optical-based sensors. Furthermore, with some

specific modifications done to the surface, LPFG can be applied to detect different elements due to its unique property, *i.e.* the sensitivity to external parameters. In this chapter, gold nanoparticle was coated onto the gratings section of LPFG to modify its surface. Gold nanoparticles were chosen as the sensing agent due to its reactions with mercury that led to the formation of another substance, amalgam (Levlin *et al.*, 1999). To date, not much research has been done on employing LPFG for the real-time monitoring of mercury (II) ions in water.

## **5.2 Mercury in the Environment**

Mercury is a kind of heavy metal that occurs naturally in the crust of the Earth. In the periodic table, it is represented by the symbol “Hg” and has an atomic number of 80. Due to its bio-accumulative property and toxicity towards the environment and living beings, mercury has become a serious issue when it is released into the environment, both in the atmosphere and in water (Kidd *et al.*, 2003).

### **5.2.1 Sources of Mercury**

Over the years, there have been reports that the emissions and levels of mercury in the environment are increasing day by day. An estimation of the global emission of mercury into the environment was in the range of 5000 to 8000 metric tonnes each year (Romanov *et al.*, 2017). The sources of the emission of mercury into the environment can be divided into two categories.

The first category is induced by emissions from natural geological activities, including volcanic activities and eruptions, forest fires and the weathering of rocks (Pirrone *et al.*, 2010).

However, it has been reported that the main factor which causes the release of mercury into the environment is due to anthropogenic activities, which comprises at least 50 percent of all mercury emissions (Gworek *et al.*, 2017). According to data reported in 2010, the amount of mercury released into the atmosphere caused by anthropogenic activities alone was estimated to be 1960 metric tonnes, while emission into oceans was at least 1000 metric tonnes (UNEP, 2013). Different activities conducted by humans that can cause the emission of mercury includes the combustion of fossil fuels and coal, the mining of metals, and the emission of hazardous chemical waste from industries and medical processes (Gade *et al.*, 2015).

### **5.2.2 Impacts of Mercury**

Mercury is an element that is very dangerous, and can lead to significant issues to both the environment and human health. Due to the high persistency of mercury, all sources of mercury are of concern as it can be re-introduced into the environment through natural processes such as evaporation of water. On the other hand, those that are emitted into the atmosphere will be transported and deposited on the surface of Earth again by rain (Lourie *et al.*, 2003). Mercury is hazardous because of its ability to bio-accumulate and bio-magnify in the ecosystems and bodies of living beings, in other words, its

concentration tends to increase with time (Schmitt *et al.*, 2011). Mercury contamination has long been known to be toxic to both public health and environment.

#### *5.2.2.1 Environmental Impacts*

Ecological disturbance is the major environmental impact found due to the contamination of mercury. Food, primarily fish, has become the most significant source of mercury exposure for the general population. Fish and aquatic life are known as the main source of food for many animals including birds. When water sources such as oceans and rivers are contaminated by mercury, it will then be ingested by aquatic life and fish. The health of predators that mainly rely on aquatic life as a food source such as loons and eagles will be damaged. For instance, the ability to reproduce of Minnesota loons might be affected and impaired due to the intake and accumulation of mercury (Ensor *et al.*, 1992). On the other hand, another example of the influence of mercury to the environment was seen at the Minamata Bay, after the serious mercury poisoning incident caused by a chemical plant. Serious neurological effects were observed in the animals and wildlife that lived near the Minamata Bay (Yorifuji *et al.*, 2013). Birds were found to be experience difficulty in flying, and exhibited abnormal behaviour. Furthermore, wildlife that was exposed to mercury were found to have organ impairment such as liver and kidney damage. Also, the emission of mercury is suggested to have affected the ecosystem of the nature. For example, the contamination of mercury caused the reduction in microbiological activity, which is crucial to

the terrestrial food chain. As a result, all the other species within that food web are then affected and causing an ecological imbalance (Driscoll *et al.*, 2007).

#### 5.2.2.2 Health Impacts

All humans are exposed to a certain low level of mercury in their daily lives, often through chronic exposure (continuous or intermittent long-term contact). However, due to the increase of the pollution caused by mercury, the exposure of humans to mercury has greatly accelerated. Human exposure to mercury can occur through different channels. One of the major routes is through the consumption of aquatic life, especially fish (Ruiz-Guzman *et al.*, 2014). As mentioned earlier, the mercury contaminants that are emitted into the environment and water bodies will be ingested, then bio-accumulate in the tissues of aquatic life and fish. Consequently, the contaminant is passed up the natural food chain and eventually reaches humans (Driscoll *et al.*, 2007). Hence, fish have become the most significant source of mercury exposure for the other population.

Exposure to mercury can lead to a variety of health impacts. First and foremost, mercury is a well-known neurotoxin, which can cause serious damage to the neurological system. High exposure to mercury may cause adverse effects to both the brain and spinal cord of human bodies. Symptoms such as tremors, loss of memory, insomnia and motor dysfunction might occur in human bodies due to the high exposure to mercury (Bernhoft *et al.*, 2012). A research was conducted in 2000 to observe the effect of mercury exposure

to the nerve system, where they found out that the presence of mercury inhibits the binding of GTP to the brain tubulin, thereby inhibiting the polymerization of tubulin into microtubules. Also, the research has demonstrated that the exposure to mercury ions causes the failing of neuronal somata to sprout. The research has concluded that mercury is a potential etiological factor in neurodegeneration (Leong *et al.*, 2001).

The greatest risk is for foetuses or young children because of the ongoing developing process of their brain and nervous systems. The exposure of the foetus towards mercury usually occurs when the contaminant in the pregnant mother's bloodstream is transported across the placenta into the foetus (Minai *et al.*, 2016). Low doses of mercury in the bodies of pregnant women have been shown to have impacts on the foetuses which includes the poor performance on neurobehavioral tests, particularly on tests of attention, fine-motor function as well as verbal memory, language, visual-spatial abilities. In addition, the exposure to mercury can destroy and impair different organs in human bodies, including the gastrointestinal and renal organs. Moreover, the exposure to mercury can alter the heart rate of human bodies which then lead to the increment of heart attack risk and cause disturbances to the human immune processes. Recent epidemiological studies found out the associations between exposure to low level of mercury content and adverse cardiovascular effects. One of the most serious mercury poisoning cases happened in Minamata, Japan, in 1956, due to the release of mercury in the industrial wastewater by a chemical factory. Symptoms such as muscle weakness, loss of peripheral vision and hearing were first discovered within

the population who stayed near the Minamata Bay. The poisoning then worsened and issues such as insanity, coma and fatalities were discovered within weeks of the discovered mercury poisoning symptoms (Semionov *et al.*, 2018).

Realizing the severe consequences of this issue, an international treaty was designed and approved in 2013 by approximately 140 countries as a global effort to protect the natural ecosystem and human health from further threats by mercury, which named as the “Minamata Convention on Mercury”. This convention addressed the control and reductions of the content of mercury used and the waste emitted in industries and different processes (Selin *et al.*, 2018). Apart from this, the management of mercury has become an important issue to the world due to the harmful effects of mercury exposure. Particularly, attention has been drawn in finding measurements, not only for reducing and limiting the release of mercury into the environment, but also for the monitoring and detection of mercury in water bodies. Different techniques and methods to monitor mercury content have been proposed and demonstrated over the last few decades.

### **5.3 History of Mercury Detection**

Over the years, many researches were conducted to detect mercury in water. Among the sensors proposed, optical-based type sensors were the most commonly used devices, and they can be classified into colourimetric, Fluorescent and Surface Enhanced Raman Scattering (SERS) sensors.

### 5.3.1 Colourimetric Sensor

The colourimetric sensor was one of the sensors utilised for mercury detection. Sensing using the colourimetric sensor usually involves the collection of analytes from the site, followed by testing in a laboratory. The response of the sensor towards the analytes can be easily read by naked human eyes. Also, it can be investigated concisely using UV-vis spectrometry (Duan *et al.*, 2015). In the detection of mercury (II) ions by colourimetric sensor, gold nanoparticles were one of the most commonly used colourimetric reporters because of their strong absorption properties and high visible-region extinction coefficients. The main mechanism of mercury (II) ions detection in colourimetric sensor is based on the fact that mercury (II) ions could induce the re-dispersion and aggregation reaction of gold nanoparticles, and as a result, generates a colour change in the solution varying from red to blue, depending on the concentration of mercury (II) ions added. This colour-change behaviour depends on the interparticle distance of gold nanoparticles, where the colour will change from red to blue when the interparticle distance between the gold nanoparticles becomes less than the average particle diameter. One of the examples of mercury (II) ions detection by colourimetric sensor was proposed in 2015 (Du *et al.*, 2015). The gold nanoparticles used in the investigation was decorated with a thymine derivative modified with quaternary ammonium salt (N-T). The initial colour of the modified gold nanoparticles solution was red with a SPR band at 520 nm. After 1  $\mu$ M of mercury (II) ions was added into the system, the red colour of the solution changed to blue, with a new SPR peak appearing at 650 nm.

### 5.3.2 Fluorescent Sensor

Fluorescent sensors were also able to detect mercury. Similarly, the analytes were usually collected from the real environment such as river water before it was filtered and tested in the laboratory. The mechanism of a fluorescent sensor in detecting analytes is based on analyzing the change of intensity and wavelength of fluorescents after mercury (II) ions was added. One of the commonly used fluorescent sensors is the quantum dot (QD) based sensor. After being excited by different wavelengths of light, QDs emit fluorescence and the intensity of fluorescent signals can be used to indicate changes in the surface. The basis of the QD-based fluorescent sensor is on their sensitivity to the surface states. Any physical or chemical interactions between the analytes and the surface of QDs leads to changes in the efficiency of the radiative electron-hole recombination, resulting in luminescence quenching or activation of QDs. In mercury detection, the interaction between mercury ions and the QDs results in a fluorescence quenching that can be explained by the electron transfer process between the surface of QDs and mercury ions. One of the mercury sensing applications using QD was reported in 2011, where an ensemble of QDs/DNA/gold nanoparticles was used to detect mercury (II) ions. When mercury (II) ions were added to the solution containing the DNA-conjugated QD and gold nanoparticles, hybridization of DNA occurred, causing the nanoparticles to be brought into close proximity with the QDs. As a result, energy transfer occurred and led to the quenching of fluorescence. The result of the conducted research confirmed that the intensity of fluorescent was reduced with the presence of mercury (II) ions. Also, it was

shown that the brightness of the QD diminished remarkably after the addition of 1  $\mu\text{M}$  of mercury (II) ions (Li *et al.*, 2011).

### **5.3.3 Surface Enhanced Raman Scattering (SERS) Sensor**

On the other hand, another optical-based sensor that was demonstrated for the detection of mercury was the Surface Enhanced Raman Scattering (SERS) sensor. SERS is a powerful analytical technique that can provide enhanced Raman signals of the molecules or ions adsorbed on a metallic substrate. Usually the SERS signal can be enhanced with the help of a plasmonic nanostructure. In SERS sensing application, gold nanoparticles are one of the most commonly used substrates due to their optical response in the visible region of the electromagnetic spectrum. When the gold nanoparticles aggregate, an intense electric field which is often called “hotspot” occurs, and a strong SERS signal is observed. The detection route in SERS is based on the inhibited aggregation of nanoparticles or the removal of Raman reporters from the aggregated nanoparticles substrate surface with the presence of mercury (II) ions. An example of mercury detection with SERS was demonstrated in 2009. The interaction between gold nanoparticles and Mercury (II) ions caused the changes in SERS signal of the reporter molecule. This was because the aggregation reagent on the nanoparticles surface was replaced by mercury ions and the binding of mercury ions onto the gold nanoparticles surface affected the aggregation of nanoparticles, which, as a result led to a decrement in the SERS signal (Wang *et al.*, 2009).

There is a main similarity found in all the sensors discussed above, in which most of them focused on the active sampling technique, where the solutions to be analysed were collected from the real site first before the quick test and detection in the laboratory. Hence, if the detection and test needs to be extended outside laboratory, limitations are found with all these sensors as they cannot be directly deployed in the real scenario for real-time monitoring purposes. Hence, the modified LPFG proposed in this chapter aimed to overcome this limitation, as past research has proven that LPFG can be deployed kilometres away and no electric source is required at the sensing point (Yong *et al.*, 2017).

On the other hand, it can be observed that gold nanoparticles are one of the widely used reporters and sensing agents towards mercury (II) ions. Due to the natural affinity of gold for mercury, gold nanoparticles were chosen as the sensing agent in this research to be coated onto the LPFG surface. The main sensing mechanism of this modified LPFG was based on the reaction between gold nanoparticles and mercury (II) ions which then induced the responses of the LPFG.

## **5.4 Gold Nanoparticles coated LPFG**

### **5.4.1 Interaction of Gold Nanoparticles with Mercury**

Gold is known as the neighbour element of mercury in the periodic table. The unique physical properties of these two metals have led to the

inspiration of many investigations and research, especially after the discovery of the adsorption and reaction in between these two metals. (James *et al.*, 2012) The process of bringing gold particles into contact with mercury is known as amalgamation, where a new compound called amalgam is formed after the reaction between gold and mercury (Levlin *et al.*, 1999). As discussed earlier, gold particles were used widely in various kinds of sensors to detect mercury due to their reactions. In this research, gold nanoparticles were used as the sensing agents to be coated onto LPFG to capture mercury ions in water as well.

#### **5.4.2 Synthesis of Gold Nanoparticles**

The gold nanoparticles, AuNP, that were employed in this research were synthesized according to the Frens method developed in 1973 (Frens *et al.*). Generally, the nanoparticles were formed through the basic reduction between gold (III) chloride trihydrate ( $\text{HAuCl}_4 \cdot 3\text{H}_2\text{O}$ ) and trisodium citrate dihydrate ( $\text{Na}_3\text{C}_6\text{H}_5\text{O}_7 \cdot 2\text{H}_2\text{O}$ ). One advantage of using the Frens method in synthesizing gold nanoparticles is that the size of nanoparticles can be controlled by adjusting the mole ratio between the gold and citrate. Initially, both gold (III) chloride trihydrate and trisodium citrate dehydrate were prepared before the synthesis process. 0.01 wt% of gold (III) chloride trihydrate was prepared by dissolving 0.01 g of gold (III) chloride in 100 ml of deionised water. On the other hand, 1 wt% of trisodium citrate dehydrate was prepared by dissolving 1 g of sodium citrate 2-hydrate in 100 ml of deionized water. After that, 50 ml of 0.01 wt% gold (III) chloride trihydrate solution was

heated and stirred to boiling point. Subsequently, a small amount of 1 wt% trisodium citrate dehydrate solution was added gradually to the boiled gold (III) chloride trihydrate solution in a drop-wise method. The solution was then kept heated and stirred until a colour change was discovered. The yellow colour of the solution changed to blue and finally into reddish purple, indicating the formation of nanoparticles. The citrate ions were used as both reducing and capping agents in stopping the particle growth and agglomeration so that the nano size of gold can be attained. Gold nanoparticles that were synthesized through this method will be in the nanosphere shape. In addition, the sizes of the gold nanoparticles produced were in the range from 50 nm to 80 nm.

#### **5.4.3 Coating process of LPFG**

Chapter 4 discussed thin film coating as one of the methods adopted to sensitize the arc-induced LPFG, where polyelectrolytes layers were deposited onto the fiber gratings to modify the cladding index and enhance its sensitivity. In this chapter, the PE-coated LPFG was further modified with the deposition of gold nanoparticles (AuNPs) onto the PE layers. The AuNPs were immobilized onto the LPFG surface using the ESA technique. In the previous chapter, a desired number of polyelectrolytes bilayers (PDDA/PSS)<sub>n</sub>, had already been deposited onto the gratings surface and the outermost layer of the coating was negatively-charged PSS. Before further modifying the LPFG surface with AuNP, another layer of positively-charged PDDA needed to be coated above the outermost PSS layer. This is because the surface of the AuNP synthesized using citrate-reduction method was covered with citrate

anions, which caused the surface to become negatively-charged (Turkevich et al., 1951; Lim et al., 2014) Hence, an extra layer of positively-charged PDDA must be coated to attract the opposite charges of the nanoparticles towards the gratings surface. The electrostatic forces between the negatively charged AuNP and the positively charged PDDA resulted in the formation of a uniformly distributed self-assembly monolayer of gold nanoparticles on the fiber gratings (Tan *et al.*, 2018). The structure of the PE-AuNP coated LPFG is as shown in Figure 5.1.

After the deposition of AuNPs, the coating of gold nanoparticles on the surface of the LPFG was investigated by using a field emission scanning electron microscope (FESEM) (JEOL JSM-6701F). The coated section of LPFG was cut to less than 1 cm length and was adhered to the holder by using carbon tape. After that, the sample was sputtered with gold palladium alloy and mounted onto a stage and the surface morphology of coated section was observed.

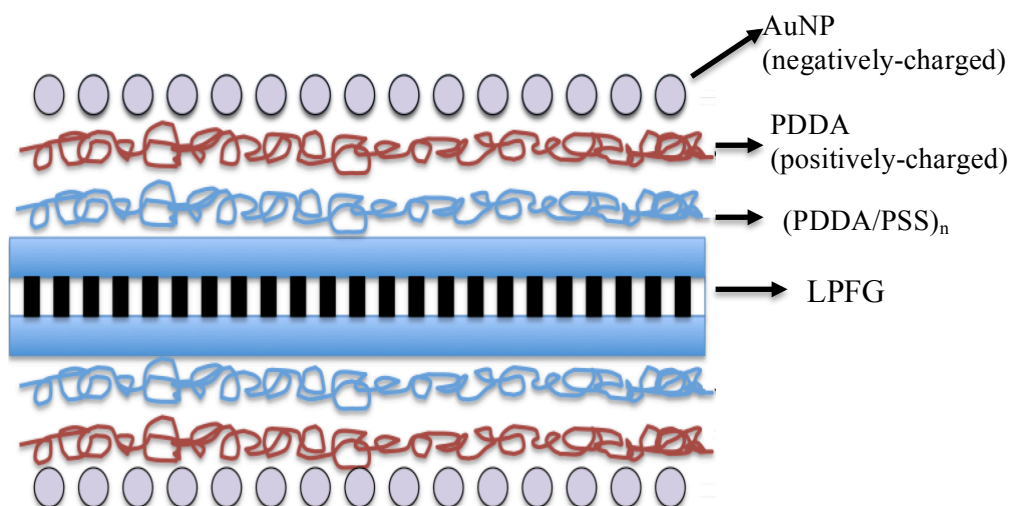


Figure 5.1 Schematic diagram of the PE-AuNP coated LPFG

#### 5.4.4 Experimental Setup

The mercury (II) solutions used in this experiment were prepared from the mercury standard solution (Wako, 100 mg/L, Japan). Five different concentrations of mercury (II) solutions were tested, ranging from 0.5 ppm to 10.0 ppm. The mercury solutions were prepared by diluting the standard solution according to the ratio of standard solution and water as shown in Table 5.1.

Table 5.1 Volume of mercury standard solution and deionised water required to prepare mercury (II) solutions with different concentrations

| Concentrations (ppm) | Mercury standard solution (mL) | Water (mL) |
|----------------------|--------------------------------|------------|
| 0.5                  | 0.5                            | 99.5       |
| 1.0                  | 1.0                            | 99.0       |
| 2.0                  | 2.0                            | 98.0       |
| 5.0                  | 5.0                            | 95.0       |
| 10.0                 | 10.0                           | 90.0       |

The setup used in this experiment was a double-pass configuration which was same as the configuration discussed in Chapter 4, with the purpose of further improving the sensitivity of LPFG (Loh *et al.*, 2015). Similarly, two optical circulators were used in the setup so that the light passes through the LPFG twice to increase the transmission attenuation of resonance wavelength. The position of LPFG was fixed by two fiber clamps, and a constant tension of 18cN was attached to the LPFG throughout the experiments to ensure the gratings were kept straight and to avoid any bending effect on the LPFG. Mercury (II) solutions were dropped into the fixture container where the gratings part of the fiber was placed to allow the whole gratings to be fully soaked in the solution.

During the experiment, the coated LPFG was initially immersed in deionized water until the response reached to a stable state. Subsequently, the coated LPFG was soaked in every concentration of mercury (II) solution for

an hour (starting from lowest concentration to highest concentration) until the response of LPFG plateaued. In between different concentrations of mercury (II) solutions, the LPFG was rinsed with deionized water to remove the residue from the previous measurand. Experiments were conducted in a controlled room with a constant temperature of  $24.2\text{ }^{\circ}\text{C} \pm 0.2\text{ }^{\circ}\text{C}$  to avoid the temperature cross sensitivity of the LPFG. The power fluctuation of the broadband light source was recorded to be within the range of  $\pm 0.01\text{ dBm}$ .

## **5.5 Results and Discussions**

### **5.5.1 Coating of Gold Nanoparticles**

As shown in Figure 5.2, the resonance wavelength of LPFG was shifted to the lower wavelength after the deposition of gold nanoparticles layer. This is because the coating of the AuNP layer increased the effective refractive index of fiber cladding and reduced the differential effective indices between core and cladding mode. As a result, the resonance wavelength encountered a blue shift.

On the other hand, the FESEM results of the PE-AuNP coated LPFG is illustrated in Figure 5.3. As observed from the SEM image, the nanoparticles were distributed uniformly on the fiber surface. Furthermore, the diameters of the particles were in the range from 50 nm to 80 nm (Frens *et al.*, 1973; Kumar *et al.*, 2012).

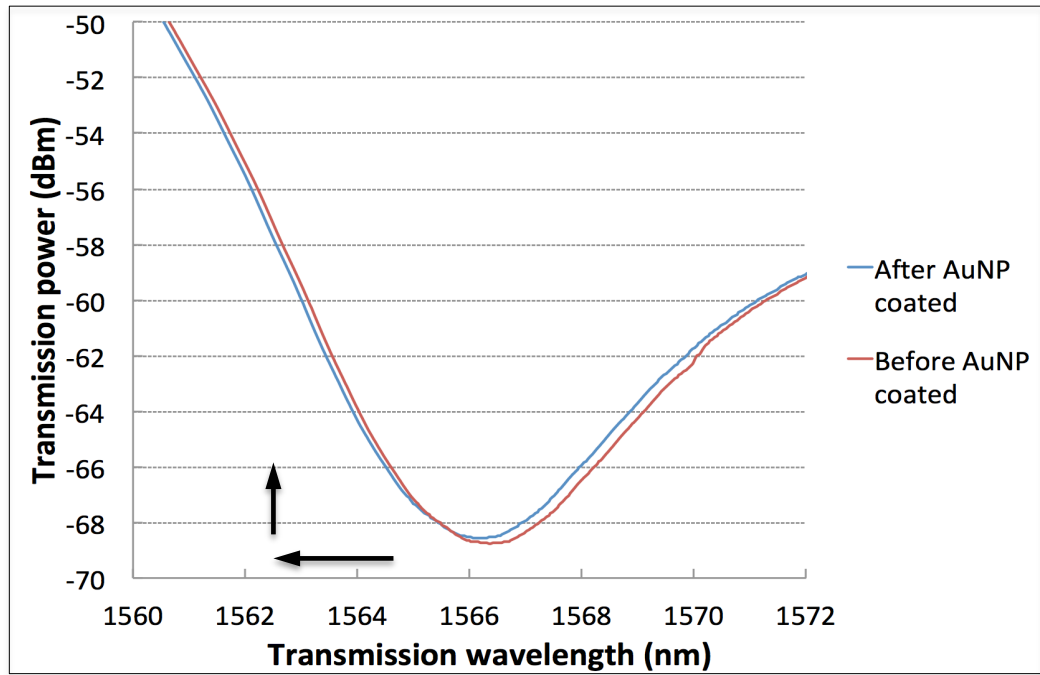


Figure 5.2 Wavelength shift of LPFG resonance wavelength after the deposition of AuNPs

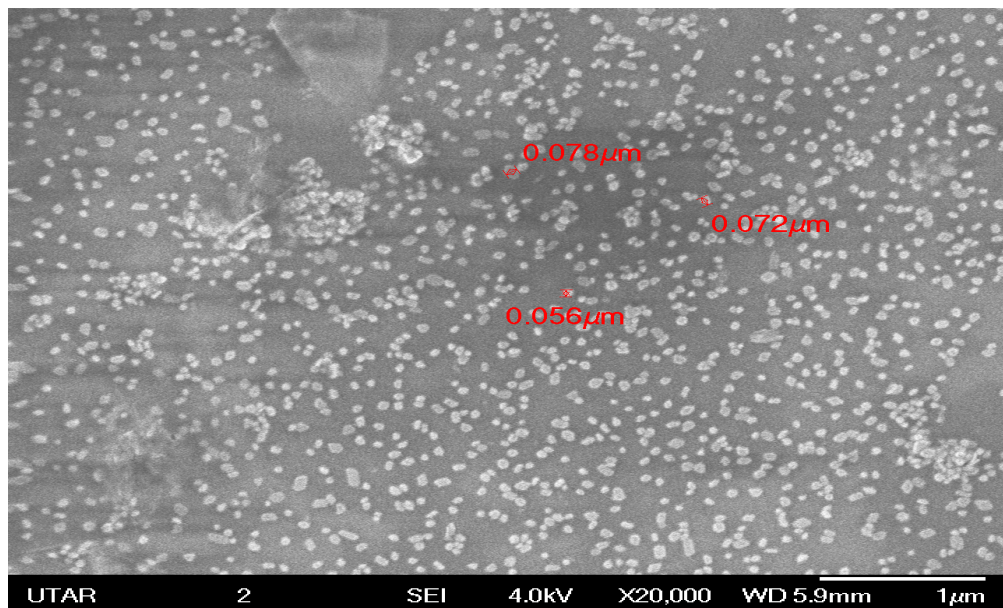


Figure 5.3 FESEM image of the gratings surface after the deposition of AuNPs at magnification of 20,000x

### 5.5.2 Mercury (II) Ions Detection with PE-AuNP Coated LPFGs

In the experiment of mercury (II) ions detection, the PE–AuNP coated LPFG was first immersed in deionized water and its response stabilised after a duration of around an hour. The PE–AuNP coated LPFG was then tested with different concentrations of mercury solutions including 0.5 ppm, 1.0 ppm, 2.0 ppm, 5.0 ppm and 10.0 ppm within a duration of 5 hours, with change in concentration done after every 60 minutes. As shown in Fig. 5.4, the PE–AuNP coated LPFG encountered a total shift of 1.34 nm to a longer wavelength over 5 hours while the transmission power of the LPFG encountered a total increment of 1.74 dBm.

It was observed that the increment of the transmission power was significant in the first 10 to 30 minutes for every concentration of mercury solution. For instance, in Figure 5.5(a), in 0.5 ppm mercury (II) ion solution, the rate of transmission power shifting in the first 30 minutes was 0.0231 dBm/min. When the PE–AuNP coated LPFG was soaked in 1.0 ppm mercury solution, the rate of transmission power was 0.0533 dBm/min for the first 10 minutes. However, the rate of increment of the transmission power after the first 10 minutes became lower; at around 0.0028 dBm/min (the slope from the graph is almost flat). On the other hand, for 2.0 ppm mercury (II) ion solution, the rate of power increment was 0.0107 dBm/min for the first 10 minutes whereas for the next 50 minutes, the rate dropped to 0.0005 dBm/min. The rates of transmission power increment for the first 10 minutes in 5.0 ppm and 10.0 ppm solutions were 0.0045 dBm/min and 0.0009 dBm/min, respectively.

Both rates dropped to 0.0008 dBm/min and 0.0005 dBm/min after the first 10 minutes, respectively. These results show that the response of the coated LPFG reached a saturation state after the first 10 minutes of reaction with 2.0 ppm mercury (II) solutions as the rate afterwards was close to zero. For the resonance wavelength shifting, as shown in Figure 5.5(b), the first 10 minutes of the experiment in 0.5 ppm mercury(II) ion concentration resulted in a wavelength shift of 0.55 nm, with a rate of 0.0553 nm/min. The rate of wavelength shift dropped to 0.006 nm/min for the next 10 minutes. However, the wavelength remained the same for the last 40 minutes in 0.5 ppm of mercury (II) ion solution. For 1.0 ppm, the transmission wavelength shifted to longer wavelength at a rate of 0.006 nm/min for the first 10 minutes and the transmission notch remained at the same wavelength for the next 50 minutes. The same situation was observed for the 2.0 ppm concentration, where the notch encountered a red shift with a rate of 0.05 nm/min for the first 20 minutes and the notch remained at same wavelength for the next 40 minutes. In 5.0 ppm concentration, the transmission notch shifted in the first 10 minutes with a rate of 0.004 nm/min and remained the same position for the next 50 minutes. However, for 10.0 ppm of mercury, the transmission notch of the LPFG did not shift and remained at the same wavelength throughout the 60 minutes.

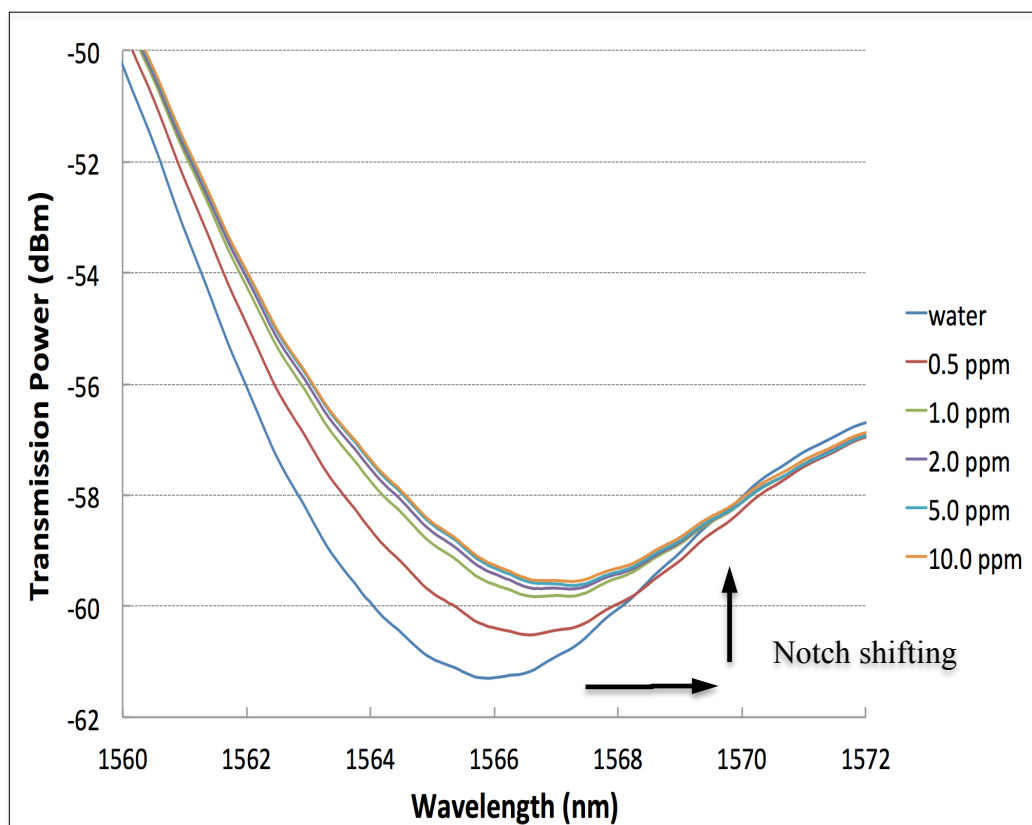
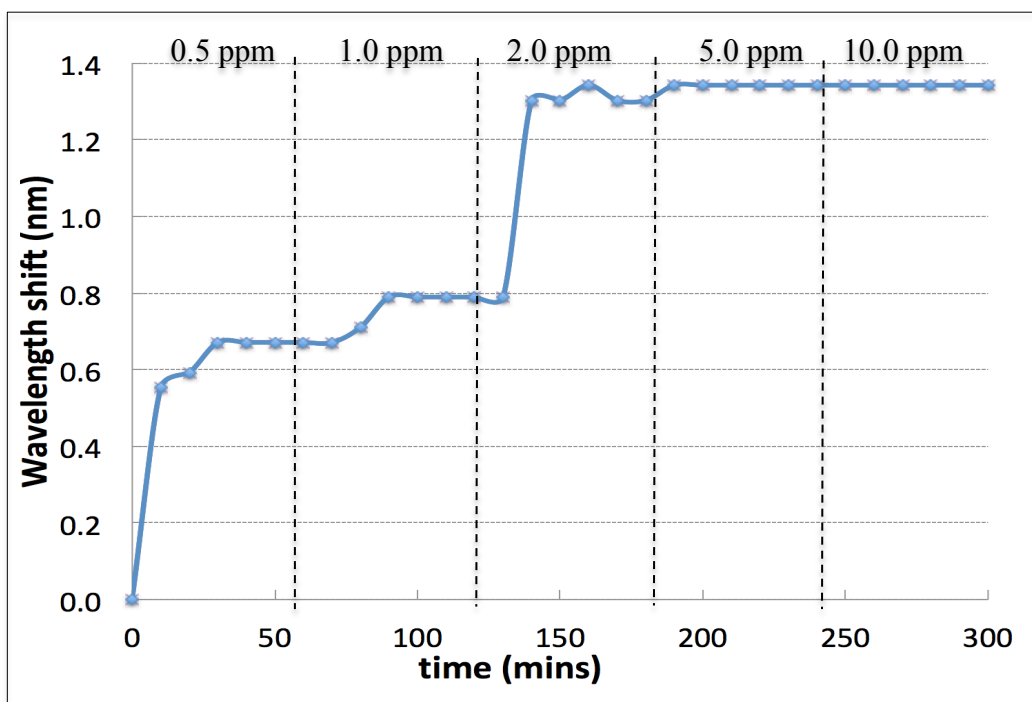
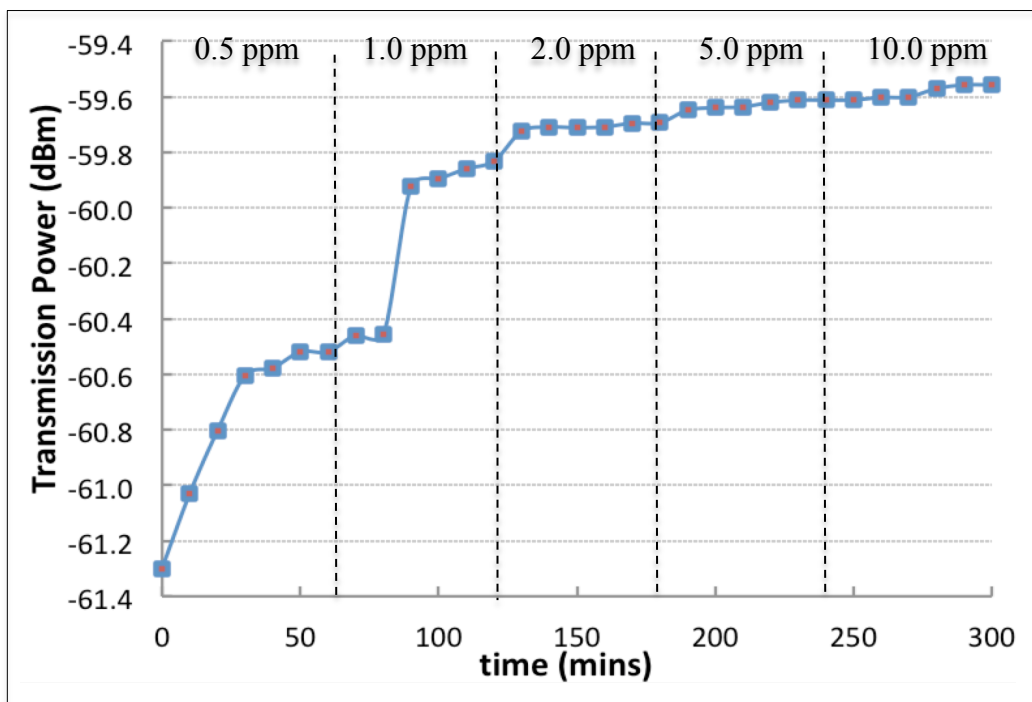


Figure 5.4 Transmission response of the first PE-AuNP coated LPFG towards mercury (II) solutions



(a)



(b)

Figure 5.5 (a) Wavelength shift (b) Transmission power responses of PE-AuNP coated LPFG (first LPFG) towards different concentrations of mercury over time

The exact same experiment was conducted with another PE-AuNP coated LPFG to confirm the findings. The results of the second PE-AuNP coated LPFG are shown in Figure 5.6 and Figure 5.7. The second coated LPFG behaved similar to the first LPFG in mercury solutions, in which its resonance wavelength shifted to a longer wavelength and its transmission power increased. The resonance wavelength of this LPFG encountered a total red-shift of 1.12 nm and a total power increment of 1.673 dBm after immersing in mercury solutions ranging from 0.5 ppm to 10.0 ppm.

The increase in transmission power was most prominent in the first 10 to 40 minutes in different concentrations of mercury solutions. In 0.5 ppm of mercury (II) solutions, the rate of power increment was 0.0183 dBm/min in the first 40 minutes. However, the rate dropped to 0.0020 dBm/min in the last 20 minutes of immersion. On the other hand, the rate of transmission power was 0.0287 dBm/min for the first 20 minutes as the LPFG was soaked in 1.0 ppm of mercury (II) solutions. After 20 minutes, the rate has dropped to only 0.0022 dBm/min. For 2.0 ppm of mercury (II) solution, the rate of power increment was found to be 0.0086 dBm/min in the first 20 minutes before it dropped to only 0.0003 dBm/min for the remaining 40 minutes. Moreover, the rate of power increment in 5.0 ppm was 0.0022 dBm/min for the first 20 minutes. After that, the rate dropped to 0.0002 for the next 30 minutes. Last but not least, the rate of power increment in 10.0 ppm of solutions was 0.0030 dBm/min in the first 10 minutes. For the remaining 50 minutes, the rate dropped to only 0.0001 dBm/min. The response of LPFG was almost flat in

5.0 ppm and 10.0 ppm of mercury (II) solutions due to the saturation state achieved.

As for the shifting of resonance wavelength shown in Figure 5.7(b), the rate of wavelength shift in the first 20 minutes of experiment in 0.5 ppm mercury (II) ion concentration was 0.0280 nm/min. The rate of wavelength shift dropped to 0.0040 nm/min for the next 20 minutes. However, the wavelength remained the same for the last 20 minutes in 0.5 ppm of mercury (II) ion solution. In addition, for 1.0 ppm concentration, the transmission wavelength shifted to a longer wavelength at a rate of 0.008 nm/min for the first 30 minutes and the transmission notch remained at the same wavelength for the next 30 minutes. Similarly, for 2.0 ppm concentration, the resonance wavelength encountered a red shift with a rate of 0.0067 nm/min for the first 30 minutes and the notch remained at same position for the next 30 minutes. In 5.0 ppm concentration, the transmission notch shifted in the first 10 minutes, with a rate of 0.004 nm/min and remained the same for the remaining 50 minutes. Lastly, for 10.0 ppm of mercury, the transmission notch of the LPFG remained at the same wavelength throughout the 60 minutes experiment.

The responses of both PE–AuNP coated LPFGs were due to the reaction between gold nanoparticles and mercury (II) ions, which led to the production of amalgam on the LPFG surface (Levlin *et al.*, 1999). Mercury amalgam is the alloy produced from the interaction of zero valent mercury with gold nanoparticles due to the high chemical affinity of mercury towards gold. The production of amalgam on the fiber surface changed the effective

refractive index of the LPFG. As a result, the resonance wavelength was shifted to the longer wavelength and the transmission power of LPFG was increased. As the concentration increases, the resonance wavelength shifted to a longer wavelength until a point where the entire deposited AuNP reacted with mercury and reached a saturation point. This situation can be seen from the response of coated LPFG in 10 ppm mercury solution, in which the transmission wavelength remained at the same wavelength.

As mentioned in the experimental setup section, the coated LPFG was rinsed with deionised water before changing the mercury solution to higher concentration. During the experiment, it was discovered that the resonant wavelength of the LPFG did not go back to the original wavelength (the resonant wavelength before tested with mercury ions solution). This is due to the production of amalgam onto the surface of the coated LPFG from the reaction between mercury (II) ions and gold nanoparticles. Even after rinsing with deionised water to remove the mercury residue, the amalgam was still changing the effective refractive index of the LPFG. From this observation, it can be concluded that this LPFG sensor is not reusable unless the coatings on the used LPFG is removed and re-coated with new PE-AuNP coatings.

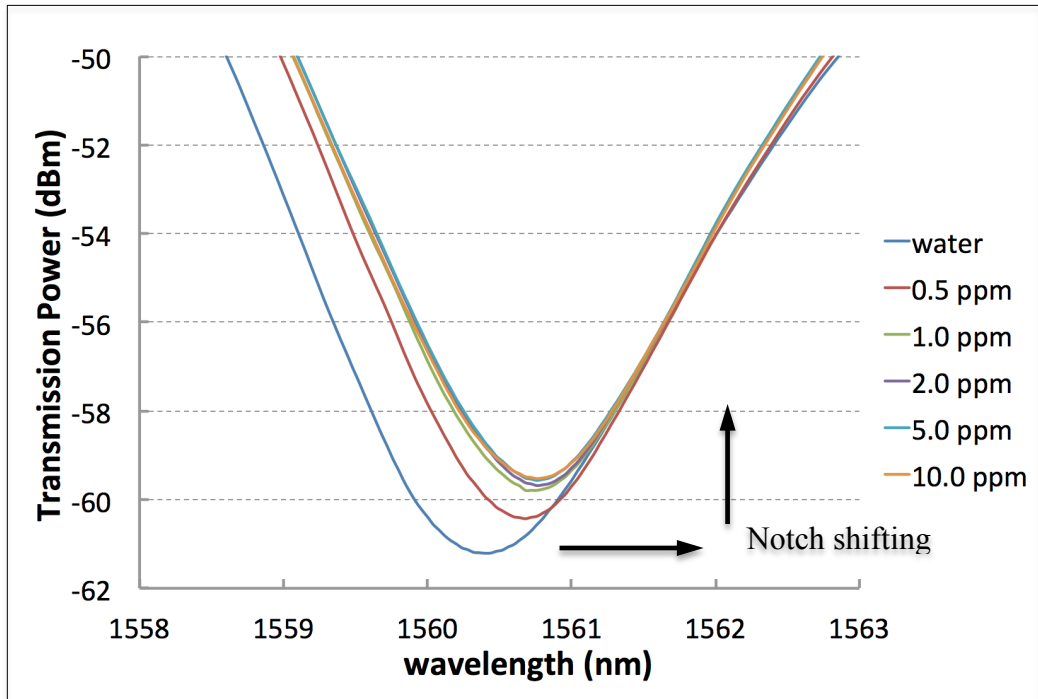
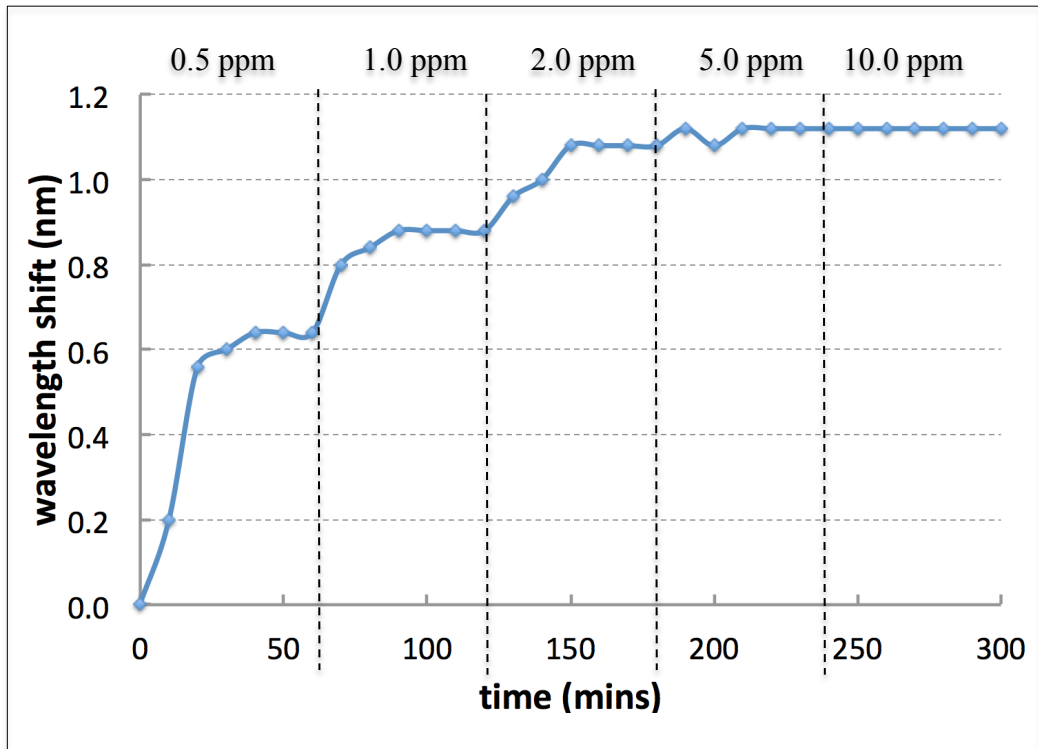
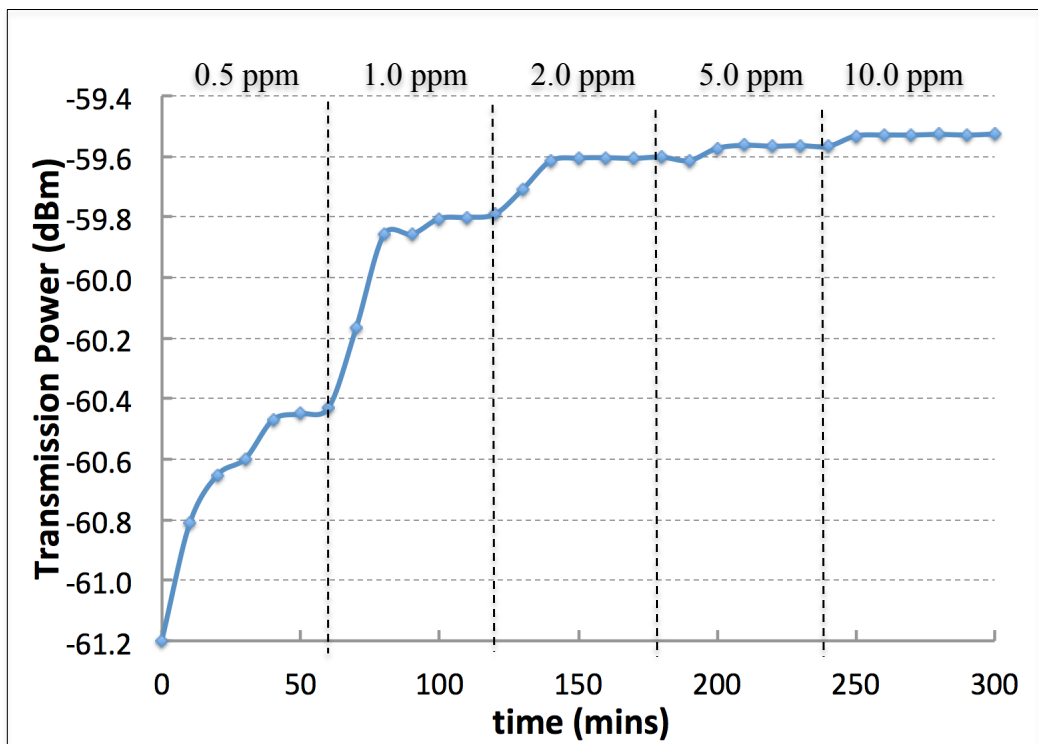


Figure 5.6 Transmission response of the second PE-AuNP coated LPFG towards mercury (II) solutions



(a)



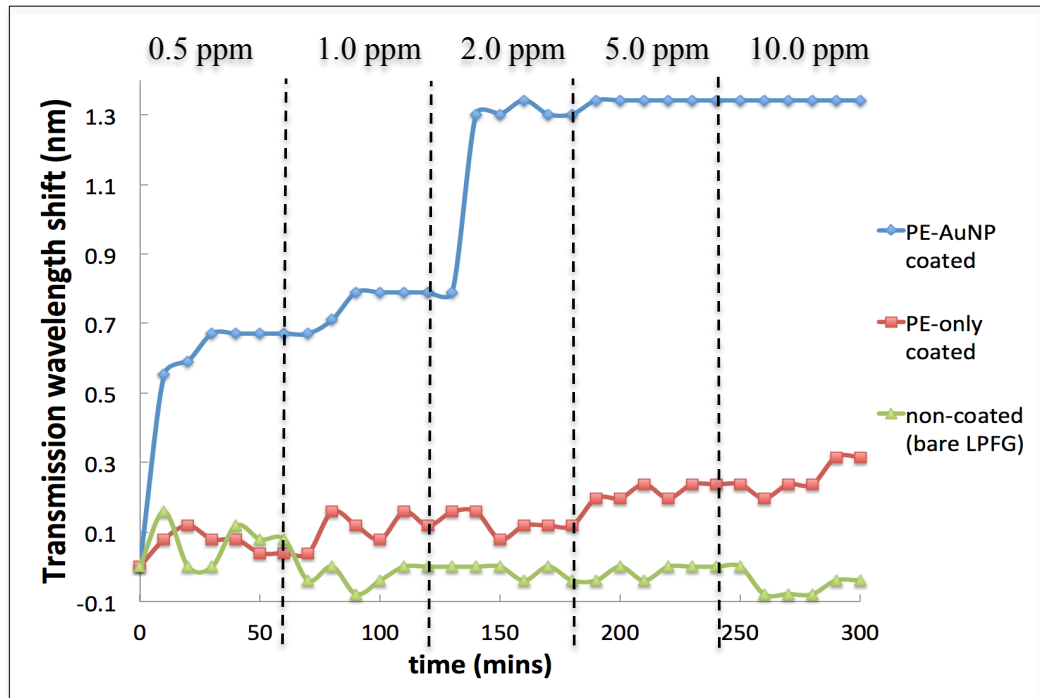
(b)

Figure 5.7 (a) Wavelength shift (b) Transmission power responses of PE-AuNP coated LPFG (second LPFG) towards different concentrations of mercury over time

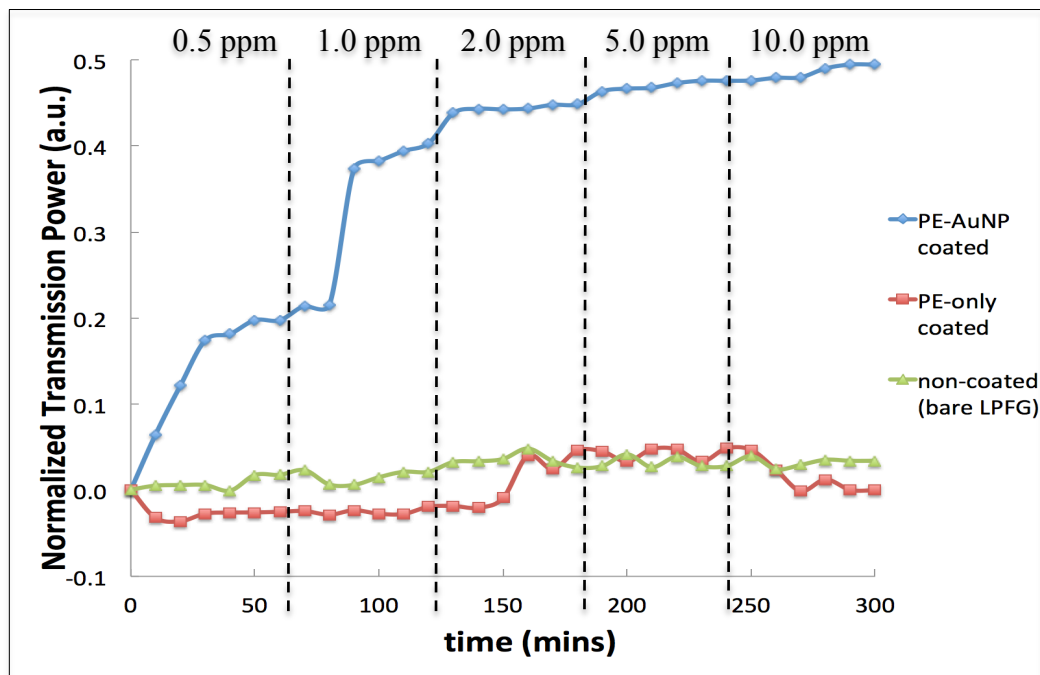
### **5.5.3 Comparison of Responses among Non-coated, PE-only Coated and PE-AuNP Coated LPFGs towards Mercury (II) Ions**

Next, in order to confirm the reaction between mercury (II) ions and gold nanoparticles layer, the experimental procedures were repeated with uncoated LPFG and PE-only coated LPFG (with optimized number of PE bilayers only). The purpose of this experiment is to compare the responses of the LPFGs with and without AuNPs coated towards mercury (II) ions. Figure 5.8(a) and (b) show the comparisons of the normalized transmission power and resonance wavelength shift of the first PE–AuNP coated LPFG (LPFG 1), PE-only coated LPFG and the uncoated LPFG. From Figure 5.8, both the normalized transmission power and the resonance wavelength shift of the PE–AuNP coated LPFG increased as the concentration of mercury solution increased, up to a point where the saturation state was reached. On the contrary, for the uncoated LPFG, both the normalized transmission power and resonance wavelength shift did not show significant responses towards the mercury solution. As the concentration increased, both the normalized transmission power and resonance wavelength shift remained almost constant. The shift of resonance wavelength of PE–AuNP coated LPFG in mercury solution was almost 33.5 times compared to the uncoated LPFG. The increase in transmission power of PE–AuNP coated LPFG in mercury solution was around 14.5 times of the uncoated LPFG.

Similar to the uncoated LPFG, the normalized transmission power and resonance wavelength shift of the PE-only coated LPFG did not show prominent changes with increasing mercury (II) ions concentration compared to the PE–AuNP coated LPFG as shown in Figure 5.8 (a) and (b). The increase in normalized transmission power of PE–AuNP coated LPFG was 10.3 times compared to PE-only coated LPFG while the resonance wavelength shift of the PE–AuNP coated LPFG was 4.5 times compared to the wavelength shift of PE-only coated LPFG. The response of the PE-only coated LPFG towards different mercury (II) concentrations compared to the uncoated LPFG was relatively better due to the improved sensitivity of the LPFG caused by the deposition of PE layers.



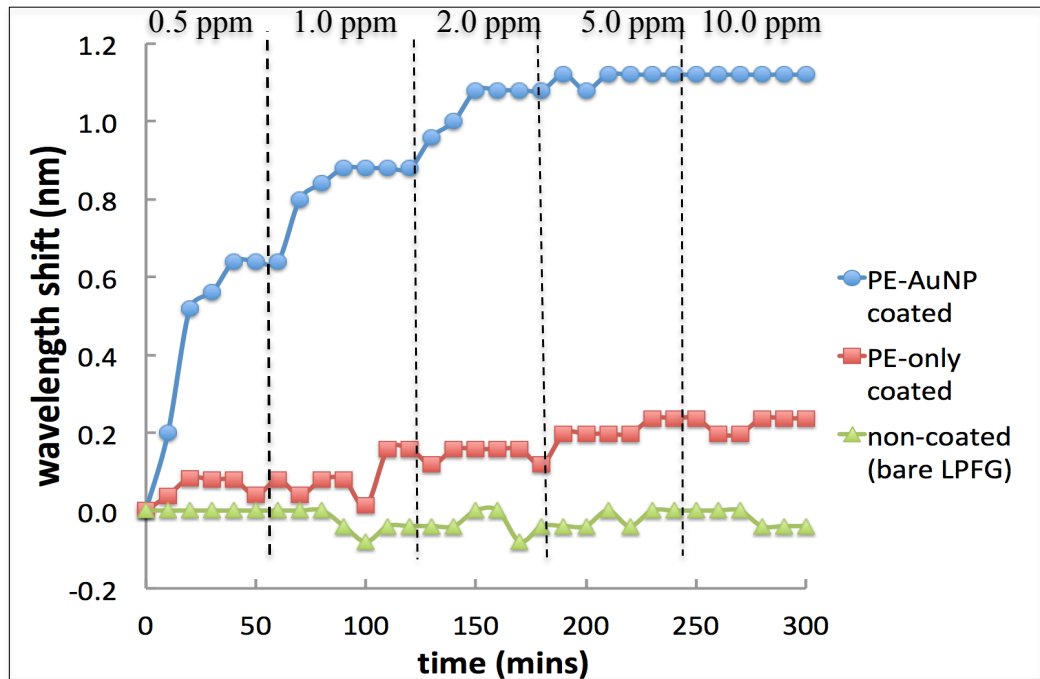
(a)



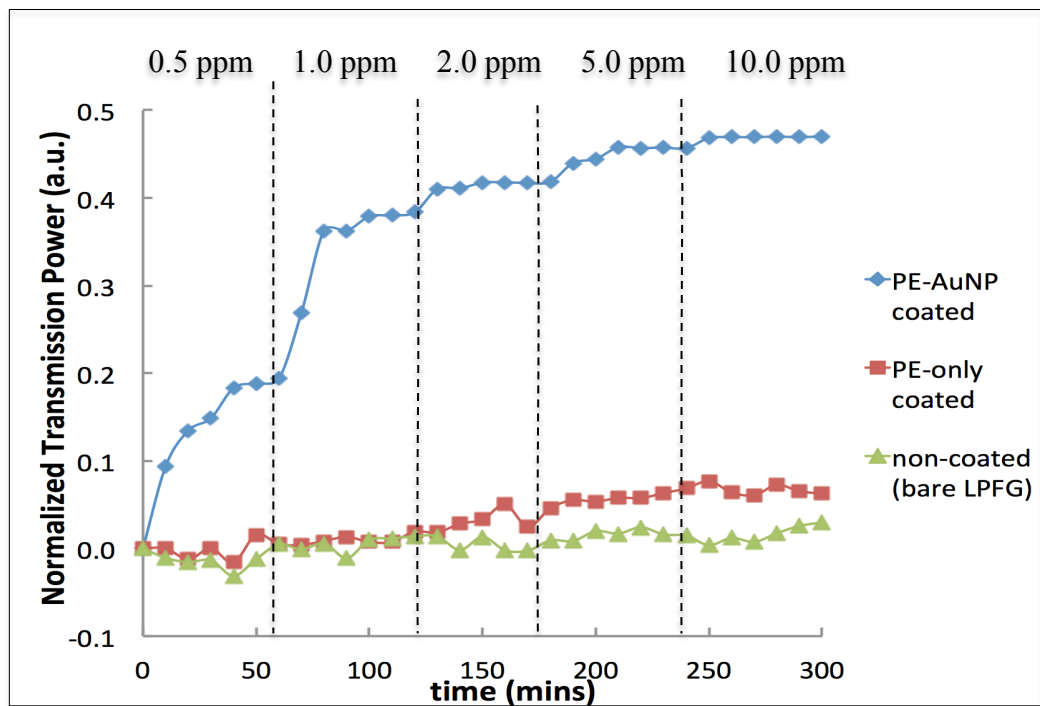
(b)

Figure 5.8 First comparison of (a) resonance wavelength shift of non-coated LPFG, PE-only coated LPFG and PE-AuNP coated LPFG; (b) normalized transmission power of non-coated LPFG, PE-only coated LPFG and PE-AuNP coated LPFG

Again, the comparison was conducted with the second PE-AuNP coated LPFG to confirm the consistency of findings. The comparison of the normalized transmission power and resonance wavelength is shown in Figure 5.9(a) and (b). Both the uncoated LPFG and PE-only coated LPFG did not show a prominent response towards the increment in concentrations of mercury (II) solutions. On the contrary, both the normalized transmission power and the resonance wavelength shift of the PE-AuNP coated LPFG increased as the concentration of mercury solution increased, until it reached to a point where the response plateaued. The shift of resonance wavelength of PE-AuNP coated LPFG in mercury solution was almost 28.1 times compared to the uncoated LPFG. If compared to the PE-only coated LPFG, the wavelength shift of PE-AuNP coated LPFG was 4.7 times higher. On the other hand, the increase in transmission power of PE-AuNP coated LPFG in mercury solution was around 15.8 times the uncoated LPFG, and 7.2 times the PE-only coated LPFG. From these comparisons, it can be concluded that gold nanoparticles are suitable to be used as the sensing agent towards mercury (II) ions due to their unique reaction in forming amalgam.



(a)



(b)

Figure 5.9 Second comparison of (a) resonance wavelength shift of non-coated LPFG, PE-only coated LPFG and PE-AuNP coated LPFG; (b) normalized transmission power of non-coated LPFG, PE-only coated LPFG and PE-AuNP coated LPFG

## 5.6 Summary

In this chapter, a novel PE–AuNP coated LPFG sensor that is applicable for real-time monitoring had been successfully demonstrated and tested for the detection of mercury (II) ions in water. It had proven that the coated LPFG was able to detect mercury (II) solutions. The deposition of PE–AuNP layers further modified the surface of arc-induced LPFG where AuNPs were used as the sensing agents that captured mercury (II) ions. Generally, the resonance wavelength of the PE–AuNP coated LPFG shifted to a longer wavelength and the transmission power increased throughout the duration of 5 hours exposure to varied concentrations. For both resonance wavelength and transmission power, the rate of change was the highest in the first 10 to 30 minutes of soaking in the mercury (II) solutions until the saturation point was achieved. These responses of the PE–AuNP coated LPFGs were then compared with uncoated and PE-only coated LPFGs. Negligible changes in the resonance wavelength and transmission power were observed for the uncoated and PE-only coated LPFGs. The response of PE–AuNP coated LPFG compared to other LPFGs was caused by the formation of amalgam on the PE–AuNP LPFG surface due to the reaction of mercury (II) ions with AuNP. Nonetheless, the lifespan of LPFG is one of the main drawbacks if employed LPFG as a sensor in water bodies as the structure of LPFG is very easily broken by any external force caused by environmental factors. Therefore, there is a need to construct a structure which can protect the LPFG sensor to prolong its lifespan for long-term monitoring of mercury (II) ions. The structure to strengthen and protect the LPFG is discussed in next chapter.

## CHAPTER 6

### A NOVEL HYBRID LPFG-DGT SENSOR SYSTEM FOR LONG-TERM MONITORING OF MERCURY (II) IONS

In this chapter, the final stage of the work conducted in this research is discussed in details. As demonstrated in the earlier chapters, the surface of the sensitized arc-induced LPFG was further deposited and modified with gold nanoparticles as the sensing agent towards mercury (II) ions. The results proved that the modified LPFG was able to detect mercury (II) ions in water. However, it is known that LPFG is very brittle and easily breakable due to its silica-based structure. Due to this, further improvement was done to the structure of the sensor in the last phase of this research so that the modified LPFG is well protected and can be used for long-term monitoring, as long-term data is an essential aspect in environmental studies. A hybrid structure, which is very similar to the Diffusive Gradient in thin Film (DGT) device, is introduced in this chapter to strengthen the structure of the LPFG sensor system. The coated LPFG was embedded as the innermost layer of the structure and it was covered with diffusive gel and membrane filter layers. Again, the hybrid sensor was tested with different concentrations of mercury (II) solutions to validate the effect of the structure towards the responses of the LPFG towards mercury (II) ions.

## 6.1 Introduction

In environmental studies, long-term monitoring is often an important aspect to be considered. It can be defined as the collection of data of certain parameters at an environmental site over a prolonged period of time (Dodds *et al.*, 2012). There are a few reasons why the collection of long-term data is valuable to environmental research. First and foremost, it has been illustrated that a sufficient collection of data of an environmental parameter can help to appraise and evaluate the quality of the environment better because long-term data offers a more solid proof and understanding for researchers to make future decisions and measures to be taken. In addition, the long-term background data collected can be utilized to estimate and discover certain important environmental patterns and trends and help to identify rare events that could occur. Although normal short-term monitoring may help to conduct a routine investigation about an environmental study so that the basic measures to be taken can be decided, the identification of undesirable patterns or changes is equally essential for the outcome of ongoing surveillance (Magnuson *et al.*, 1990; Lohner *et al.*, 2013; Carrie *et al.*, 2014). The same goes to the monitoring of mercury content in water. Long-term detection is a crucial process to achieve a more accurate prediction about a water body. However, most of the mercury sensors proposed, including the optical-based sensors that were discussed previously in Section 5.3, were meant for fast investigation and short-term detection purposes in a laboratory instead of a collection of long-term data at the real site. Hence, a sensor structure that can

be used to monitor mercury contents in water over a longer period of time is needed.

In an earlier phase, experiments have proven that the proposed PE-AuNP coated LPFG were able to detect mercury (II) ions in water. On the other hand, the research conducted by Yong *et al.* demonstrated that LPFG can be deployed multi-kilometers away from the laboratory for detection purposes (2017). Also, LPFG is resistant to corrosion and is insensitive to electromagnetic interference (Bock *et al.*, 2007). All these evidences show that LPFG is suitable to be deployed in the real environment for remote and real-time monitoring of mercury in water. However, when it comes to long-term monitoring, the PE-AuNP coated LPFG alone is not suitable to be used due to the limited lifespan induced by harsh environmental factors. The brittle silica-based structure of LPFG can be easily broken by any stress or force caused by the environment (Du *et al.*, 2017). Due to this reason, a durable structure which can fully protect the LPFG sensor over a long period of time and prevent it from being damaged needs to be constructed to allow the sensor to be deployed for collecting long-term data.

In this study, a protective structure that can seal the LPFG was constructed based on the basic structure of a long-term monitoring device that was proposed in 1994, which was named as DGT (Davison *et al.*). The DGT device is a commonly used passive sampling technique for collecting long-term data of a water body, in which the device is deployed directly in a real aqueous environment (Zhang *et al.*, 1995). This indicates that the DGT device

has a durable and strong structure that can protect the sensor over a long period of deployment time in harsh environments. The main purpose of this research phase is to utilize the features of the DGT structure to overcome the limitation found in the LPFG device, *i.e.* its brittle structure. A hybrid LPFG-DGT sensor that combined the PE-AuNP coated LPFG and the durable structure of DGT device was constructed in this research to prolong the lifespan of the LPFG for long-term monitoring purposes. The PE-AuNP modified LPFG was well sealed within the DGT structure so that the sensor can provide real-time data over a longer duration. This is the first ever reported investigation on combining the features of both LPFG and DGT as a hybrid sensor for mercury (II) ions detection. The hybrid structure was experimented with different concentrations of mercury (II) solutions to observe its detection ability.

## **6.2 Diffusive Gradient in Thin Films**

In 1994, a sensor device that is suitable to be used for in-situ and long-term water monitoring, *i.e.* DGT was proposed by Zhang and Davison *et al.* This technique was employed in the monitoring of different heavy metals such as mercury and cadmium (Wang *et al.*, 2016; Amato *et al.*, 2014). It utilized passive sampling technique, in which the DGT device was deployed for a period of time in an aqueous environment before it is retrieved and analysed in a laboratory.

The DGT device employs a three-layer structure that consists of a resin-impregnated binding gel layer, a diffusive gel layer as well as a membrane filter. The function of the membrane filter is to act as a size-selective outer membrane, blocking suspended particles contained in water from entering the device and allowing only elements that are smaller than a certain size to pass through (Nordblad *et al.*, 2008). Besides that, it helps to hold the gel layers in the device. On the other hand, the critical role of the diffusive gel layer is to lead and allow only certain particles which are smaller than the gel pore size to diffuse through the gel and reach the binding layer (Zhang *et al.*, 1999; Docekalova *et al.*, 2005). Last but not least, the function of the innermost binding gel layer is to attract and accumulate the targeted metal ions (Pouran *et al.*, 2014). The illustration of the DGT structure is shown in Figure 6.1. The membrane filter is placed as the outermost layer covering the diffusive gel layer, whereas the innermost binding gel layer is placed right beneath the diffusive layer. These three layers are enclosed and sealed within a plastic device, leaving only the uppermost membrane filter to be exposed to solutions through the DGT window (Huang *et al.*, 2016).

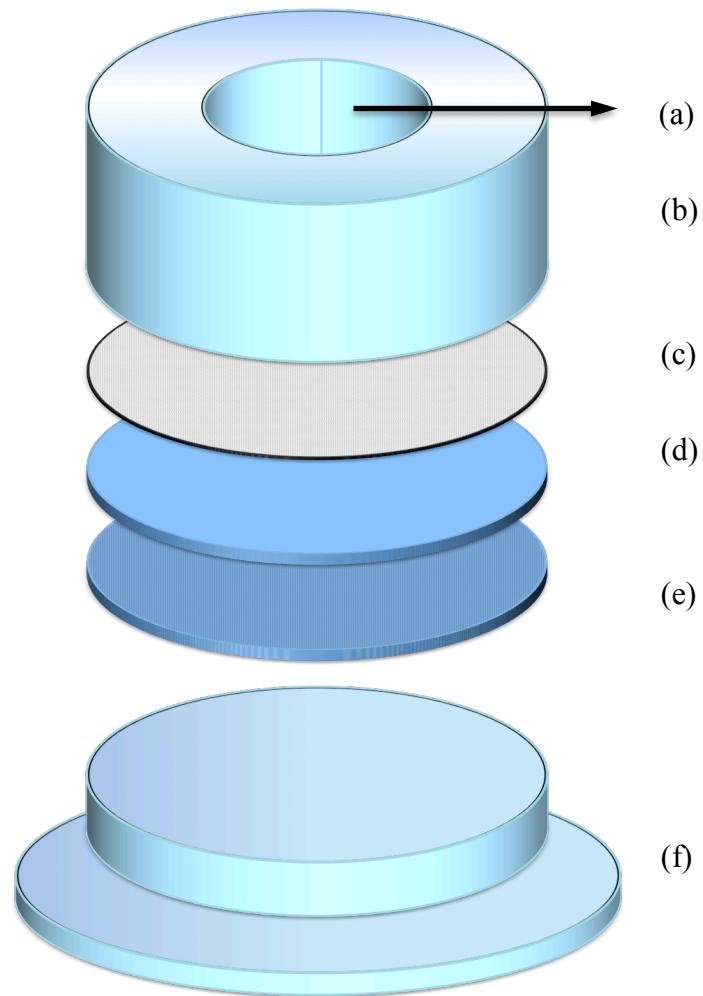


Figure 6.1 Structure of DGT (a) window, (b) cap, (c) membrane filter, (d) diffusive gel layer, (e) resin gel layer, (f) plastic base.

When the DGT is first deployed in water, there will be no metal ion that binds to the resin layer and hence the concentration of metal ions on the resin gel surface is effectively zero. As a result, a gradient of concentration is created across the measurand and resin layer, which then induces the movement of metal ions from measurand to pass through the diffusive layer and accumulate on the innermost binding layer (Divis *et al.*, 2005). After retrieving the device from the water reservoir, the binding gel within the DGT must be analysed by either the inductively coupled plasma mass spectrometry (ICP-MS) or Atomic Absorption Spectrometry (AAS) method to determine if metal ions had accumulated. Furthermore, the binding gel layer must be treated and stored carefully before conducting the analytical process. For instance, the DGT device must be rinsed thoroughly and stored at a temperature of 4 °C within three weeks of retrieval. Subsequently, the binding gel is required to be disassembled from the DGT probe and sliced into thin slices before it is weighed and extracted in HNO<sub>3</sub> for a day. The analytical procedure will only be conducted after these elution processes (Simpson *et al.*, 2012).

One main limitation found in the DGT device is that it does not allow real-time and remote monitoring of water bodies as it requires the retrieval of the device and extra analysing procedures to determine the presence of a certain metal ion. Generally, it is mainly used for in situ and long-term detection purposes. Even though on-site monitoring is close to real-time monitoring, the presence of a certain metal in water bodies can be determined only after the retrieval and elution processes of the DGT device. However, if

the deployed sensor allows the collection of real-time data, in some cases it can help build a stronger understanding about the environmental parameter. Therefore, the introduction of the hybrid LPFG-DGT sensor in this research overcomes not only the limitation of the LPFG structure, but also the problem of the lack of real-time data in the DGT device.

### **6.3 Hybrid LPFG-DGT Sensor System for the Detection of Mercury (II) Ions**

#### **6.3.1 Structure of Hybrid LPFG-DGT Sensor**

In this proposed hybrid LPFG-DGT sensor, the structure is rather similar to the conventional DGT device. As described in Section 6.2, the conventional DGT is made up of a three-layer structure, which consists of an innermost binding gel layer, a diffusive gel layer as well as a layer of outermost membrane filter. In this proposed hybrid structure, the innermost binding phase layer is replaced by the polyelectrolyte (PE)–gold nanoparticles (AuNP) coated LPFG. The PE-AuNP coated LPFG is placed beneath the diffusive hydrogel layer and the diffusive gel layer is covered with an outer layer of a membrane filter. The whole structure is protected and sealed properly in between plastic plates, leaving only the upper membrane filter to be exposed to the measurand through the small window of the plastic structure. The structure of the hybrid LPFG-DGT is illustrated in Fig. 6.2.

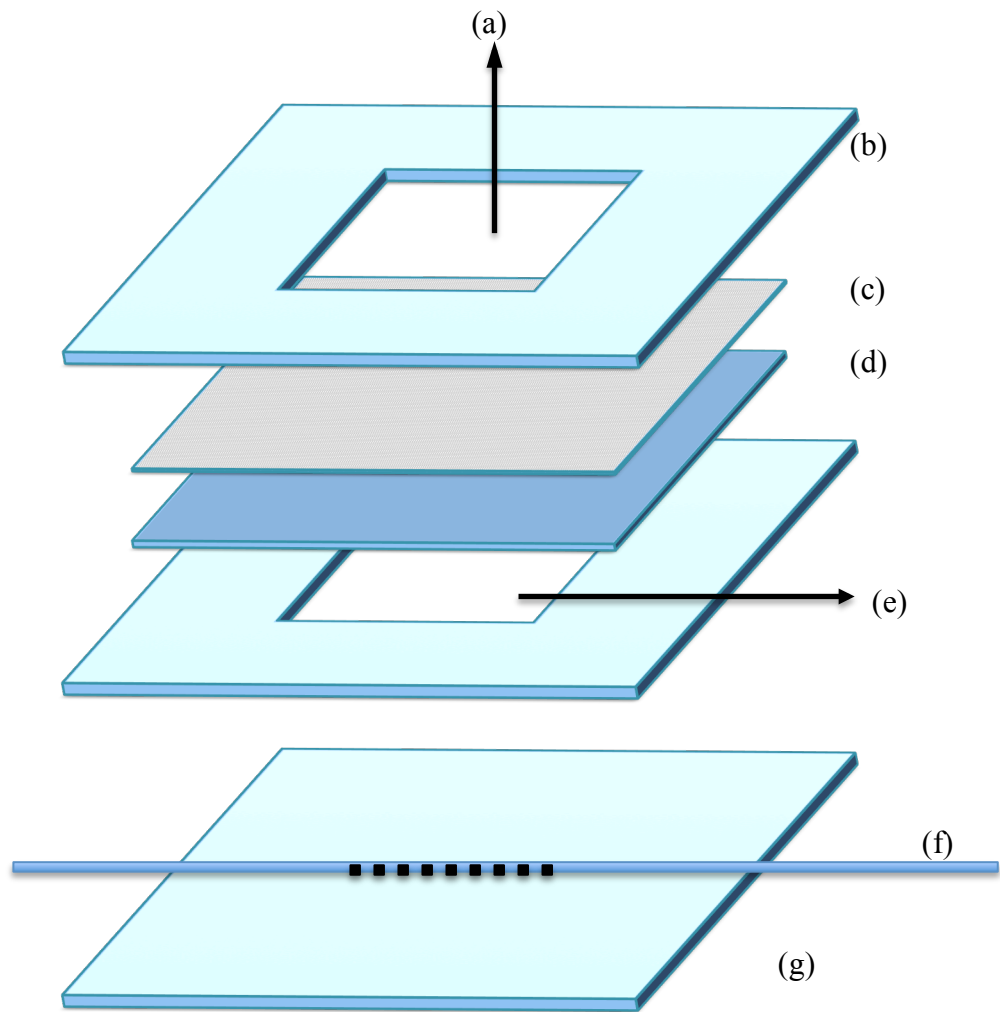


Figure 6.2 Structure of the hybrid LPFG-DGT DGT (a) window, (b) upper plastic plate, (c) membrane filter, (d) diffusible gel layer, (e) window that exposed fiber gratings section, (f) PE-AuNP coated LPFG, (g) base (plastic plate with a groove in the middle for positioning of the LPFG); the upper and base plates were glued and sealed together into a sealed structure similar to DGT device.

From the illustration of the hybrid LPFG-DGT sensor structure, the PE-AuNP coated LPFG was covered with a layer of diffusive gel. In conventional DGT, different types of diffusive layers were used for different metal detection. In mercury detection, the agarose gel type was the most commonly proposed diffusive layer (Divis *et al.*, 2009). The diffusive gel layer employed in this research was similar to the agarose gel used in DGT device for mercury detection. A 1.5 % (w/v) diffusive gel solution was first prepared by dissolving agarose powder (Apical Scientific Sdn. Bhd., Malaysia) in appropriate amounts of deionised water at a temperature of 80 °C. The mixture was then placed and heated in a boiling water bath and stirred gently until the agarose powder was all dissolved and the mixture became transparent. Finally, the hot gel mixture was placed in between two plates and left to cool down to its gelling temperature in which the diffusive gel layer started to form (Docekalova *et al.*, 2005). After that, the diffusive gel was immersed in DI water before use in the hybrid device.

In constructing the hybrid LPFG-DGT structure, the PE-AuNP coated LPFG was placed on a plastic plate where a groove was made in the middle to allow the positioning of the LPFG. Another plastic plate was then placed on top of the PE-AuNP coated LPFG with a small window in the middle to expose only the PE-AuNP coated LPFG gratings section. Next, the synthesized diffusive gel layer was placed on top of the window, followed by a layer of membrane filter. The membrane filter used in this hybrid structure was similar to the membrane used in the conventional DGT structure, *i.e.* polyethersulphone filter with pore size of 0.45  $\mu\text{m}$  (DGT Research Ltd., UK.)

The hybrid sensor was then closed and sealed with another windowed plastic plate placed on top of the membrane filter.

#### **6.4 Experimental Setup**

In this experiment, a similar setup as in Section 5.4.1 was used, in which double-pass system was employed to improve the sensitivity of LPFGs. However, weight was not attached to the fiber in this experiment as the LPFG was already kept straight within the hybrid LPFG-DGT structure, hence extra weight to prevent the bending effect was not required. The experiment setup of the hybrid structure is shown in Figure 6.3.

Similarly, five mercury (II) solutions with different concentrations were tested in the experiment, and their concentrations were exactly the same as in Chapter 5, which ranged from 0.5 ppm up to 10.0 ppm. The response of the hybrid sensor towards mercury (II) ions was tested by filling the window of the hybrid sensor system with different concentrations of mercury (II) solutions. Firstly, DI water was used as the control solution to ensure that the response of the PE-AuNP coated LPFG was stabilised. After its response stabilised, the DI water was removed and replaced with different concentrations of mercury (II) solutions. The window of the hybrid structure was filled with every concentration of mercury (II) solution for a duration of time until the response observed in OSA plateaued, indicating that the LPFG response had become stable. Before changing the measurand to a higher concentration of mercury (II) solution, the window of the hybrid sensor must

be rinsed thoroughly with DI water to remove the residue from the previous solution. Furthermore, these experiments were conducted in a controlled room with a constant temperature of  $24.2\text{ }^{\circ}\text{C} \pm 0.2\text{ }^{\circ}\text{C}$ .

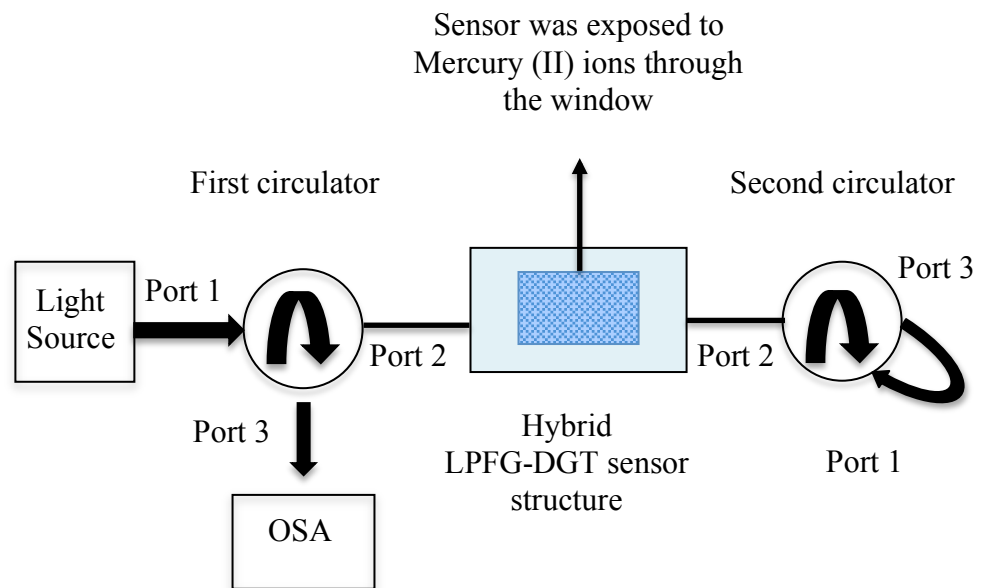


Figure 6.3 Experimental Setup of mercury detection by the hybrid LPFG-DGT sensor

## 6.5 Results and discussion

### 6.5.1 Mercury (II) ions Detection with Hybrid LPFG-DGT

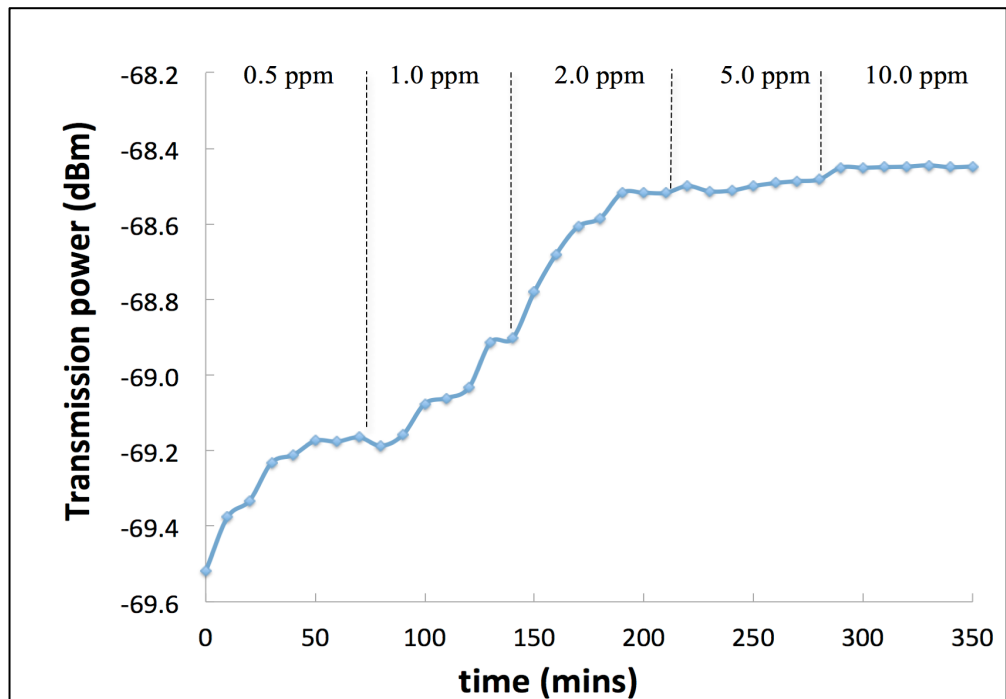
The first experiment conducted in this final stage of research aimed to determine whether the proposed hybrid LPFG-DGT sensor system is able to detect the presence of mercury (II) ions. The hybrid sensor was first exposed to deionized water until its response stabilized. Consequently, the experiment continued with five different concentrations of mercury (II) ion solutions, *i.e.* increasing from 0.5 ppm to 10 ppm. The results of the experiments are shown in Figure 6.4 and Figure 6.5.

From the results, it can be observed that the resonance wavelength of the hybrid LPFG-DGT structure encountered a total red shift of 0.8 nm to a longer wavelength and a total increment of 1.071 dBm in the transmission power. For each different concentration, the output spectra of the LPFG-DGT hybrid sensor reached stability around 70 minutes of exposure to the different concentrations of mercury (II) ion solutions. It was also observed that for the hybrid LPFG-DGT structure, the rate of reaction was the highest in the first 40 minutes to 50 minutes of exposure to every concentration of mercury (II) solution. After the first 40 to 50 minutes, the reaction started to slow down and in the end reached a plateau.

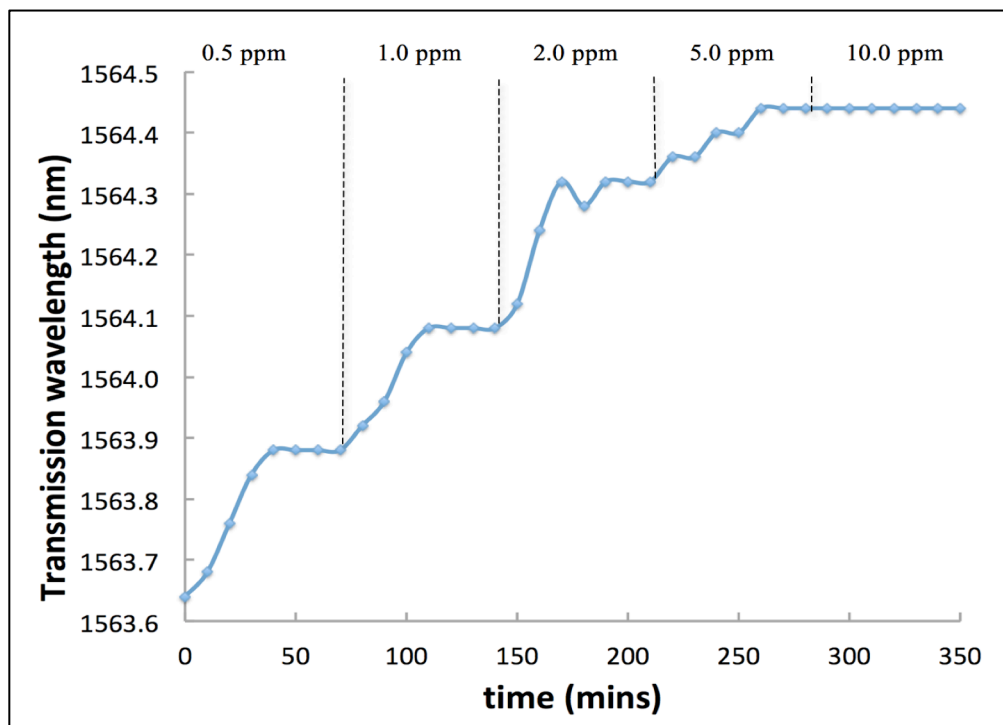
For 0.5 ppm of mercury (II) ion solution, the transmission power of the resonance notch encountered a total increment of 0.354 dBm in the first 50

minutes, whereas for the next 20 minutes, the transmission power remained the same. In the first 60 minutes of exposure to 1.0 ppm of mercury (II) ion solution, the increment of transmission power was around 0.274 dBm but it remained at the same level after 60 minutes of exposure in 1.0 ppm of mercury (II) ion solution. On the other hand, for 2.0 ppm of mercury (II) solution, the sensor encountered an increment in transmission power of 0.385 dBm in the first 50 minutes and remained at the same level beyond this duration. The response of the hybrid sensor became slower in 5.0 ppm of mercury (II) solutions, *i.e.* encountered only 0.032 dBm of increment in transmission power. Finally, as the LPFG-DGT hybrid sensor was exposed to 10.0 ppm of mercury (II) ion solution, the response became saturated, *i.e.* increased only 0.022 dBm in the first 10 minutes of exposure and remained the same afterwards.

On the other hand, in 0.5 ppm and 1.0 ppm of mercury (II) ion solutions, the resonance wavelength encountered a total shift of 0.24 nm and 0.20 nm respectively in the first 40 minutes of exposure time and remained at the same wavelength after that. In 2.0 ppm and 5.0 ppm of solutions, the notch shifted for a total of 0.24 nm and 0.12 nm in the first 50 minutes of exposure, respectively. However, the resonance notch of the hybrid sensor remained the same in 10.0 ppm of mercury (II) solutions because the saturation state had been reached and no further reaction occurred in between the gold nanoparticles and mercury (II) ions.



(a)



(b)

Figure 6.4 (a) Transmission power response; (b) Transmission wavelength shift of the first hybrid sensor towards mercury (II) solutions

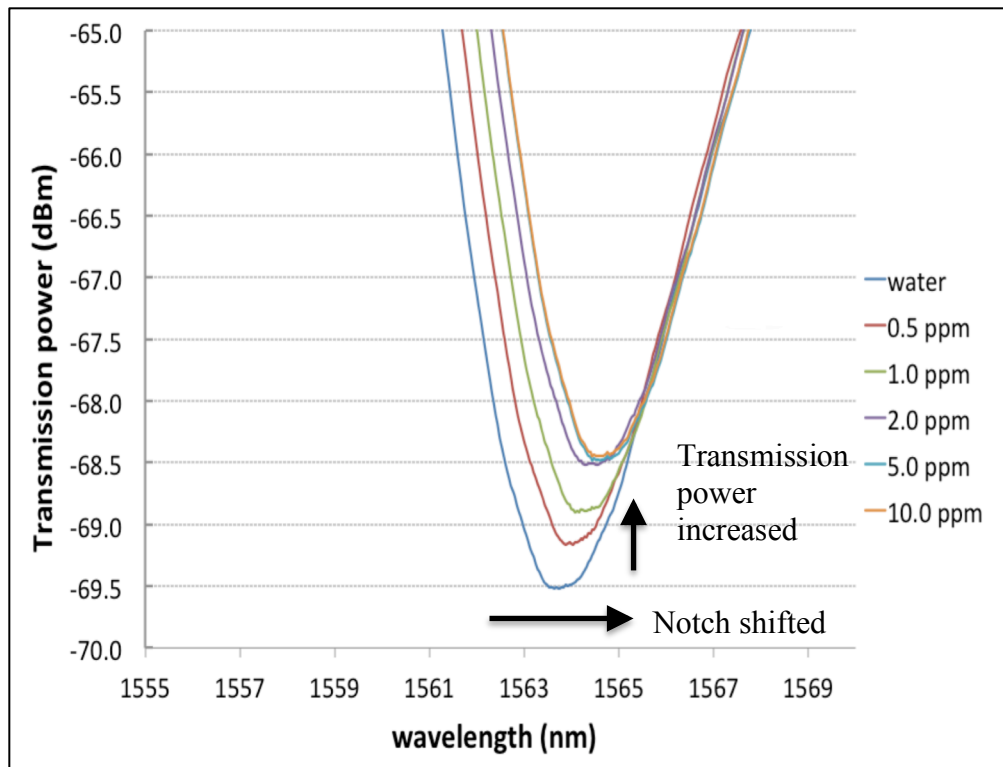


Figure 6.5 Transmission response of the first hybrid sensor towards mercury solutions

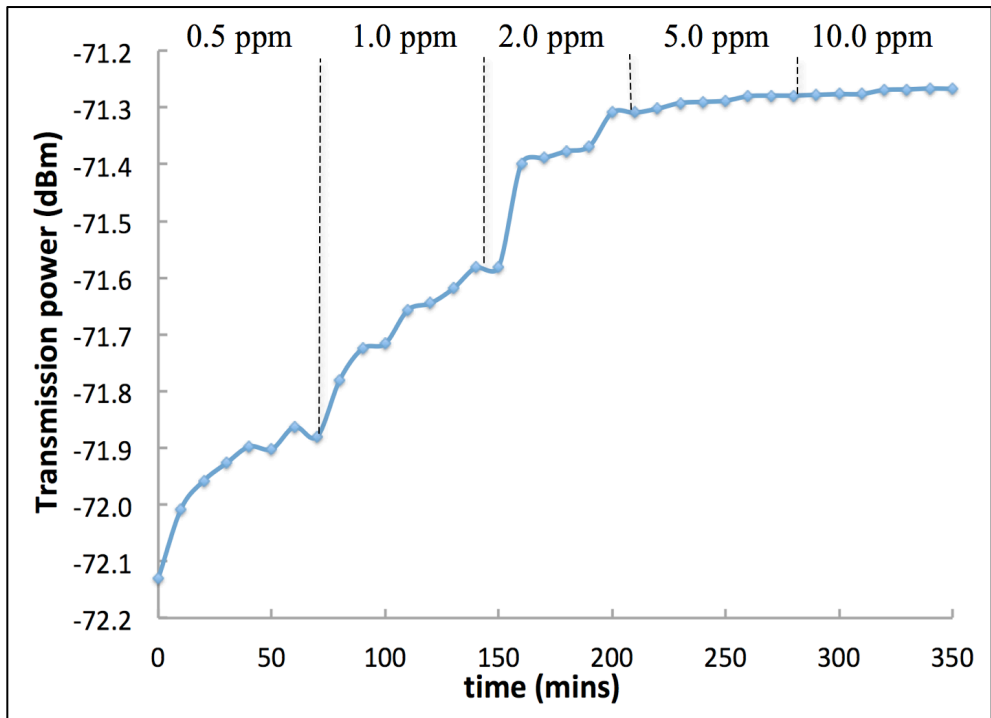
A similar experiment was repeated with another hybrid LPFG-DGT structure to confirm the findings. The results of the second hybrid structure are shown in Figure 6.6. From the results, it can be observed that the sensor had a similar response as the first hybrid structure. The resonant wavelength of the second hybrid structure encountered a total red shift of 0.68 nm to a longer wavelength and a total increment power of 0.864 dBm.

For 0.5ppm of mercury (II) ion solution, the transmission power of the resonance notch encountered a total increment of 0.233 dBm in the first 40 minutes, whereas for the next 30 minutes, the transmission power remained almost the same as the response had stabilised in the mercury (II) solution. When the hybrid sensor was exposed to 1.0 ppm of mercury (II) ion solution, the increment of transmission power was around 0.298 dBm. On the other hand, for 2.0 ppm of mercury (II) solution, the sensor encountered an increment in transmission power of 0.272 dBm in the first 60 minutes and remained at same level beyond this duration. The response of the hybrid sensor became smaller in 5.0 ppm of mercury (II) solution; it encountered only 0.030 dBm of increment in transmission power. Lastly, as the second LPFG-DGT hybrid sensor was exposed to 10.0 ppm of mercury (II) solution, the response became saturated; its transmission power had increased only 0.012 dBm in the first 20 minutes of exposure and remained the same afterwards.

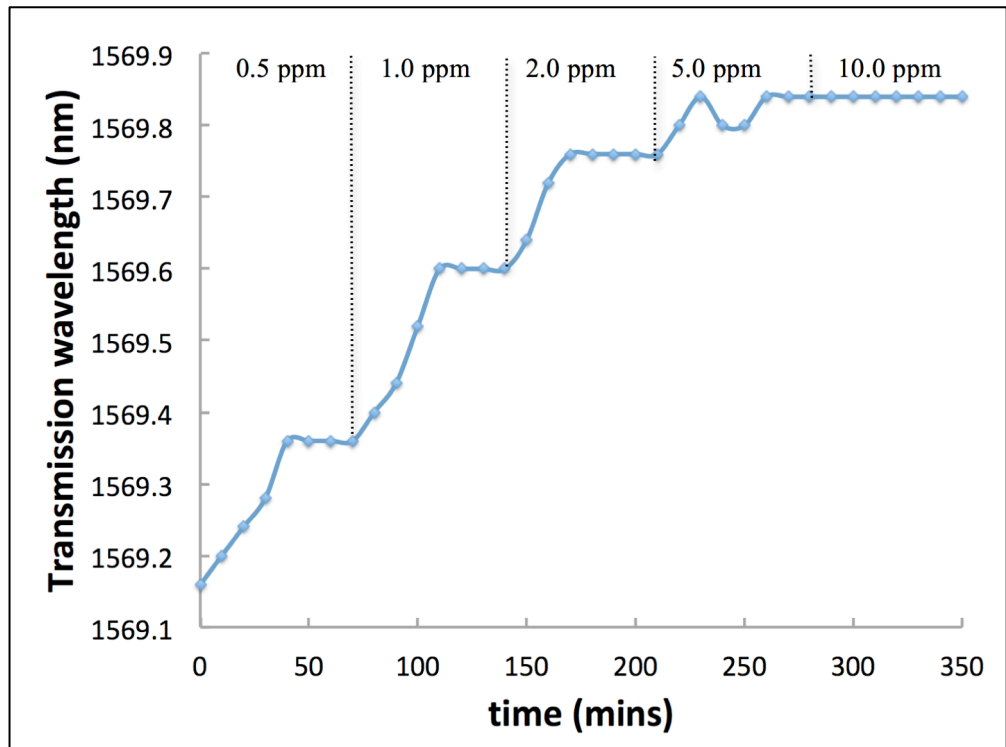
On the other hand, in 0.5 ppm of mercury (II) solutions, the resonance wavelength encountered a total shift of 0.24 nm to a longer wavelength in the first 40 minutes of exposure time and remained at the same wavelength after

that. When the sensor was exposed to 1.0 ppm of mercury (II) solution, the resonant wavelength shifted a total of 0.24 nm to a longer wavelength and the position of the notch remained the same for the remaining 30 minutes. In 2.0 ppm of mercury (II) solution, the notch shifted for a total of 0.16 nm in the first 30 minutes and the response plateaued after that. In addition, the resonant wavelength encountered a total red shift of 0.08 nm in the first 20 minutes of exposure, respectively. However, the resonance notch of the hybrid sensor remained the same in 10.0 ppm of mercury (II) solution.

The results of both hybrid structures show that the proposed sensor system is able to detect mercury as its resonant wavelength had shifted to a longer wavelength and its minimum transmission power had increased when the sensors were exposed to mercury (II) solutions.



(a)



(b)

Figure 6.6 (a) Transmission power response; (b) Transmission wavelength shift of the second hybrid sensor towards mercury (II) solutions

## 6.5.2 Comparison of Performances between Hybrid and Open Structure

### Sensor

The second part of the experiment was conducted to investigate the roles of the membrane filter and diffusive gel layer in the hybrid structure. Another structure was constructed without the presence of both membrane filter and diffusive gel layers and the illustration of this open structure is shown in Figure 6.7 below. The PE-AuNP coated LPFG in this open structure was exposed directly to the measurand due to the absence of both upper layers. Similarly, this open structure was then tested with mercury (II) solutions with five different concentrations.

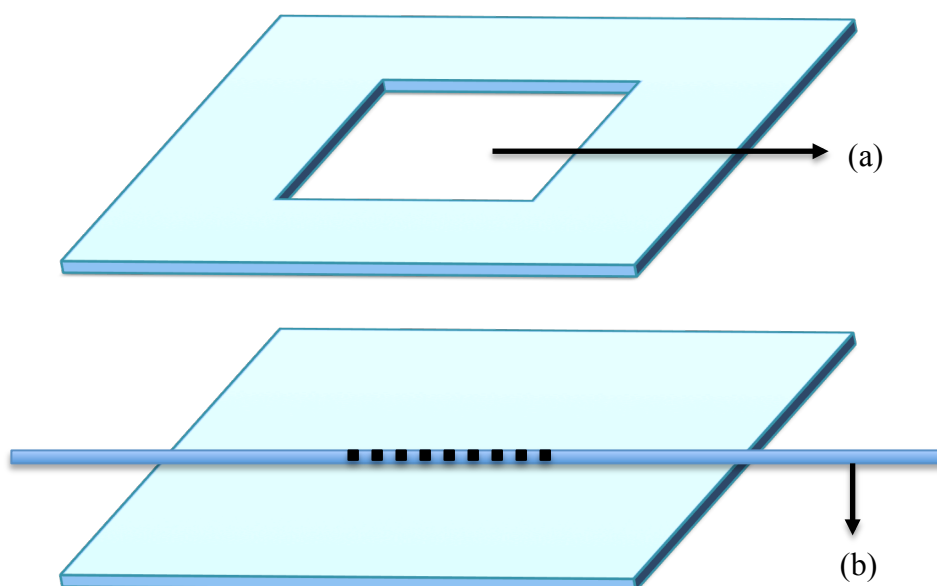
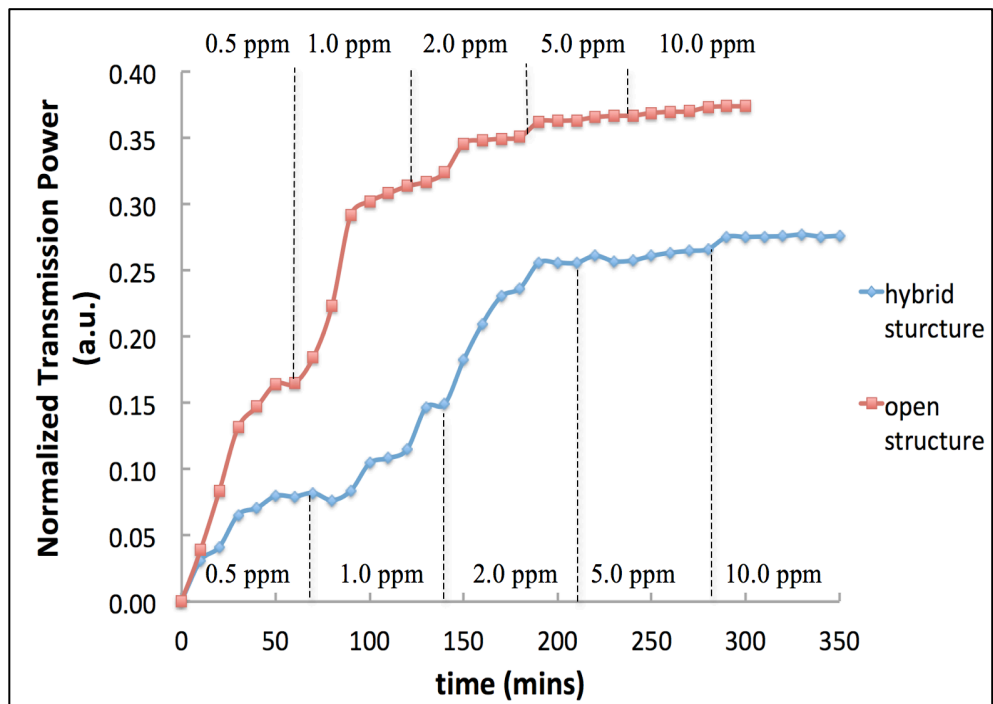


Figure 6.7 Diagram of the open structure sensor (a) window that exposed fiber gratings section, (b) PE-AuNP coated LPFG; both the upper plastic plate and base plate were glued together to seal the structure

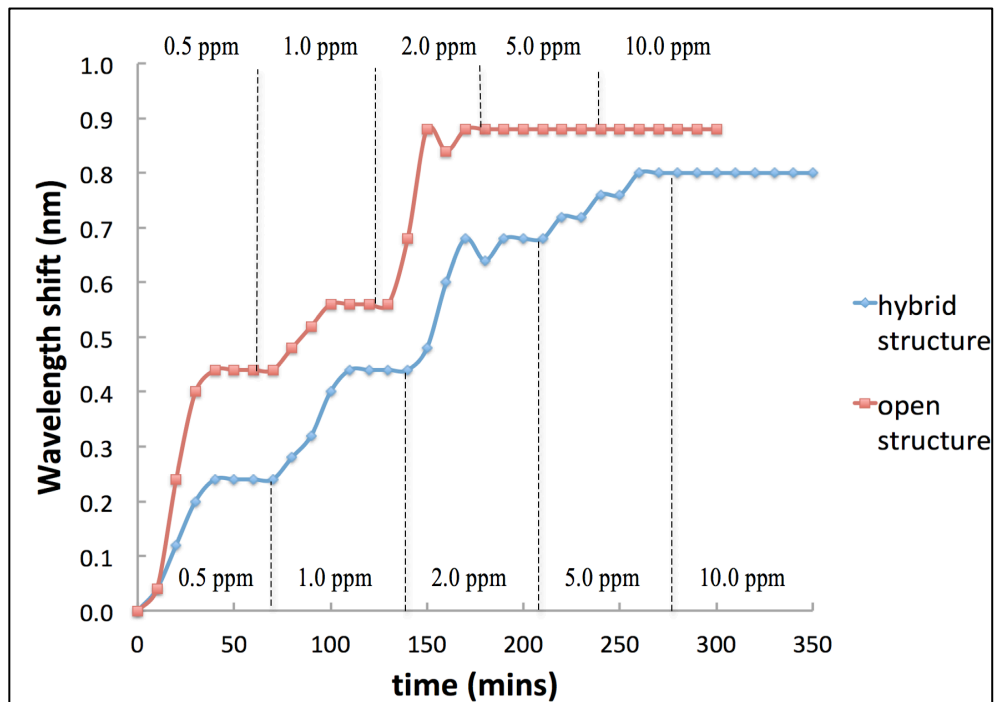
The results of the first open structure sensor were compared to the responses of LPFG-DGT hybrid sensor, as shown in Figure 6.8. It can be observed that the open structure sensor had a response that was similar in trend as the hybrid sensor structure. However, the response rates to reach plateau between the open and hybrid structure were different, as summarized in Table 6.1. In general, the open structure sensor responded faster when exposed to the mercury (II) ions than the hybrid structure sensor indicating the role of the diffusive gel in reducing the flow of mercury (II) ions towards the PE-AuNP coated LPFG. Also, the comparison results showed that the responses of both open and hybrid structure reached saturation state after immersion in mercury (II) ions for a period of time. This was because the gold nanoparticles coated on LPFGs in both structures had fully reacted with the mercury (II) ions. Therefore, this proves that the presence of DGT structure and gel layer will not influence the reaction of gold nanoparticles towards mercury (II) ions.

Table 6.1 First comparison of response rate for the hybrid LPFG-DGT structure and open structure

| Concentrations<br>(ppm) | Hybrid LPFG-DGT<br>Structure<br>(Rate) |                                  | Open Structure<br>(Rate)            |                                  |
|-------------------------|----------------------------------------|----------------------------------|-------------------------------------|----------------------------------|
|                         | Transmission<br>power<br>(a.u/ min)    | Wavelength<br>shift<br>(nm/ min) | Transmission<br>power<br>(a.u/ min) | Wavelength<br>shift<br>(nm/ min) |
| 0.5                     | 0.0016                                 | 0.0060                           | 0.0033                              | 0.0147                           |
| 1.0                     | 0.0012                                 | 0.0040                           | 0.0045                              | 0.0030                           |
| 2.0                     | 0.0016                                 | 0.0080                           | 0.0018                              | 0.0107                           |
| 5.0                     | 0.0002                                 | 0.0020                           | 0.0004                              | No change                        |
| 10.0                    | 0.0002                                 | No change                        | 0.0002                              | No change                        |



(a)



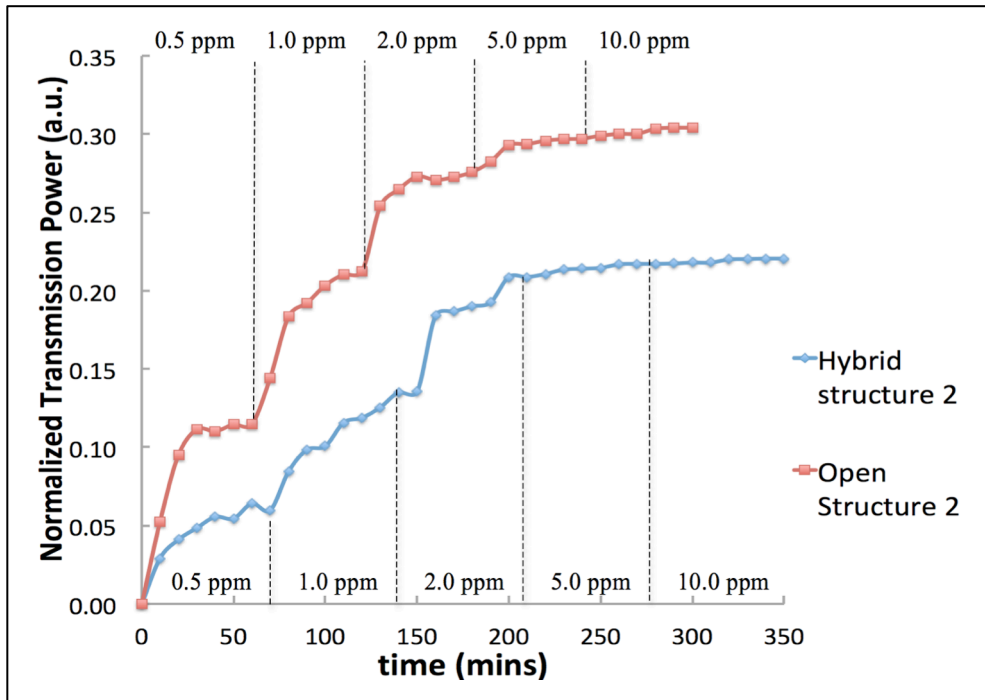
(b)

Figure 6.8 First comparison of (a) Normalized transmission power; (b) Wavelength shift between the hybrid and open structure

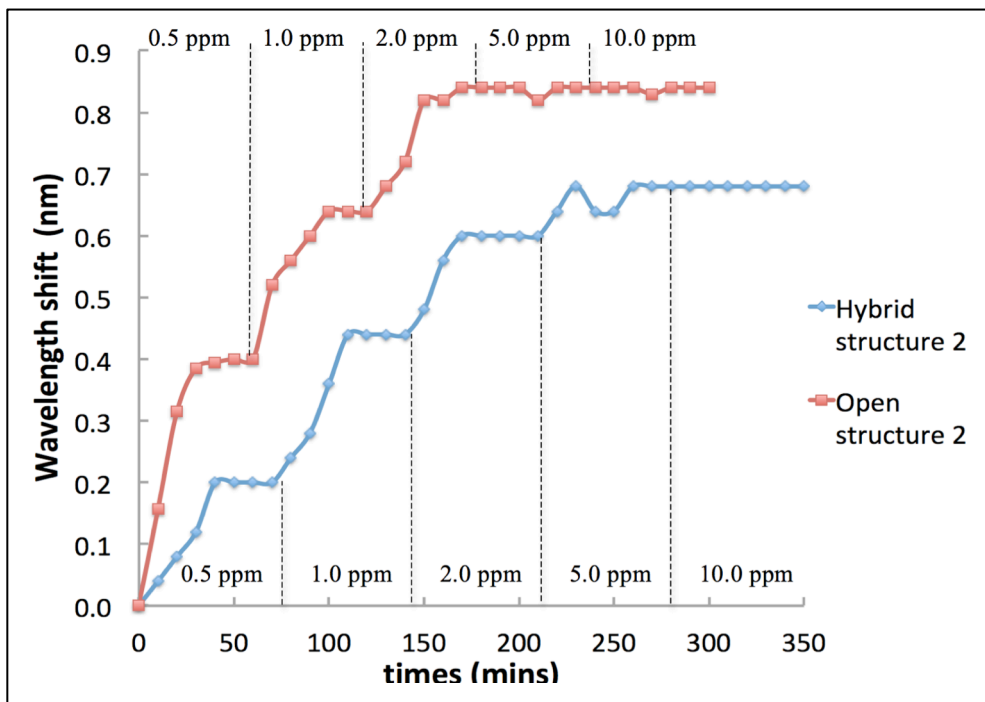
Similarly, the experiment was conducted with another open structure and the result was compared to the second hybrid structure to determine the consistency of results. Results showed that both second comparison conducted in this section led to the similar conclusion as the first comparison discussed previously (the first open and hybrid structure). The response rates for both structures are summarized into Table 6.2. Furthermore, the comparisons between the second open structure sensor and the second hybrid structure are shown in Figure 6.9.

Table 6.2 Second comparison of response rate for hybrid and open structure

| Concentrations<br>(ppm) | Hybrid LPFG-DGT<br>Structure<br>(Rate) |                                  | Open Structure<br>(Rate)            |                                  |
|-------------------------|----------------------------------------|----------------------------------|-------------------------------------|----------------------------------|
|                         | Transmission<br>power<br>(a.u/ min)    | Wavelength<br>shift<br>(nm/ min) | Transmission<br>power<br>(a.u/ min) | Wavelength<br>shift<br>(nm/ min) |
| 0.5                     | 0.0010                                 | 0.0048                           | 0.0038                              | 0.0133                           |
| 1.0                     | 0.0011                                 | 0.0060                           | 0.0025                              | 0.0080                           |
| 2.0                     | 0.0012                                 | 0.0053                           | 0.0021                              | 0.0067                           |
| 5.0                     | 0.0001                                 | 0.0016                           | 0.0005                              | No change                        |
| 10.0                    | 0.0001                                 | No change                        | 0.0001                              | No change                        |



(a)



(b)

Figure 6.9 Second comparison of (a) Normalized transmission power; (b) Wavelength shift between the hybrid and open structure

In conventional DGT, the use of different types of diffusive layers demonstrated the critical role of their pore sizes for allowing only certain elements with smaller sizes than the pore to pass through (Pouran *et al.*, 2014). Similarly, in this LPFG-DGT hybrid sensor structure, the diffusive gel layer allowed the mercury (II) ions to diffuse from the measurand (where the mercury (II) ions were in higher concentration) to the innermost LPFG region (where the mercury (II) ion was not present initially), until equilibrium state was achieved. Due to this extra process of diffusion in the LPFG-DGT hybrid sensor structure, the response time of the PE-AuNP coated LPFG was longer as extra time was needed for the mercury (II) ions to diffuse through the gel layer and reach an equilibrium state. Once the mercury (II) ions diffused out of the diffusive gel and reached the PE-AuNP coated LPFG, the ions reacted with AuNP coated on the LPFG to form amalgam, thus changing the effective refractive index of the LPFG's cladding. As a result, the resonance notch of the LPFG sensor shifted because of its sensitivity towards changes in effective refractive index of the cladding.

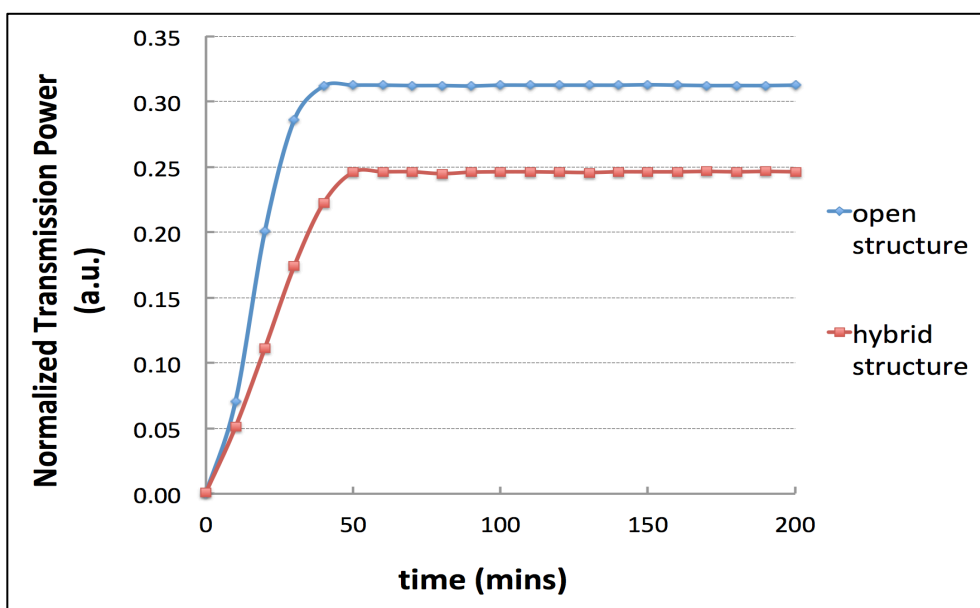
To confirm the root cause of the prolonged response time, additional experiments were conducted to both structures with concentration of mercury (II) ions fixed at 2.0 ppm. The results obtained are shown in Figure 6.10 where again, the response rates of the open structure sensor was higher if compared to the hybrid sensor structure. For the transmission power of both LPFGs, the response rate of the open structure and hybrid structure were 0.0078 a.u./min and 0.0049 a.u./min, respectively, before reaching plateaus. On the other hand, for wavelength shift, the response rate of the open structure was 0.032 nm/min

while the rate for the hybrid structure was 0.018 nm/min. In addition, the maximum shift of resonance wavelength and the increment of normalized transmission power of both open and hybrid structures were at different saturating levels. This scenario can be explained by the concentrations of mercury (II) ions surrounding the coated LPFG. In the open sensor structure, the PE-AuNP coated LPFG was directly exposed to the applied mercury (II) solutions, therefore all the mercury (II) ions were attracted towards the LPFG without barrier and reacted with the nanoparticles on the grating surface to form amalgam (Levlin et al., 1999), thus affecting the resonance wavelength. On the contrary, for the LPFG-DGT hybrid structure, the number of mercury (II) ions that was able to reach to the LPFG surface was limited by the diffusion process of metal ions through the diffusive gel layer. When the mercury (II) solution was applied onto the window of the hybrid sensor, the metal ions will continuously diffuse in and out of the diffusive gel layer until a point where the number of mercury (II) ions between the outer and innermost layers of the hybrid structure are the same, *i.e.* equilibrium state. Due to this, the number of mercury (II) ions that actually reached the innermost layer and reacted with the AuNP on the LPFG surface in the hybrid structure was lower than in the open structure. Thus, the saturating level of the open structure was higher than the hybrid structure.

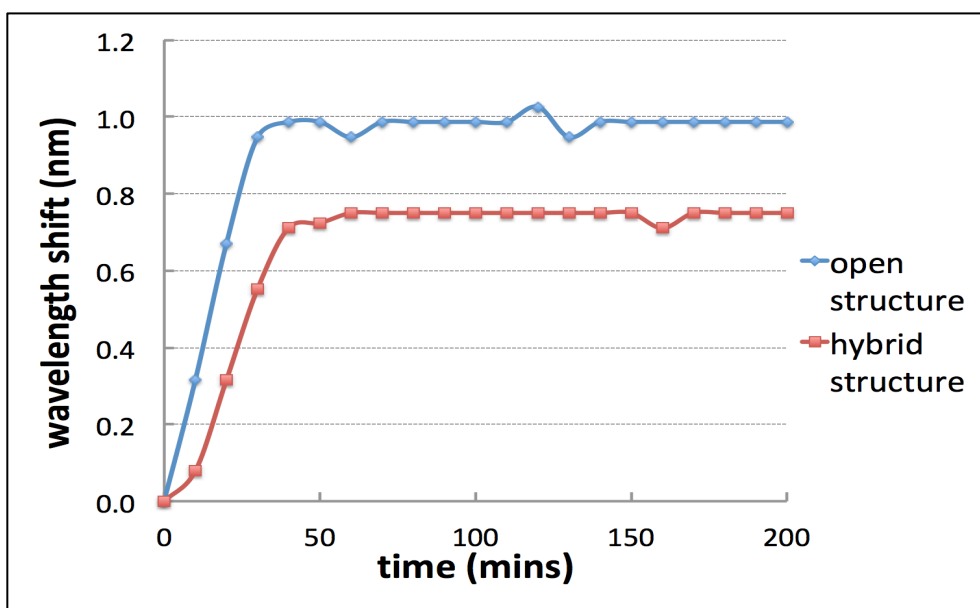
This phenomenon of the equilibrium state can be explained by the concentration volume equation as below:

$$C_{after} = \frac{C_{before}V_1}{V_2} \quad (6.1)$$

In this case,  $C_{before}$  represents the concentration of the original mercury (II) solution and  $C_{after}$  represents the final concentration of mercury (II) ions inside and outside the gel after the diffusion had reached an equilibrium. Furthermore,  $V_1$  is the volume of measurand applied to the window of the sensor while  $V_2$  is the volume of both the measurand and gel. The volume of the gel is taken into consideration in the experiment because the mercury ions have gradually diffused into the gel throughout the experiment. In other words, this phenomenon is similar to dilution, *i.e.*, the process where the concentration of a solute decreased when adding more solvent (in this case the diffusive gel). The movement and diffusion of mercury (II) ions from the original measurand into the gel gradually decreased the number of mercury (II) ions in the original measurand and after equilibrium state was reached, the number of mercury (II) ions inside and outside of gel will be the same. Thus, according to the equation (6.1),  $C_{after}$  will be lower than  $C_{before}$  due to the increment in total volume,  $V_2$ . The diffusion of mercury (II) ions through gel can be described as the diagram shown in Figure 6.11.



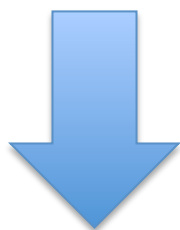
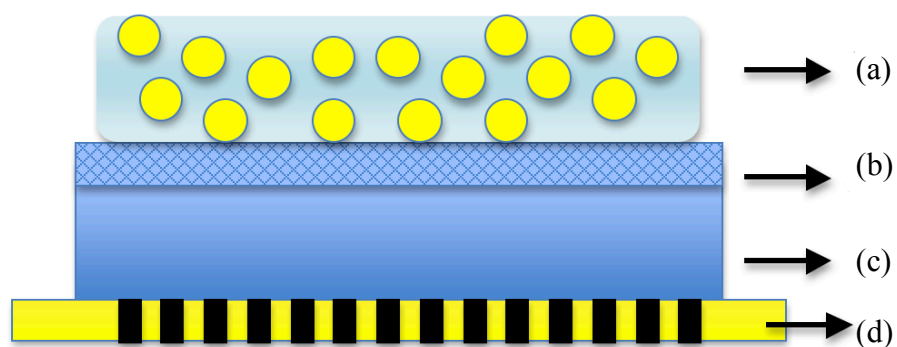
(a)



(b)

Fig. 6.10 Comparison of (a) Normalized transmission power; (b) wavelength shift between open structure and hybrid structure in 2.0 ppm mercury (II) solution

**Initial Stage:**



**Equilibrium State (Concentration within and outside of the gel are similar):**

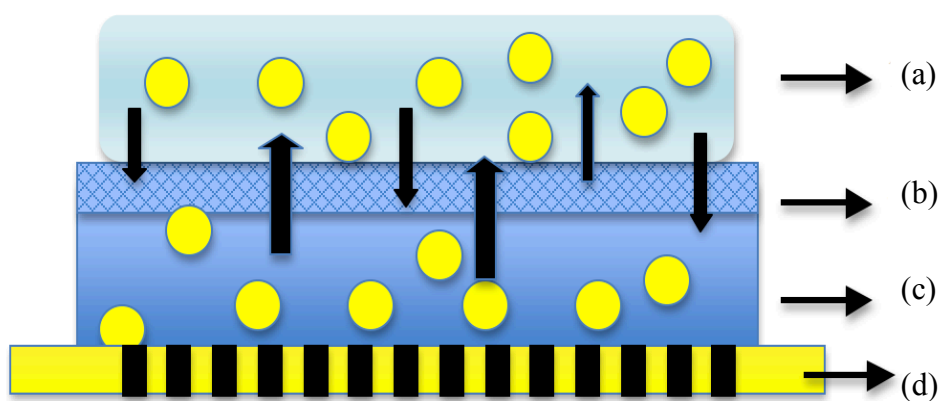


Figure 6.11 Diffusion of mercury (II) ions across diffusive gel until equilibrium is achieved; (a) Mercury (II) solution (original measurand), (b) membrane filter, (c) diffusive gel layer, PE-AuNP coated LPFG

According to all results obtained above, the proposed hybrid sensor can be used for real-time and long-term monitoring of mercury (II) ions. With the DGT structure, the innermost LPFG was well sealed and protected by both the membrane filter and gel layer. Also, the DGT structure prevented the LPFG to be influenced by outer disturbances, thus providing a stable and constant sensing condition which was an important aspect in long-term monitoring applications. On the other hand, the hybrid sensor demonstrated in this research allowed us to conduct real-time monitoring as the data of the sensor response can be collected and investigated from time to time.

## **6.6 Summary**

A novel hybrid LPFG-DGT sensor system that was designed for the detection of mercury (II) ions present in water had been successfully developed and tested. This proposed hybrid sensor introduces the possibility to overcome the demerit of usual sensors as it can be directly deployed in water bodies to provide real-time detection, instead of a quick detection in a laboratory. Furthermore, the hybrid sensor demonstrated is capable to be used for long-term monitoring due to the structure of DGT that provides a good protection and offers a stable sensing condition for the LPFG in detecting mercury (II) ions. The experiment results showed that the response rate of the hybrid structure was slower than the open structure due to the presence of the diffusive gel layer that prolonged the movement of the mercury (II) ions before reaching the PE-AuNP coated LPFG sensor. However, the response trends of both open and hybrid structures were similar to each other, indicating

that the presence of the gel structure did not affect the performance of PE-AuNP coated LPFG in detecting mercury (II) ions. This mechanism makes the proposed LPFG-DGT sensor system suitable to be used for long-term monitoring of mercury (II) ions in water bodies. Also, it has the capability for near real-time and remote monitoring when used in a fiber sensor network.

## CHAPTER 7

### CONCLUSIONS AND FUTURE RECOMMENDATIONS

#### 7.1 Conclusion

The research presented in this thesis had mainly focused on the development of a novel hybrid LPFG-DGT sensing system that demonstrates the potential for real-time, in situ and long-term monitoring of mercury (II) ions in water. Throughout the different phases of research, the objectives and research gaps mentioned in the beginning of this thesis have been achieved and fulfilled. The first objective mentioned in Chapter 1 was achieved in Chapter 3 and 4. The second objective was fulfilled in Chapter 5, whereas the third objective was achieved in last stage of research, *i.e.* Chapter 6.

In early phase of this research, LPFG was fabricated particularly with the electrical arc discharge technique. The sensitivity of LPFGs towards the external index had been successfully characterized as it is the key parameter that allows them to be used as sensors. Through the first two phases of research, it has been proven that it is possible to enhance the sensitivity of the LPFGs towards external index for both wavelength-based and transmission-based interrogations, by enlarging their wavelength shift and transmission variation in accordance to different refractive indices. Also, both enhancement techniques employed in this research do not require complicated processes to

modify the physical structure of the LPFG. It has been shown that the wavelength shift of LPFG was successfully enlarged by coating multi-layer polyelectrolytes onto the LPFG surface. On the other hand, the transmission attenuation of LPFG towards different refractive indices was successfully increased by applying double-pass configuration into the experimental setup.

The third stage of this research aimed to achieve the second objective of this research by further modifying the surface of LPFG so that it can be used to detect mercury (II) ions. Throughout this phase of research, it was shown that there was a possibility to further tailor the surface of LPFG with gold nanoparticles through the ESA technique. Also, it was found that gold nanoparticles were suitable sensing agents to be used in monitoring mercury (II) ions due to their ability to capture mercury (II) ions. The novel combination of coating agents used in this research, *i.e.* polyelectrolytes-gold nanoparticles had not been demonstrated for mercury sensing, so far, by other researches. Due to its ability in monitoring mercury (II) ions as well as the potential of being deployed kilometres away from the laboratory, the PE-AuNP coated LPFG sensor presented in this research introduces the possibility to overcome the shortcomings discovered in other optical-based mercury sensors, which are limited only to laboratory testing.

Last but not least, the work conducted in the final stage of this research had successfully constructed a novel hybrid LPFG-DGT sensing system which is suitable to be used for real-time and long-term monitoring of mercury (II) ions. This novel hybrid system overcomes the problem of the short lifespan

discovered in LPFG. Generally, the durable structure of the hybrid system sealed the PE-AuNP coated LPFG as the innermost layer within the structure and helped to prevent the LPFG from being broken by environmental factors. By constructing this hybrid structure, it brings the possibility to deploy the sensor in water bodies over a longer period of time for long-term collection of background data. On the other hand, the results obtained through this research proved that this hybrid sensor allows the collection of near real-time data as the responses of the sensor can be investigated from time to time. In conclusion, throughout this whole research, a hybrid DGT-LPFG sensor had been proposed and constructed with the main purpose to provide real-time and long-term data in monitoring the contents of mercury (II) ions in water.

## **7.2 Future Recommendations**

According to the studies conducted in this research, there are a number of topics that require further investigation and improvement. In this thesis, the focus is given mainly to the mercury (II) ions detection using LPFG, hence, attention is required to be given to the hybrid LPFG-DGT structure in future works. It is important to carry out further research concerning the improvement of the performance of the hybrid structure.

- Improvement of the hybrid sensor to allow the sensor to be able to detect mercury (II) ions at even lower concentrations. On the contrary, improvement can be done to the sensor so that it can be used to detect higher concentration as well.

- An investigation on the influences of different diffusive gel layers towards the diffusion of mercury (II) ions; in other words, to observe the effect of applying different gel layers in the hybrid structure towards its performance in mercury (II) detection.
- Conduction of next phase of testing, preferably in a real water bodies, which consist of mercury content to evaluate the performance of the hybrid sensor in a real scenario.
- More investigations can be conducted to observe the influence of other factors towards the response of this hybrid sensor, also to confirm the specificity and selectivity of this sensor.
- Further testing is warranted to investigate the stability of the hybrid sensor in protecting the LPFG in a real scenario which may be harsh towards the deployment of the sensor.
- Further modifications to the sensor in order to achieve a more advanced sensing structure. For instance, to modify the sensor into a portable device might be a good start.

## PUBLICATIONS

### Journal Papers

Tan, S.Y., Yong, Y.T., Lee, S.C., Rahman, F.A., 2015. Review on an arc-induced long period fiber grating and its sensor applications, *J. Electromagn. Waves Appl.* 29, pp. 703–726.

Tan, S.Y., Lee, S.C., Okazaki, T., Kuramitz, H., Rahman, F.A., 2018. Detection of Mercury (II) Ions in Water by Polyelectrolyte - Gold Nanoparticles Coated Long Period Fiber Grating Sensor, *Optics Communication* 419, pp. 18-24.

Tan, S.Y., Lee, S.C., Kuramitz, H., Rahman, F.A., 2018. A Novel Hybrid Long Period Fiber Grating-Diffusive Gradient in Thin Films Sensor System for the Detection of Mercury (II) Ions in Water. (Submitted)

Okazaki, T., Imai, K., Tan, S.Y., Yong, Y.T., Rahman, F.A., Hata, N., Taguchi, S., Ueda, A., Kuramitz, H., 2015. Fundamental study on the development of fiber optic sensor for real-time sensing of CaCO<sub>3</sub> scale formation in geothermal water, *Analytical Science*.31, pp. 177-183.

## REFERENCES

Abbaspour, S., 2011. Water Quality in Developing Countries, South Asia, South Africa, Water Quality Management and Activities that Cause Water Pollution, 2011 International Conference on Environmental and Agriculture Engineering IPCBEE ,15, pp. 94-102.

Akki, J.F., Lalasangi, A.S., Raikar, P.U., Srinivas, T., Laxmeshwar, L.S., and Raikar, U.S., 2013. Core-cladding mode resonances of long period fiber grating in concentration sensor, IOSR Journal of APplied Physics (IOSR-JAP), 3(3), pp. 41-46.

Allsop, T., Floreani, F., Jedrzejewski, K.P., Marques, P.V.S., Romero, R., Webb, D.J., and Bennion, I., 2006. Spectral characteristics of tapered LPG device as a sensing element for refractive index and temperature, Journal of Lightwave Technology, 24(2), pp. 870-878.

Alwis, L., Bremer, K., Sun, T., and Kenneth T. V. Grattan, Analysis of the Characteristics of PVA-Coated LPG-Based Sensors to Coating Thickness and Changes in the External Refractive Index, IEEE Sensors Journal, 13(3), pp. 1117-1124.

Amato, E.D., Simpson, S.L., Jarolimek, C.V., Jolley, D.F., 2014. Diffusive gradients in thin films technique provide robust prediction of metal bioavailability and toxicity in estuarine sediments, Environ. Sci. Technol., pp. 4485–4494.

Ayala, J.M.E., Chavez, R.I.M., Garcia, J.C.H., and Laguna, R.R., 2012. Long period fiber grating produced by arc discharges, Fiber Optic Sensors, pp. 296-316.

Behrens, S.H., Grier, D.G., 2001. The charge of glass and silica surfaces. J. Chem. Phys., 115, pp. 6716-6721.

Bernhoft, R.A., 2012. Mercury Toxicity and Treatment: A Review of the Literature, Journal of Environmental and Public Health, 2012, pp. 1-10.

Bhatia, V., 1999. Applications of long-period gratings to single and multi-parameter sensing, Optics Express, 4, pp. 457-466.

Bock, W.J., Chen, J.H., Mikulic, P., Eftimov, T., 2007. A Novel Fiber-Optic Tapered Long-Period Grating Sensor for Pressure Monitoring, IEEE Transactions on Instrumentation and Measurement., 56, pp. 1176-1180.

Caucheteur C, Chah K, Lhomme F, Debliquy M, Lahem D, Blondel M, Megret P. Enhancement of cladding modes coupling in tilted Bragg gratings owing to cladding etching. In: Proceedings of 2005 IEEE/LEOS Workshop on Fibres and Optical Passive Components; 2005 June 22–24; Mondello.

Carrie, R.L., Ruth, D.Y., Gregory, G.L., Douglas, A.B., Charles, T.D., Gregory, B.L., Jason, A.L., Nina, S., 2014. Evaluating the efficiency of environmental monitoring programs, *Ecological Indicators* 39, pp. 94-101.

Chan, K.P., Tan, C.S., Teng, W.S., Rahman, F.A., Soon, S.C. 2010. Feasibility study of long period grating as an optical biosensor for dengue virus detection – an alternative approach to dengue virus screening. Paper presented at: IEEE EMBS Conference on Biomedical Engineering & Sciences (IECBES 2010), Nov 30–Dec 2 2010 Kuala Lumpur, Malaysia.

Chávez, R.I.M., Rios, A.M., Gomez, I.T., Chavez, J.A.A., 2008. Selvas-Aguilar R, Estudillo-Ayala J. Wavelength band-rejection filters based on optical fiber fattening by fusion splicing. *Opt. Laser Technol.*, 40, pp. 671–675.

Cheng, A.Z., Swaminathan, R., Layer By Layer (LbL) Self-assembly Strategy and its applications, *Nanotechnology Engineering*, University of Waterloo, pp. 1-5.

Chiang, K.S., Liu, Y.Q., Ng, M.N., Dong, X.Y., 2000. Analysis of etched long-period fibre grating and its response to external refractive index, *Electronics Letters*. 36, pp. 966-967.

Colaco, C., Caldas, P., Chibante, R., and Rego, G., 2015. Arc-induced gratings in the turning points, 24th International Conference on Optical Fibre Sensors, 9634 of Proceedings of SPIE, September 2015 Curitiba, Brazil.

Correy, T.B., 1982. What makes an electric welding arc performs its required functions. US Department of Energy.

Czapla, A., 2015. Spectral properties of long-period fiber gratings with nematic liquid crystals. PhD dissertation, Université du Québec en Outaouais, Canada.

Davis, D.D., Gaylord, T.K., Glytsis, E.N., and Mettler, S.C., 1998. CO<sub>2</sub> laser-induced long-period fibre gratings: spectral characteristics, cladding modes and polarisation independence, *Electron. Lett.*, 34, pp. 1416-1417.

Davison, W., Zhang, H., 1994. In situ speciation measurements of trace components in natural waters using thin-film gels, *Nature*. 367, pp. 546-548.

Decher, G., 1997. Fuzzy Nanoassemblies: Toward Layered Polymeric Multicomposites, *Science*, 277, pp. 1232- 1237.

Desai, N, SmtVanitaben, 2014. A study on the water pollution based on the environmental problem. *Indian Journal of Research*, 3(12), pp. 95-96.

Dianov, E.M., Karpov, V.I., Grekov, M.V., Golant, K.M., Vasiliev, S.A., Medvedkov, O.I., Khrapko, R.R., 1997. Thermo-induced long-period fibre gratings. In: 23rd European Conference on Optical Communication (ECOC '97), Sep 22–25 1997, Edinburgh.

Dianov, E.M., Kurkov, A. S., Medvedkov, O. I., and Vasiliev, S. A., 1996. Photoinduced long-period fiber grating as a promising sensor element, *European Conf. Solid State Transducers Eurosensors*, pp. 128.

Ding, J.F., Zhang, A.P., Shao, L.Y., Yan, J.H., He, S., 2005. Fiber-taper seeded long-period grating pair as a highly sensitive refractive-index sensor. *IEEE Photon. Technol. Lett.*, 17, pp. 1247–1249.

Divis, P., Leermakers, M., Docekalova, H., Gao, Y., 2005. Mercury depth profiles in river and marine sediments measured by the diffusive gradients in thin films technique with two different specific resins, *Anal Bioanal Chem* 382, pp. 1715–1719.

Divis, P., Szkandera, R., Brulik, L., Docekalova, H., Matus, P., Bujdos, M., 2009. Application of New Resin Gels for Measuring Mercury by Diffusive Gradients in a Thin-films Technique, *Analytical Sciences*. 25, pp. 575-578.

Docekalova, H., Divis, P., 2005. Application of diffusive gradient in thin films technique (DGT) to measurement of mercury in aquatic systems, *Talanta*. 65, pp. 1174-1178.

Dodds, W.K., Robinson, C.T., Gaiser, E.E., Hansen, G.J.A., Powell, H., Smith, J.M., Morse, N.B., Johnson, S.L., Gregory, S.V., Bell, T., Kratz, T.K., McDowell, W.H., 2012. Surprises and Insights from Long-Term Aquatic Data Sets and Experiments, *BioScience.*, 62, pp. 709–721.

Driscoll, C.T., Han Y.J., Chen, C.Y., D.C. Evers Kathleen Fallon Lambert Holsen, T.M., Kamman, N.C., Munson, R.K., 2007. Mercury Contamination in Forest and Freshwater Ecosystems in the Northeastern United States, *BioScience*, 572, pp. 17–28.

Du Y., Chen, Y.Z., Zhu, C., Zhuang, Y.Y., Huang, J., 2017. An embeddable optical strain gauge based on a buckled beam, *Review of Scientific instruments*, 88, 115002.

Du, C., Zhao, Y., Wang, Q., Xia, F., 2017. Sensitivity-optimized long-period fiber gratings for refractive index and temperature sensing, *Instrumentation Science & Technology*, pp. 1-15.

- Du, J.J., Wang, Z.K., Fan, J.L., Peng, X.J., 2015. Gold nanoparticle-based colorimetric detection of mercury ion via coordination chemistry, *Sensors and Actuators*. 212, pp. 481-486.
- Duan, J., Zhan, J.H., 2015. Recent developments on nanomaterials-based optical sensors for Hg<sup>2+</sup> detection, *Science China Materials*. 58, pp. 223-240.
- Dwivedi, A.K., 2017. Researches in water pollution: a review, *International Research Journal of Natural and Applied Sciences*, 4(1), pp. 118-142.
- Enomoto, T., Shigehara, M., Ishikawa, S., Danzuka, T., Kanamori, H., 1998. Long-period fiber grating in a pure-silica-core fiber written by residual stress relaxation. In: *Optical Fiber Communication Conference and Exhibit. Proceeding of Optical Fiber Communication Conference (OFC '98)*, 22 Feb –27 Feb 1998, San Jose, CA, USA.
- Ensor, K.L., Helwig, D.D. and Wemmer, L.C. 1992. in *Mercury and Lead in Minnesota Common Loons*, published by the MPCA Water Quality Division in 1992.
- Erdogan T., 1997. Fiber grating spectra. *J. Lightwave Tech.*,15, pp.1277–1294.
- Erdogan, T., 1997. Cladding-mode resonances in short- and long- period fiber grating filters, *J. Opt. Soc. Am. A*, 14(8), pp. 1760-1773.
- Fen, Y.W., Yunus, W.M.M., Yusof, N.A., 2011. Detection of Mercury and Copper Ions Using Surface Plasmon Resonance Optical Sensor, *Sensors and Materials*, 23, pp. 325–334.
- Fernandes, A.B, Barros, F.L, Peçanha F.M., 2012. Toxic Effects of Mercury on the Cardiovascular and Central Nervous Systems. *Journal of Biomedicine and Biotechnology*, pp. 1-11.
- Frazao, O., Falate, R., Baptista, J.M., Fabris, J.L., Santos, J.L., 2005. Optical bend sensors based on a long-period fiber grating monitored by an optical time-domain reflectometer. *Opt. Eng. Lett.*, 44, pp. 1–3.
- Frens, G., 1973. Controlled nucleation for the regulation of the particle size in monodisperse gold solutions, *Nat. Phys. Sci.*, 241, pp. 20–22.
- Fujimaki, M., Ohki, Y., Brebner, J. L., and Roorda, S., 2000. Fabrication of long-period optical fiber gratings by use of ion implantation, *Opt. Lett.*, 25, pp. 88-89, 2000.
- Gade, D., 2015. Mercury Emissions from Coal-Fired Powerplants. *Environmental Management & Risk Assessment (PH 560)*. Paper 4.

- Georges, H., Abdelrafik, M., 2002. Electric-arc-induced gratings in non-hydrogenated fibres: fabrication and high-temperature characterizations, *Journal of Optics A: Pure and Applied Optics*, 4(2).
- Gouvie, C.A.J., Baptista J.M., Jorge P.A.S., 2013. Chapter 13 Refractometric optical fiber platforms for label free sensing In: *Current developments in optical fiber technology*, pp. 345–372.
- Gworek, B., Kalabun, O.B., Kijenska, M., Jakubowska, J.W., 2016. Mercury in Marine and Oceanic Waters—a Review, *Water Air Soil Pollut.*, 227(10), pp. 1-19.
- Gworek, B., Dmuchowski, W., Baczewska, A.H., Brągoszewska, P., Bemowska-Kalabun, O., Wrzosek-Jakubowska, J., 2017. Air Contamination by Mercury, Emissions and Transformations—a Review. *Water, Air, and Soil Pollution.*, 228(4).
- Halder, J.N., Islam, M.N., 2015. Water pollution and its impact on the human health. *Journal of environment and human*, 2(1), pp. 36-46.
- Harada, M., 1995. Minamata Disease: Methylmercury Poisoning in Japan Caused by Environmental Pollution, *Critical Reviews in Toxicology*, 25, pp. 1-24.
- Haseena, M., Malik, M.F., Javed, A., Arshad, S., Asif, N., Zulfiqar, S. and Hanif, J., 2017. Water pollution and human health, *Review Article - Environmental Risk Assessment and Remediation*. 1 pp. 16-19.
- Heflin, J.R., Figura, C., Marciu, D., Liu, Y., Claus, R., 1999. Thickness dependence of second-harmonic generation in thin films fabricated from ionically self-assembled monolayers, *Appl. Phys. Lett.*, 74, pp. 495-497.
- Hossain, M.Z., 2015. Water: the most precious resource of our life, *Global Journal of Advanced Research.*, 2, pp. 1436-1445.
- Huang, J.Y., Bennett, W.W., Welsh, D.T., Li, T.L., Teasdale, P.R., 2016. Development and evaluation of a diffusive gradients in a thin film technique for measuring ammonium in freshwaters, *Analytica Chimica Acta*. 904, pp.83-91.
- Huang, Q.D., Yu, Y.Q., Ou, Z.L., Chen, X., Wang, J.S., Yan, P.G., and Du, C.L., 2014. Refractive index and strain sensitivities of a long period fiber grating, *Photonic Sensors*. (4), pp. 92-96.
- Huang, W.P., 1994. Coupled-mode theory for optical waveguides: an overview, *Optical Society of America*. 11(99), pp. 963-983.
- Huang, W.P., Mu, J.W., 2009. Complex coupled-mode theory for optical waveguides, *Optics express*. 17, pp.19134-19152.

- Huang, Y., Tang, F., Liang, X., Chen, G., Xiao, H., Azarmi, F., 2014. Steel bar corrosion monitoring with long-period fiber grating sensors coated with nano iron/silica particles and polyurethane, *Struct. Health Monit.: Int. J.* 14 , pp. 178–189.
- Humbert, G., Malki, A., 2002. Characterizations at very high temperature of electric arc-induced long-period fiber gratings, *Optics Communications*, 208(4–6), pp. 329–335.
- Humbert, G., Malki, A., 2002. Electric-arc-induced gratings in non-hydrogenated fibres: fabrication and high-temperature characterizations. *J. Opt. A: Pure Appl. Opt.* 4, pp. 194–198.
- Hwang, I.K., Yun, S.H., Gentsch, E., and Kim, B.Y., 1999. Profile-controlled long-period fiber gratings based on periodic microbends, *Proceeding of International Conference on OFC*, pp. 177-179.
- Hwang, I.K., Yun, S.H., Kim, B.Y., 1999. Long-period fiber gratings based on periodic microbends. *Opt. Lett.*, 24, pp. 1263–1265.
- Ishaq, I.M., Quintela, A, James, S.W., Ashwell,,G.J., Lopez-Higuera, J.M. and Tatam, R.P., 2005. Modification of the refractive index response of long period gratings using thin film overlays, *Sensors and Actuators B: Chemical*, 107(2), pp. 738-741.
- Ivanov, O.V., 2004. Wavelength shift and split of cladding mode resonances in microbend long-period fiber gratings under torsion," *Optics Communications*, vol. 232, pp. 159-166.
- Ivanov, O.V., Rego, G., 2007. Origin of coupling to antisymmetric modes in arc-induced long-period fiber gratings. *Optics Express*,15(21), pp. 13936–13941.
- James, J.Z., 2012. Mercury sensing with optical responsive gold nanoparticles. PhD thesis, University of California, Berkeley.
- James, S.W., Tatam, R.P., 2003. Optical fibre long-period grating sensors: characteristics and application, *Meas. Sci. Technol.*,14, pp. 49-61.
- Kaminow, I.P., Li, T., editors. *Optical fiber telecommunications IV-A: components*. Waltham, M.A.: Academic Press; 2002. p. 1–876.
- Kashyap, R., 1999. *Fibre Bragg Gratings*. Academic, New York.
- Kersey, A.D., 1996. A Review of Recent Developments in Fiber Optic Sensor Technology, *Opt. Fiber Technol.*, 2, pp. 291–317.
- Khadri, D., Belhadj, W., Gamra, D., Abdelmalek, F., and Bouchriha, H., 2012. On the validity of the effective index method for long period grating photonic crystal fibers, *Materials Sciences and Applications*, 3(5).

Kidd, K.A., Bootsma, H.A., Hesslein, R.H., Lockhart, W.L., Hecky, R.E., 2003. Mercury concentrations in the food web of Lake Malawi, East Africa. *J Great Lakes Res.*, 29, pp. 258–266.2.

Kim, M.W., Lee, D.W., Hong, B., Chung, H.Y., 2002. Performance characteristics of long-period fiber gratings made from periodic tapers induced by electric-arc discharge. *J. Korean Phys. Soc.*, 40, pp. 369–373.

Kondo, Y., Nouchi, K., and Mitsuyu, T., 1999. Fabrication of long-period fiber gratings by focused irradiation of infrared femtosecond laser pulses, *Opt. Lett.*, 24(10), pp. 646-648.

Korposh, S., James, S., Tatam, R., Lee, S.W., 2013. Optical Fibre Long-Period Gratings Functionalised with Nano-Assembled Thin Films: Approaches to Chemical Sensing. In Laborde, C. C. (Editor), *Current Trends in Short and Long Period Fiber Gratings*. (pp. 63-86). Intech.

Kosinski, G., Hill, S. M., Vengsarkar, A. M., Eyck, T., and Alexander, C., 2010. Methods for making long-period fiber gratings, European Patent Specification.

Kosinski, S.G., Vengsarkar, A.M., 1998. Splicer-based long-period fiber gratings. In: *Optical Fiber Communication Conference and Exhibit. Proceeding of Optical Fiber Communication Conference (OFC '98)*; 22 Feb 27 Feb 1998; San Jose, CA.

Krohn, D.A., 2015. *Fiber optic sensors-Fundamental and applications*, Instrument Society of America.

Kumar, D., Meenan, B.J., Mutreja, I., D'sa, R., Dixon, D., 2012. Controlling the size and size distribution of gold nanoparticles: a design of experiment study, *Int. J. Nanosci.* 1250023.

L. Y. Shao, J. Zhao, X. Y. Dong, H. Y. Tam, C. Lu, and S. He, "Long-period grating fabricated by periodically tapering standard single-mode fiber," *Applied Opt.*, vol. 47, no. 10, pp. 1549-1552, Apr 2008.

Laffont, G., Ferdinand, P., 2000. Fiber Gragg Grating-induced coupling to cladding modes for refractive index measurements, *Proceedings of SPIE* 4185 , pp. 326-329.

Lazaro, J.M., Quintela, A., Allende, P.B.G., Mirapeix, J., Galindez, C., and Higuera, J.M.L., 2009. High temperature fiber sensor based on a thermo-mechanical written," *Proc. of SPIE* 7503, 20th International Conference in Optical Fibre Sensors.

Lee, B. H., Liu, Y., Lee, S. B., Choi, S. S., Jang, J. N., 1997. Displacements of the resonant peaks of a long-period fiber grating induced by a change of ambient refractive index, *Optics Letter*, 23, pp. 1769-1771.

Lee, S.C., Yong, Y.T., Yeap, K.H., Rahman, F.A., 2013. An asymmetric tapered long period fiber grating: fabrication and characterization. In: Photonics (ICP). 2013 IEEE 4th International Conference on Photonics (ICP); 2013 Oct 28–30, Melaka, Malaysia.

Lee, S.T., George, N.A., Sureshkumar, P., Radhakrishnan, P., Vallabhan, C.P.G., and Nampoori, V.P.N., Chemical sensing with microbent optical fiber, *Opt. Lett.* 26, pp. 1541-1543.

Leong, C.C.W., Syed, N.I., and Lorscheider, F.L., Retrograde degeneration of neurite membrane structural integrity of nerve growth cones following in vitro exposure to mercury 2001, *Neuroreport* 12.4, pp. 733-737.

Levine, C.R., Yanai, R.D., Lampman, G.G., Burns, D.A., Driscoll, C.T., Lawrence, G.B., Lynch, J.A., Schoch, N., 2014. Evaluating the efficiency of environmental monitoring programs, *Ecological Indicators*, 41, pp. 94–101.

Levlin, M., Ikävalko, E., Laitinen, T., 1999. Adsorption of mercury on gold and silver surfaces, *Fresenius Journal of Analytical Chemistry*, 365, pp. 577–586.

Li, M., Wang, Q.Y., Shi, X.D., Hornak, L.A., Wu, N.Q., 2011. Detection of Mercury(II) by Quantum Dot/DNA/Gold Nanoparticle Ensemble Based Nanosensor Via Nanometal Surface Energy Transfer, *Anal. Chem.*, 83, pp. 7061-7065.

Li, Q., Qian, Y., Yu, Y., Wu, G., Sui, Z., Wang, H., 2009. *Opt. Commun.*, 282, pp. 2446–2450.

Li, Q.S., Zhang, X.L., He, H., Meng, Q., Shi, J., Wang, J.N., Dong, W.F., 2014. Improved detecting sensitivity of long period fiber gratings by polyelectrolyte multilayers: The effect of film structures, *Opt. Commun.* 331, pp. 39–44.

Li, Q.S., Zhang, X.L., Yu, Y.S., Qian, Y., Dong, W.F., Li, Y., Shi, J.G., Yan, J.T., Wang, H.Y., 2011. Enhanced sucrose sensing sensitivity of long period fiber grating by self-assembled polyelectrolyte multilayers, *Reactive & Functional Polymers*, 71, pp. 335–339.

Libish, T.M., Linesh, J., Bobby, M.C., Biswas, P., Bandyopadhyay, S., Dasgupta, K., Radhakrishnan, P., 2011. Fiber optic sensor for the adulteration detection of edible oils, *optoelectronics and advanced materials-rapid communications.*, 5, pp. 68-72.

Libish, T.M., Linesh, J., Matthews, B.C., Sebastian, M., 2011. Glucose concentration sensor based on long period grating fabricated from hydrogen loaded photosensitive fiber, *Sensors and Transducers*, 129, pp. 142-148.

- Lim, J., Lee, N.E., Lee, E., Yoon, S., 2014. Surface modification of citrate-capped gold nanoparticles using CTAB micelles, *Bull. Korean Chem. Soc.* 35, pp. 2567–2569.
- Lin, H.S., Mokhtar, M.R., Rashid, H.A.A., Rahman, F.A., 2009. Simultaneous sensing system for identical long-period gratings sensors using subcarrier multiplexing, *Laser Phys.*, 19, pp. 1453–1456.
- Lin, H.S., Mokhtar, M.R., Rashid, H.A.A., Rahman, F.A., 2009. Simultaneous sensing system for identical long-period gratings sensors using subcarrier multiplexing, *Laser Phys.* 19, pp. 1453–1456.
- Linesh, J., Libish, T.M., Bobby, M.C., Radhakrishnan, P., Nampoore, V.P.N. 2011. Periodically tapered LPFG for ethanol concentration detection in ethanol-gasoline blend. *Sens. Transd. J.*,125, pp. 205–212.
- Loh, MC, Rahman FA, Kuramitz H, Yong YT. Method to sensitize an arc-induced LPFG-based sensor using double-pass configuration. *Microw. Opt. Technol. Lett.* 2014 ;56: 2766–2769.
- Loh, M.C., Yong, Y.T., Kuramitz, H., Teh, P.C., Rahman, F.A., 2015. Double-pass configuration to enhance the sensitivity of a polyelectrolyte-coated arc-induced long-period fiber grating, *J. Electromagn. Waves Appl.* 29 , pp. 1908–1916.
- Lohner, T. W., & Dixon, D. A. (2013). The value of long-term environmental monitoring programs: an Ohio River case study. *Environmental Monitoring and Assessment*, 185(11), 9385–9396.
- Lourie, B., Glenn, W., 2003. Mercury in the environment: a primer, pollution probe foundation.
- Magnuson, J.J., and Bowser, C.J., 1990. A network for longterm ecological research in the United States. *Freshwater Biology*, 23, pp. 137–143.
- Medlock, R., 1989. Fibre optics in process-control, *Control Instrum*, 21(4), pp. 105–108.
- Minai, M., 2016. Methylmercury and Human Embryonic Development, *Embryo Project Encyclopedia*.
- Mountfort, F.H., 2009. A path integral approach to the coupled-mode equations with specific reference to optical waveguides, Master Thesis, Dept.of Science, University of Stellenbosch.
- Myers, D.N., 2015. Foundations of Water Quality Monitoring and Assessment in the United States, Chapter 2. In: *Food Energy and Water*, 2015. pp. 21-92.

- Mysliwiec, M., Grochowski, J., Krogulski, K., Mikulic, P., Bock, W. J., and Smietana, M., 2013. Effect of wet etching of arc-induced long-period gratings on their refractive index sensitivity, *Acta Physica Polonica*, 124(3), pp. 521-524.
- Nordblad, F., 2008. Evaluation of In-Situ Sampling Methods for Trace Metal Measurements in Natural Waters Using Thin Films. PhD thesis, University of Technology, Sweden.
- Patrick, H.J., Kersey, A.D., Bucholtz, F., 1998. Analysis of the response of long period fibre gratings to external index of refraction, *J. Lightwave Technol.* 16, pp. 1606–1642.
- Pawari, M.J., Gawande, S., 2015. Ground water pollution & its consequence. *International journal of engineering research and general science.*, 3(4), pp. 773-776.
- Petrovic, J.S., Dobb, H., Mezentsev, V.K., Kalli, K., Webb, D.J., and Bennion, I., 2007. Sensitivity of LPGs in PCFs fabricated by an electric arc to temperature, strain, and external refractive index, *Journal of Lightwave Technology*, 25(5), pp. 1306-1312.
- Pink, D.H., 2006. Investing in tomorrow's liquid gold, *World J. Anal. Chem.*, 2, pp. 42–46.
- Pirrone, N., 2010. Global mercury emissions to the atmosphere from anthropo- genic and natural sources. pp. 4721-22.
- Poole, C.D., Meester, J.P., Presby, H.M., 1994. Two-mode fibre spatial-mode converter using periodic core deformation. *Electron. Lett.* 30, pp. 1437–1438.
- Pouran, H.M., Martin, F.L., Zhang, H., 2014. Measurement of ZnO nanoparticles using diffusive gradients in thin films: binding and diffusional characteristics, *Anal Chem.*, 12, pp. 5906-13.
- Rees, N.D., James, S.W., and Tatam, R.P., 2002. Optical fiber long-period gratings with Langmuir-Blodgett thin-film overlays, *Opt. Lett.*, 27(9), pp. 686-688.
- Rego, G., 2013. A review of refractometric sensors based on long period fibre gratings, *Scientific World Journal*, 2013, pp. 1 –14.
- Rego, G., 2006. Arc-induced long-period fibre gratings: fabrication and their applications in optical communications and sensing. PhD dissertation. Portugal: University of Porto.
- Rego, G., 2009. Annealing of arc-induced gratings at high temperatures, *Electron. Lett.*, 45(19), pp. 972-974.

- Rego, G., 2016. Arc-Induced Long Period Fiber Gratings, *Journal of Sensors*. (2016), pp. 1-14.
- Rego, G., Santos, L.M.N.B.F., Schroder, B., Marques, P.V.S., Santos, J.L., and Salgado, H.M., 2004. In situ temperature measurement of an optical fiber submitted to electric arc discharges, *IEEE Photonics Technology Lett.*,16(9), pp. 2111-2113.
- Rice, K.M., Walker, E.M. Jr., Wu, M.Z., Gillette, C., Blough, E.R., 2014. Environmental mercury and its toxic effects, *J. Prev. Med. Public Health* 47, pp. 74–83.
- Rios, A.M., Hernandez, D. M., and Gomez, I. T., 2009. Highly sensitive cladding-etched arc-induced long-period fiber gratings for refractive index sensing, *Optics Communications*, 283, pp. 958-962.
- Rios, A.M., Hernandez, D.M., Gomez, I.T., 2010. Highly sensitive cladding-etched arc-induced long-period fiber gratings for refractive index sensing. *Opt. Commun.*, 283, pp. 958–962.
- Rocha, J.B.T., Aschner, M., Dórea, J.G., Ceccatelli, S., Farina, M., & Silveira, L.C.L., 2012. Mercury Toxicity. *Journal of Biomedicine and Biotechnology*, 2012, 831890.
- Romanov, A.V., Ignatieva, Y.S., Morozova, I. A., Speranskaya, O. A., Tsitser, O. Y., 2017. Mercury pollution in Russia: problems and recommendations.
- Ruiz-Guzman, J.A., Marrugo-Negrete, J.L., Diez, S., 2014. Human Exposure to Mercury Through Fish Consumption: Risk Assessment of Riverside Inhabitants of the Urrá Reservoir, Colombia, *Human and Ecological Risk Assessment: An International Journal*. 20, pp.1151-1163.
- Schmitt, C.J., Stricker, C.A., Brumbaugh, W.G., 2011. Mercury bioaccumulation and biomagnification in Ozark stream ecosystems, *2 Ecotoxicology and Environmental Safety* 74, pp. 2215–2224.
- Selin, H., Keane, S.E., Wang, S., Selin, N.E., Davis, K., & Bally, D., 2018. Linking science and policy to support the implementation of the Minamata Convention on Mercury. *Ambio*, 47, pp. 198–215.2
- Semionov, A., 2018. Minamata Disease—Review. *World Journal of Neuroscience*, 8, pp. 178-184.
- Shu, X.W., Zhang, L., and Bennion, I., 2002. Sensitivity characteristics of long-period fiber gratings, *Journal of Lightwave Technology*, 20(2), pp. 255-266.

Silva, C., Coelho, J. M. P., Caldas, P., and Jorge, P., 2012. Fibre sensing system based on long-period gratings for monitoring aqueous environments, In *Fiber Optic Sensors*, pp. 318-342.

Simpson, S.L., Yverneau, H., Cremazy, A., Jarolimek, C.V., Price, H., Jolley, D.F., 2012. DGT-induced copper flux predicts bioaccumulation and toxicity to bivalves in sediments with varying properties. *Environmental Science and Technology* 46, pp. 9038-9046.

Smietana, M., Bock, W. J., and Mikulic, P., 2011. Temperature sensitivity of silicon nitride nanocoated long-period gratings working in various surrounding media, *Meas. Sci. Technol.*, 22(11), 115203.

Smietana, M., Bock, W.J., 2011. Influence of fabrication technology on metrological properties of long period fiber gratings for pressure measurements. XVIII IMEKO TC4 Symposium and IX Semetro Metrologia 2011, pp. 254-257.

Smietana, M., Bock, W.J., Mikulic, P., Chen, J., 2010. Pressure Sensing in High-Refractive-Index Liquids Using Long-Period Gratings Nanocoated with Silicon Nitride. *Sensors*. 12, pp. 11301-11310.

Smietana, M., Bock, W.J., Mikulic, P., Chen, J., 2011. Increasing sensitivity of arc-induced long-period gratings – pushing the fabrication technique toward its limits. *Meas. Sci. Technol.*, 22, pp. 1–6.

Smietana, M., Debowska, A.K., Mikulic, P., and Bock, W.J., 2013. Refractive index sensing with high temperature nano-coated electric arc-induced long-period gratings working at dispersion turning point, in *Proceedings of the 18th Microoptics Conference (MOC '13)*, pp. 1–2, Tokyo, Japan.

Stegall, D.B., Erdogan, T., 1999. Leaky cladding mode propagation in long-period fiber grating devices. *IEEE Photonics Technology Letters.*, 11(3), pp. 343–345.

Szymańska, M., Krogulski, K., Mikulic, P., Bock, W.J., Śmietana, M., 2014. Sensitivity of Long-period Gratings Modified by their Bending, *Procedia Engineering*, 87, pp. 1180-1183.

Tan, S.Y., Yong, Y.T., Lee, S.C., Rahman, F.A., 2015. Review on an arc-induced long period fiber grating and its sensor applications, *J. Electromagn. Waves Appl.*, 29, pp. 703–726.

Tan, S.Y., Lee, S.C., Okazaki, T., Kuramitz, H., Rahman, F.A., 2018. Detection of Mercury (II) Ions in Water by Polyelectrolyte - Gold Nanoparticles Coated Long Period Fiber Grating Sensor, *Optics Communication* 419, pp. 18-24.

Turkevich, J., Stevenson, P.C., Hillie, J., 1951. A study of the nucleation and growth processes in the synthesis of colloidal gold, *Discuss. Faraday Soc.* 11 pp. 55.

UNEP, Global Atmospheric Mercury Assessment: Sources, Emissions and Transport. [Online]. Available at: <https://www.epa.gov/international-cooperation/mercury-emissions-global-context>.

Ushio, M., 1988. Arc discharge and electrode phenomena, *Pure & App/ Chem.* 60, pp. 809-814.

Vasiliev, S.A., Dianov, E.M., Varelas, D., Limberger, H.G., and Salathe, R.P., 1996. Postfabrication resonance peak positioning of long-period cladding-mode-coupled gratings, *Opt. Lett.*, 21(22), pp.1830-1832.

Vengsarkar, A.M., Lemaire, P. J., Judkins, J. B., Bhatia, V., Erdogan, T., and Sipe, J. E., 1996. Long-period fiber gratings as band-rejection filters, *Journal of Lightwave Technology*, 14(1), pp. 58-65.

Venugopalan, T., Yeo, T.L., Sun, T., and Grattan, K.T.V., 2008. LPG-based PVA coated sensor for relative humidity measurement, *IEEE Sens.*, 8(7), pp. 1093–1098.

Villar, I.D., Achaerandio, M., Matias, I. R., and Arregui, F.J., 2005. Deposition of overlays by electrostatic self-assembly in long-period fiber gratings, *Opt. Lett.*, 30(7), pp. 720–722.

Wang, D.Y., Wang, Y., Han, M., Gong, J., 2010. Fully distributed fiber-optic biological sensing. *IEEE Photon. Technol. Lett.*, 22, pp. 1553–1555.

Wang, G.Q., Chen, C., Chen, L.X., 2009. Surface-enhanced Raman scattering in nanoliter droplets: towards high-sensitivity detection of mercury (II) ions, *Anal. Bioanal. Chem.* 394, pp.1827-1832.

Wang, P.F., Wang, T., Wang, Y., Yao, C., Liu, C., Yuan, Y., Lin, Y.P., 2016. A diffusive gradient in thin film technique for evaluation of the bioavailability of Cd in soil contaminated with Cd and Pb, *Int. J. Environ. Res. Public Health* 13, pp. 556.

Wang, Z.Y., 2005. Ionic self-assembled multilayers adsorbed on long period fiber gratings for used as biosensors, PhD. Dissertation, Electrical Engineering, Faculty of Virginia Polytechnic Institute and State University, Blacksburg, Virginia, Dec 2005.

Wang, Z.Y., Heflin, J.R., Stolen, R.H., and Ramachandran, S., 2005. Highly sensitive optical response of optical fiber long period gratings to nanometer-thick ionic self-assembled multilayer, *Applied Physics Lett.*, 86.

- Yamamoto, H. Tsutsumi, Miyoshu, Y., and Ohashi, M., 2010. Temperature characteristics of a long period fiber grating using a heat-shrinkable tube, In Communications and Photonics Conference and Exhibition on IEEE, pp.651-652.
- Yang, G.H., Dai, S.X., Cheng, G., Zhang, P.Y. and Du, Z.L., 2007. Evaluation of nano-frictional and mechanical properties of a novel Langmuir–Blodgett monolayer/self-assembly monolayer composite structure, *J. Mater. Res.* 22, pp. 2429-2436.
- Yin, G.L., Wang, Y.P, Liao, C.R., Zhou, J.T., Zhong, X.Y., Wang, G.J., Sun, B., He, J., 2014. Long Period Fiber Gratings Inscribed by Periodically Tapering a Fiber, *IEEE Photonics Technology Letters*, 26(2014), pp. 698-701.
- Yin, Z.H., Zhang, X.B., Liu, Y.Q., Pang, F.F., Wang, T.Y., 2012. Refractive index sensitivity characteristics of fiber taper long-period grating. In: *Asia Communications and Photonics Conference (ACP 2012)*, Nov 7–10, Guangzhou, China.
- Yong, Y.T., Lee, S.C., Rahman, F.A., 2015. Sensitization of hybrid LPFG-FBG refractometer using double-pass configuration. *Opt. Commun.*, 338, pp. 590–595.
- Yong, Y.T., Lee, S.C., Rahman, F.A., 2017. Fiber sensor network with multipoint sensing using double-pass hybrid LPFG-FBG sensor configuration, *Opt. Commun.*, 387, pp. 191–195.
- Yoon, M.S., Kim, H.J., Kim, S.J., and Han, Y.G., 2013. Influence of the waist diameters on transmission characteristics and strain sensitivity of microtapered long-period fiber gratings,” *Opt. Lett.*, 38(15), pp. 2669–2672.
- Yoon, M.S., Kim, S.J., Kim, H.J., and Han, Y.G., 2012. Sensitivity characteristics of micro-tapered long-period fiber grating written in tapered fiber with different diameters, *17th Opto-Electronics and Communication Conference (OECC 2012)*, pp. 779-780.
- Yorifuji, T., Tsuda, T., Harada, M., 2013. Minamata disease: a challenge for democracy and justice Late lessons from early warnings: science, precaution, innovation. European Environment Agency, Denmark, pp. 124–152.
- Zhang, H. Davison, 1995. Performance Characteristics of Diffusion Gradients in Thin Films for the in Situ Measurement of Trace Metals in Aqueous Solution, *Analytical Chemistry* 67, pp. 3391-3400.
- Zhang, H., Davison, W., 1999. Diffusional characteristics of hydrogels used in DGT and DET techniques, *Anal. Chim. Acta.* 398, pp. 329-340.

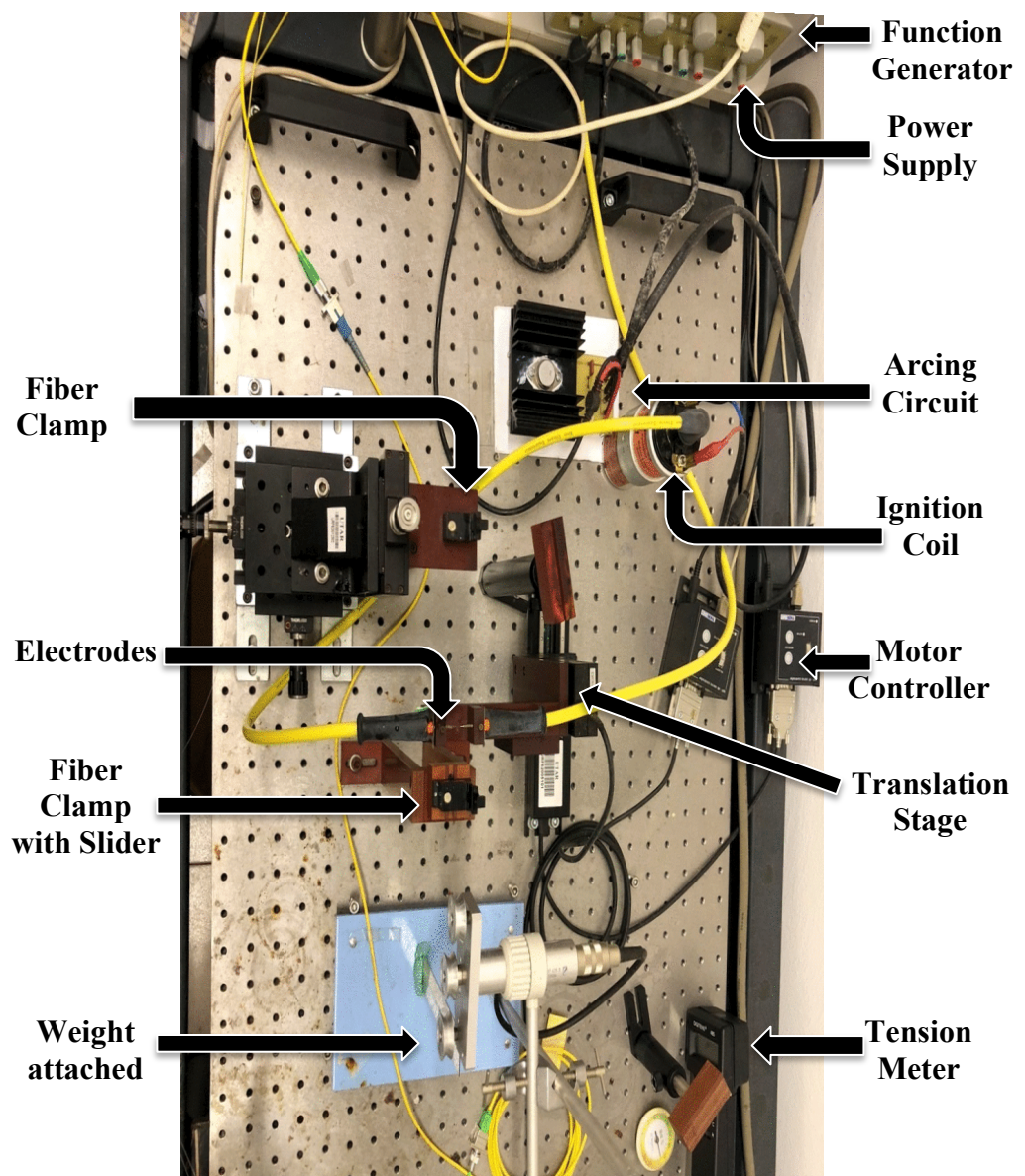
Zhang, J.R., Liu, H.R., Wu, X.K., 2009. Curvature optical fiber sensor by using bend enhanced method, *Frontiers of optoelectronics in China*. 2, pp. 204-209.

Zulkifly, M.Z.R.M., Rahman, F.A., Wong, H.Y., 2010. Arc-induced long period fiber gratings (LPFG) characterization: Comparison between cladding etched and non-etched LPFG," In *Photonics (ICP), 2010 International Conference on*. IEEE, pp.1-3.

# APPENDIX A

## FABRICATION SETUP

### (ELECTRIC ARC DISCHARGE TECHNIQUE)



# APPENDIX B

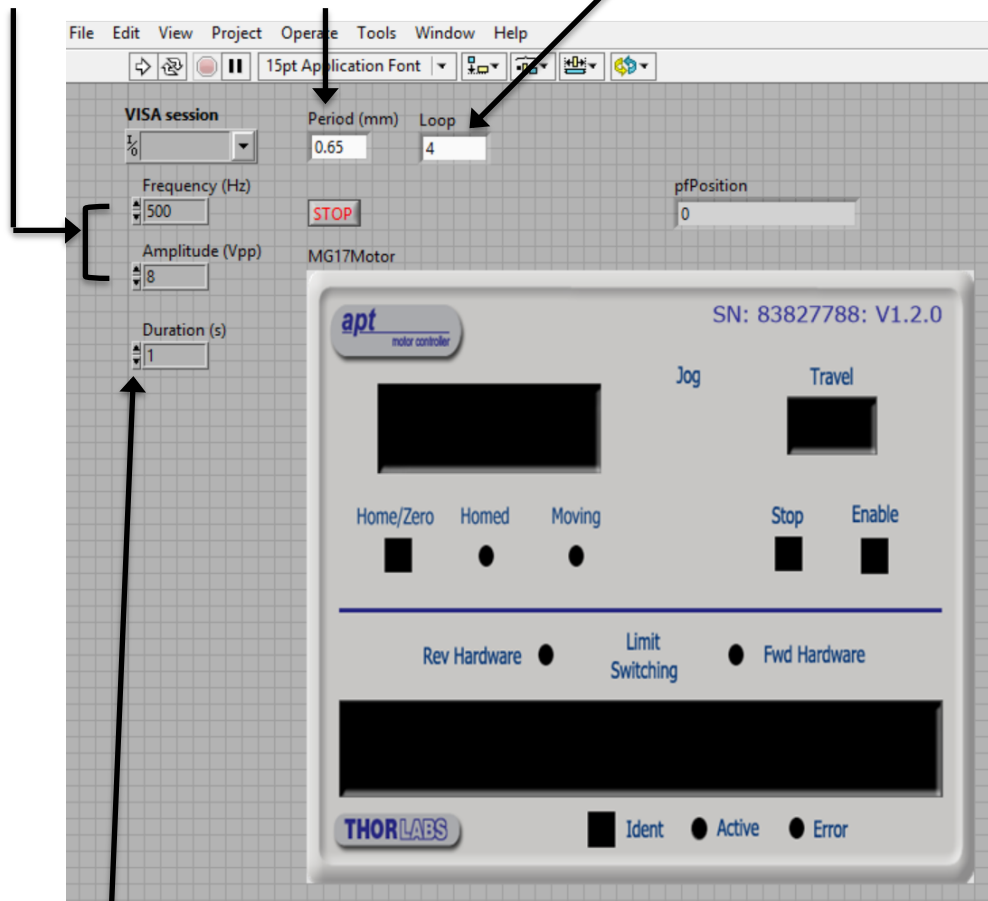
## LabVIEW PROGRAM

(CONTROLS THE FABRICATION PROCESS)

Frequency and Amplitude of Function Generator

Grating Period

Loop to control number of arcing



Arc Duration